uOttawa

L'Université canadienne
Canada's university

FACULTÉ DES ÉTUDES SUPÉRIEURES ET POSTOCTORALES

uOttawa

L'Université canadienne
Canada's university

FACULTY OF GRADUATE AND POSDOCTORAL STUDIES

Sami Kamran

AUTEUR DE LA THÈSE / AUTHOR OF THESIS

M.Sc. (Physics)

GRADE / DEGREE

Department of Physics

FACULTÉ, ÉCOLE, DÉPARTEMENT / FACULTY, SCHOOL, DEPARTMENT

Semi-empirical and Ab Initio Study of the Ideal Strengths and Elastic Properties of Covalent Crystals and FCC Metals

TITRE DE LA THÈSE / TITLE OF THESIS

Dr. K. Chen

DIRECTEUR (DIRECTRICE) DE LA THÈSE / THESIS SUPERVISOR

Dr. L. Chen

CO-DIRECTEUR (CO-DIRECTRICE) DE LA THÈSE / THESIS CO-SUPERVISOR

EXAMINATEURS (EXAMINATRICES) DE LA THÈSE / THESIS EXAMINERS

Dr. S. Godfrey

Dr. I. L'Heureux

Gary W. Slater

Le Doyen de la Faculté des études supérieures et postdoctorales / Dean of the Faculty of Graduate and Postdoctoral Studies

Semi-empirical and *Ab Initio* Study of the Ideal Strengths and Elastic Properties of Covalent Crystals and FCC Metals

by

Sami Kamran

Thesis submitted to
The Faculty of Graduate and Postdoctoral Studies
In partial fulfilment of the requirements for the Degree of
Master of Science

Ottawa-Carleton Institute for Physics
University of Ottawa

Library and Archives Canada

Published Heritage Branch

395 Wellington Street
Ottawa ON K1A 0N4
Canada

Bibliothèque et Archives Canada

Direction du Patrimoine de l'édition

395, rue Wellington
Ottawa ON K1A 0N4
Canada

Your file Votre référence
ISBN: 978-0-494-41670-9
Our file Notre référence
ISBN: 978-0-494-41670-9

NOTICE:
The author has granted a non-exclusive license allowing Library and Archives Canada to reproduce, publish, archive, preserve, conserve, communicate to the public by telecommunication or on the Internet, loan, distribute and sell theses worldwide, for commercial or non-commercial purposes, in microform, paper, electronic and/or any other formats.

The author retains copyright ownership and moral rights in this thesis. Neither the thesis nor substantial extracts from it may be printed or otherwise reproduced without the author's permission.

AVIS:
L'auteur a accordé une licence non exclusive permettant à la Bibliothèque et Archives Canada de reproduire, publier, archiver, sauvegarder, conserver, transmettre au public par télécommunication ou par l'Internet, prêter, distribuer et vendre des thèses partout dans le monde, à des fins commerciales ou autres, sur support microforme, papier, électronique et/ou autres formats.

L'auteur conserve la propriété du droit d'auteur et des droits moraux qui protège cette thèse. Ni la thèse ni des extraits substantiels de celle-ci ne doivent être imprimés ou autrement reproduits sans son autorisation.

In compliance with the Canadian Privacy Act some supporting forms may have been removed from this thesis.

While these forms may be included in the document page count, their removal does not represent any loss of content from the thesis.

Conformément à la loi canadienne sur la protection de la vie privée, quelques formulaires secondaires ont été enlevés de cette thèse.

Bien que ces formulaires aient inclus dans la pagination, il n'y aura aucun contenu manquant.

Canada

© Sami Kamran, Ottawa, Canada, 2008

Abstract

The present thesis consists of a number of studies on the elastic properties of covalently bonded crystals, the ideal strengths of a selection of face-centred cubic (FCC) metals and the anomalously large shear modulus of iridium.

Semi-empirical formulae for both bulk modulus B and shear modulus G of covalent crystals were elaborated in terms of bond length and ionicity fraction of the bonding. The resulting equations can be applied to a broad selection of covalent materials and their predictions are in good agreement with the experimental data and the results from first-principles calculations. Furthermore, the correlation between the ratio G/B and the aforementioned bonding parameters was investigated. The analysis of this relationship demonstrates that the bond length is the predominant parameter responsible for the brittle features of covalent materials.

The ideal shear and tensile strengths of FCC transition metals were examined through density functional theory (DFT)-based computations. These results allowed establishing a new indicator of ductility, namely the ratio of ideal shear strength to ideal tensile strength $\tau_m / \sigma_{<111>}$. Moreover, it was found that palladium can sustain a surprisingly long range of deformation. Based on the analysis of density of states (DOS) curves, it is suggested that creation of angular features is responsible for the notable amount of distortion suffered by palladium.

The electronic origin of the anomalously large elastic modulus and intrinsic brittleness of FCC iridium were studied using *ab initio* DFT-based calculations. The electron localisation function (ELF) and bond orders (BO) of iridium and a selection of FCC metals were calculated and then used to evaluate the directionality and the strength of the bonds. The analysis of the trend of bond strength versus elastic moduli, Cauchy pressure and the ratio of shear modulus over bulk modulus suggests that the bond strength is the primary factor that causes the abnormally high modulus of iridium and its intrinsic brittleness.

Statement of Originality

My research work presented in the current thesis was realised under Dr. Kuiying Chen's immediate supervision at the National Research Council Canada (NRC) and it was co-supervised by Dr. Liang Chen at the Department of Physics, University of Ottawa.

The semi-empirical formulae for the elastic moduli of covalent crystals presented in chapter III were solely developed by the author. The calculations reported in chapters IV and V were performed by the writer with credits attributed to Dr. Kuiying Chen for familiarising the author with the software used in this project and assisting him in solving the following problems

1- Writing the code for shear simulation;
2- Simulating FCC unit cells cut in layers along the <110> and <111> directions;

In the case of Al, Cu and Pd, Dr. Kuiying Chen has also independently verified the author's results for their ideal shear strength.

Acknowledgements

Hereby, I would like to present my deepest gratitude to Dr. Liang Chen, who has co-supervised me at the University of Ottawa and especially Dr. Kuiying Chen, my immediate co-supervisor at the National Research Council Canada (NRC), whose guidance was indispensable throughout this project. They are supervisors of great academic calibre who have always held high standards in research and have constantly evinced their professionalism. I have particularly benefited from Dr. Kuiying Chen's knowledge and experience in computational materials physics.

I am grateful to the National Research Council Canada (NRC) for permitting me to have access to their facilities for the past two years and for funding this project. I am also thankful to the National Science and Engineering Research Council (NSERC) for having provided parts of the funds used for this thesis.

Lastly, I should like to thank my parents who have supported and encouraged me during these two years.

Table of contents

ABSTRACT I

STATEMENT OF ORIGINALITY II

ACKNOWLEDGEMENTS III

TABLE OF CONTENTS IV

LIST OF FIGURES VI

LIST OF TABLES VII

LIST OF ACRONYMS VIII

CHAPTER I 1

INTRODUCTION 1

1.1 THESIS MOTIVATION AND OVERVIEW OF PREVIOUS WORKS 1
1.2 THESIS OBJECTIVES AND OUTLINE 3

CHAPTER II 5

TOTAL ENERGY CALCULATION 5

2.1 THE BORN-OPPENHEIMER APPROXIMATION 6
2.2 OVERVIEW OF DENSITY FUNCTIONAL THEORY (DFT) 7
2.2.1 The DFT Formalism 7
2.2.2 Kohn-Sham equations 9
2.2.3 Exchange and correlation energy 11
2.3 REVIEW OF VASP ALGORITHM 14
2.3.1 Outline of the VASP algorithm 14
2.3.2 Iterative methods for the diagonalisation of the Kohn-Sham Hamiltonian 16
2.3.3 Charge density mixing 20
2.3.4 Partial occupancies and Brillouin zone integration 21
2.4 PSEUDOPOTENTIAL APPROACHES AND THE PROJECTOR AUGMENTED WAVES (PAW) METHOD 22
2.5 FORCES 26

CHAPTER III 28

ELASTIC PROPERTIES 28

OF COVALENT SYSTEMS 28

3.1 ELASTIC MODULI 28
3.2 COVALENT SYSTEMS 30
3.2.1 Structure of diamond-like and sphalerite crystals 30
3.2.2 Overview of band structure 32
3.2.3 The band gap energy Eg 34
3.2.4 Ionicity fraction f_i 37
3.3 OVERVIEW OF PREVIOUS INVESTIGATIONS 39
3.4 ELASTIC MODULI OF COVALENT CRYSTALS 41

CHAPTER IV 48

IDEAL STRENGTHS OF 48

FCC METALS 48

4.1 FCC STRUCTURE 48
4.2 CALCULATION OF IDEAL STRENGTH 50

4.3 SHEARABILITY AND BOND DIRECTIONALITY 56
4.4 IDEAL STRENGTH AND DUCTILITY 57
4.5 ANALYSIS OF THE DOS OF AL, CU, IR AND PD 58

CHAPTER V 63

ORIGIN OF THE ANOMALOUS 63

ELASTIC PROPERTIES 63

OF IRIDIUM 63

5.1 METALLIC BOND 64
5.1.1 Electron localisation *64*
5.1.2 Bonding topology and interactions *68*
5.2 BOND STRENGTH 73
5.2.1 Biorthonormal functions and density matrix *73*
5.2.2 Bond order (BO) index *76*
5.2.3 LCAO approach *76*
5.3 RATIONALISATION OF THE ABNORMAL ELASTIC PROPERTIES OF IR 78

CHAPTER VI 83

CONCLUSION 83

6.1 THESIS ACHIEVEMENTS 83
6.2 SUGGESTED FUTURE WORK 85

REFERENCES 86

APPENDIX A: ATOMIC UNITS 100

APPENDIX B: ADIABATIC APPROXIMATION 101

APPENDIX C: PROOFS OF THE DFT THEOREMS 102

APPENDIX D: THE STIFFNESS AND COMPLIANCE CONSTANTS 104

APPENDIX E: SUPPLEMENT TO CHAPTER IV 106

APPENDIX F: PROPORTIONALITY OF BO WITH THE ELECTROSTATIC TERMS IN THE BORN-OPPENHEIMER HAMILTONIAN 107

APPENDIX G: CURRICULUM VITAE 110

List of Figures

Fig. 1 Outline of VASP algorithm 15
Fig. 2 Structure of diamond-like crystals 31
Fig. 3 Structure of sphalerite crystals 31
Fig. 4 Energy as a function of wave number for valence electrons of semiconductors 33
Fig. 5 Sketch of the polar coordinates (E_h, ϕ) 38
Fig. 6 Product of shear modulus with the bond length to 5.5 as a function of ionicity..42
Fig. 7 Product of bulk modulus with the bond length to 3.5 as a function of ionicity ..42
Fig. 8 The ratio R_j as a function of ionicity.....46
Fig. 9a-b Ratio of the elastic moduli as a function of ionicity and bond length.....46-47
Fig. 10 FCC structure 49
Fig. 11a-b Closed packed layers of FCC crystals along <110> and <111> directions..51
Fig. 12 Total energy of Ni as a function of the deformation shear parameter.....52
Fig. 13 Stress as a function of the shear deformation parameter 53
Fig. 14a-b Total energy and its second derivative around γ=0 54
Fig. 15 Cauchy pressure and the ratio of the deal shear strength and shear modulus as functions of shearability 56
Fig. 16 the ratio of the elastic moduli against the ratio of the ideal shear and tensile strengths 58
Fig. 17a-d DOS curves of Al, Cu, Ir and Pd for different values of γ 59-61
Fig. 18 ELF contour plot of W 68
Fig. 19a-c ELF contour plots of Al, Si and NaCl 71-72
Fig. 20 FCC based 63-atom cluster 77
Fig. 21a-c ELF contour plots of Au, Pt and Ir 78-79
Fig. 22 Comparison between BO, shear and bulk moduli, Cauchy pressure and the ratio of the elastic moduli for different FCC metals 80
Fig. 23 ELF contour plot of Pd 106

List of Tables

Table 1 Bond length and ionicity fraction of a series of covalent crystals together with the experimental and calculated values of their elastic moduli 44

Table 2 Lattice parameter, shearability, ideal shear strength, shear modulus, tensibility and ideal tensile strength of Ag, Al, Au, Cu, Ir, Ni, Pd and Pt 53

Table 3 Fermi energy of Al, Cu, Ir and Pd for different values of γ 62

Table 4 Linear correlation coefficient for BO against different elastic constants 81

Table 5 Atomic units 101

Table 6 Supplementary data on the ideal strength of FCC metals 107

List of Acronyms

Ag	Silver
Al	Aluminium
Au	Gold
BCC	Body-Centred Cubic
BO	Bond Order (index)
BZ	Brillouin Zone
CG	Conjugate Gradient (minimisation approach)
CP	Critical Point
Cu	Copper
DFT	Density Functional Theory
DOS	Density Of States
ELF	Electron Localisation Function
FCC	Face-Centred Cubic
FNN	First Nearest Neighbours
GGA	Generalised Gradient Approximation
Ir	Iridium
LCAO	Liner Combination of Atomic Orbitals
LDA	Local Density Approximation
Ni	Nickel
NNM	Non-Nuclear Maximum
PAW	Projector-Augmented Waves
Pd	Palladium
Pt	Platinum
RMM-DIIS	Residual Minimisation Method-Direct Inversion in the Iterative Subspace
RR	Rayleigh-Ritz (technique)
Si	Silicon
US	Ultrasoft (pseudopotential)
VASP	Vienna *Ab initio* Simulation Package

W	Tungsten

Chapter I
Introduction

1.1 Thesis Motivation and Overview of Previous Works

With the advent of computers capable of handling the complicated calculations arising in large-size solid systems, has come the rapidly growing necessity of rationalising the results of these computations in terms of various attributes of the chemical bonding. This increasing need originates from the fact that different macroscopic properties derivable from the electronic ground state energy of crystals such as mechanical features are not yet fully understood in relation to the atomic-scale parameters of solids. In the absence of relationships revealing the atomic level causes of the mechanical behaviour, no matter how simple they might be, computers will merely replace real experimentation with computational experimentation. In addition, the computational schemes and algorithms exploited in dealing with many-body systems still call for improvement in order to attain more efficiency, higher accuracy and better transferability to larger molecules. It is within this context that researches similar to what is presented in the current thesis gain great importance on theoretical grounds and for practical purposes. Not only our comprehension of the electronic origins of the large-scale phenomenology of crystals will be deepened through these studies, but such investigations will enable us to predict the properties of materials and synthesise new ones satisfying specific technological demands. It is noteworthy that contrary to what might be believed, one can hardly credit first-principles calculations with the invention of novel materials thus far [Eberhart 2002]. This plain observation testifies the concrete need discussed above, which serves as the foremost motivation for this thesis. As the

present work is solely aimed at shedding some light on the microscopic features governing aspects of the mechanical behaviour of solid structures, it is convenient to survey some of the research carried out in the past decades.

One of the properties that grabs the attention of the materials scientists and engineers and which will be extensively examined in the present thesis is the elastic response. In the particular case of simple metals, a simple proportionality relation between their bulk modulus and the product of the electron concentration with the Fermi energy was found [Kittel]. However, the resulting formula is of limited utility, since it usually gives predictions within a factor of 2 of the experimental values. Recently, Gilman derived expressions for both bulk and shear moduli of metals based on simplified quantum-mechanical considerations [Gilman]. The derived equations also suffer from notable deficiencies, as they ignore the effects induced by ionicity of the bonds and exchange-correlation interactions among others. Moreover, in the case of these formulae, the ratio of shear modulus over bulk modulus, which is often used to assess the ductility of materials, is a constant close to the experimental values obtained from some alkali metals like sodium. Nonetheless, it remains an aberrant result, as one expects this ratio to vary from one substance to another.

Recently, attempts have been made at elucidating the elastic moduli in terms of the concept of bond directionality. In particular, Eberhart defined bond directionality in terms of the curvatures of the charge density, and correlated it with the elastic shear constants C_{44} of a series of FCC metals [Eberhart 2001]. Although this quantitative approach attributes very strong bond directionality to iridium, an abnormal transition metal whose shear modulus will be studied in chapter V, it leads to some inconsistencies when confronted with the results of the latest investigations. For instance, it gives a low value of bond directionality for aluminium and larger ones for gold and copper, whilst it has been shown [Ogata *et al.* 2002] that aluminium has directional bonding, and that the charge distributions of gold and copper are rather spherically symmetric. Based on a *d*-band filling argument, Wills and collaborators associated the high shear modulus of iridium to its considerable BCC-FCC energy difference [Wills *et al.*]; while, Gornostyrev and co-workers suggested that the pseudocovalent effects, which occur as a result of the extremely directional charge redistribution of iridium under shear processing, are

responsible for its high shear modulus [Gornostyrev *et al.*]. Nevertheless, the electronic origin of the brittle nature of iridium still remains unknown.

The mechanical hardness, defined as the resistance of a material to external mechanical action, is another interesting property whose electronic origin has been extensively studied. For instance, Clerc and Ledbetter have utilised chemical hardness, which measures the resistance of a molecule to changes in the total number of its electrons and is related to the second derivative of the molecular energy with respect to the electron population in the molecule, to set up a semi-empirical formula for the mechanical hardness of elements and some compounds and alloys [[Clerc 1998]-[Clerc *et al.*]]. More recently, Gao and collaborators [Gao *et al.*] related the hardness of covalently bonded crystals to Phillip's homopolar band gap, which has also been linked to the thermal activation energies of these solid structures [Siethoff]. These investigations attest the predominant role played by the homoploar band gap energy in dictating the intrinsic properties of covalent systems, whose elastic moduli will be scrutinised in chapter III with regard to their band structure.

Lastly, due attention should be paid to the calculation of the ideal strength of crystals under various sorts of deformation, which constitutes another topic of increasing interest because of its practical significance. Since the early 1990's, the theoretical strengths of different metals have been estimated by means of first-principles calculations and only lately it has become known that materials with directional bonding generally tend to suffer longer ranges of distortion prior to their failure, which might occur at comparatively high stresses [Ogata *et al.* 2004]. It is noteworthy that the interested reader should consult reference [Kamran *et al.*] for a more detailed review of most research discussed in the present section.

1.2 Thesis Objectives and Outline

This thesis, in which my research work is reported, is aimed at addressing the following problems:

i- Proposing a semi-empirical description for the bulk and shear moduli of covalent crystals in terms of their atomic-scale features and determining the predominant electronic cause of their brittleness through the analysis of the G/B ratio;

ii- Suggesting new criterion for assessing the ductility of FCC metals and elucidating the abnormally long range of deformation obtained from ab initio calculations in the case of palladium;

iii- Elucidating the electronic origin of the anomalously large shear modulus of iridium and the microscopic reasons behind the resemblance observed between the failure of iridium crystals and the fatigue fracture in aluminium.

As all the calculations performed within the framework of this project, with the exception of the semi-empirical estimations of the elastic moduli of covalent crystals, are done using simulation packages based on the density functional theory, the next chapter is intended at introducing the basics of the density functional theory as well as the iterative techniques that are employed to implement it in an efficient manner. In the third chapter, semi-empirical methods for calculating the shear and bulk moduli of covalent crystals will be presented, while chapters IV and V are dedicated to the investigation of the ideal strengths of FCC metals and the peculiarly high shear modulus of iridium, respectively. The last chapter, which is followed by the bibliography and the appendices, touches on the conclusions of the present thesis and the research prospect in the field of materials physics. Lastly, it should be pointed out that in order to keep the fluidity of the text, a number of subjects such as the proofs of the Kohn-Sham theorems, which are complementary to the corpus of the text, are presented in the appendices.

Chapter II

Total Energy Calculation

As the analytical solutions of the Schrödinger equation can be obtained only in the context of a few very simple systems and the exact numerical methods do not work in the case of large number of atoms and molecules, one is constrained to use appropriate approximations and simplified computational schemes in dealing with most many-body systems of interest such as the electronic cloud in metals. During the first half of the 20^{th} century, numerous models were set forth, most of which can be classified in two categories: *(a)* the approaches focused on solving for the wave functions based on Hartree's assumption of separability[1] of the electronic wave function and *(b)* the methods in which the electron density is regarded as the main variable rather than the wave function. The first approach allowed the development of the well-known Hartree and Hartree-Fock approximations; whereas the second line of thought, initiated by Thomas and Fermi in the 1920's, ultimately led to the elaboration of the Density Functional Theory (DFT) by Hohenberg and Kohn in 1964. In what follows, we shall outline the DFT formalism, the Kohn-Sham self-consistent equations, the algorithm used in the Vienna *Ab-Initio* Simulation Package (VASP) and concepts such as pseudopotentials and projector augmented-wave functions that are exploited in VASP. Lastly, the partial occupancies and the forces will be treated in a concise fashion.

[1] Hartree approximated the many-electron wave function as a product of single-particle functions each of which satisfies a separate one-electron Schrödinger equation with a potential term arising from the average field of the other electrons.

2.1 The Born-Oppenheimer Approximation

The Born-Oppenheimer approximation, also called the adiabatic approximation, is the starting point of all models treating many-body systems. It essentially consists of an intuitive assumption that permits us to split the molecular Hamiltonian into ionic and electronic Hamiltonians that are simpler to solve.

Neglecting the relativistic effects as well as the contribution of the spin-orbital interaction, the Hamiltonian of a system of atoms with ions of Z_a charges can be written as

$$H = -\sum_a \frac{1}{2M_a}\nabla_a^2 - \frac{1}{2}\sum_i \nabla_i^2 + \sum_{a<b} \frac{Z_a Z_b}{|\vec{r}_a - \vec{r}_b|} + \sum_{\substack{i,j \\ i\neq j}} \frac{1}{|\vec{r}_i - \vec{r}_j|} - \sum_{i,a} \frac{Z_a}{|\vec{r}_i - \vec{r}_a|} \tag{2.1}$$

where $\vec{r}_i$ are the positions of the electrons and M_a corresponds to the masse of the ion a occupying the position $\vec{r}_a$. It is noteworthy that the atomic units are used here (see appendix A for details on this unit system).

As we know, the ions are considerably heavier than the electrons; consequently, they can be regarded as fixed entities with respect to the electrons. Thus, we can assume that the molecular wave function $\Psi(\vec{r}_a, \vec{r}_i)$ is separable, i.e. that it can be written as the product of the electronic wave function $\psi(\vec{r}_a, \vec{r}_i)$ and the ionic wave function $v(\vec{r}_a)$

$$\Psi(\vec{r}_a, \vec{r}_i) = v(\vec{r}_a)\psi(\vec{r}_a, \vec{r}_i) \tag{2.2}$$

As shown in appendix B, the electronic and ionic wave functions satisfy the following equations [Marchildon]

$$\left\{\frac{1}{2}\sum_i \nabla_i^2 + V\right\}\psi(\vec{r}_a, \vec{r}_i) = \varepsilon(\vec{r}_a)\psi(\vec{r}_a, \vec{r}_i) \tag{2.3}$$

and

$$\left\{\sum_a \frac{1}{2M_a}\nabla_a^2 + \varepsilon(\vec{r}_a)\right\}v(\vec{r}_a) = E(\vec{r}_a, \vec{r}_i)v(\vec{r}_a) \tag{2.4}$$

where V refers to all the potential terms in eq. (2.1) and ε is the total energy neglecting the contribution of the ionic kinetic energy. As mentioned previously, in all the calculations, the ions are assumed to be fixed; hence, only eq. (2.3) will be used to calculate the total energy.

2.2 Overview of Density Functional Theory (DFT)

2.2.1 The DFT Formalism

The two theorems, that constitute the foundation of DFT, were developed by Hohenberg and Kohn [Hohenberg and Kohn]. Here, we shall simply state the theorems and their implications; nevertheless, the interested reader can consult their proofs in appendix C. Mind that from now on, the potential contribution of the ions will be denoted as V_{ex} and that the electronic density $n(\vec{r})$ in the ground state Ψ is given by

$$n(\vec{r}) = \left|\langle \psi \,|\, \Psi \rangle\right|^2 \tag{2.5}$$

Theorem I: To within a constant, there is a one-to-one correspondence between the external potential V_{ex} (the only system specific parameter) and the electron density $n(\vec{r})$. Consequently, since V_{ex} fixes the Hamiltonian, the ground state energy is a unique functional of $n(\vec{r})$.

The one-to-one correspondence between the external potential and the density implies that if the electron density of a system is known, then one can uniquely determine the corresponding ionic potential. This statement sounds a bit counterintuitive, as one is disposed to believe that the density contains less information than the wave function used to calculate it. None the less, this theorem proves that the density and the wave function

both enclose the same amount of information and that either of them can uniquely describe the ground state properties of the system.

Theorem II: Only the correct $n(\vec{r})$, *which has to satisfy the normalisation condition (see eq. (2.8)) minimises the ground state energy functional* $E[n]$ *in the ground state* $|\Psi\rangle$

$$E[n] = \int V_{ex}(\vec{r})n(\vec{r})d\vec{r} + F[n] \tag{2.6}$$

where

$$F[n] = \langle \Psi | (T + V_{ee}) | \Psi \rangle \tag{2.7a}$$

Notice that here T denotes the kinetic energy operator and $V_{ee}(\vec{r})$ is the electron-electron interaction

$$V_{ee}(\vec{r}) = \int \frac{n(\vec{r}')}{|\vec{r} - \vec{r}'|} d\vec{r}' \tag{2.7b}$$

The normalisation condition is given by the following equation

$$N[n] = \int n(\vec{r})d\vec{r} = N \tag{2.8}$$

where N is the total number of electrons in the system.

The Hohenberg-Kohn functional *F[n]* is a universal functional that can be applied to any thinkable molecular system or solid, in view of the fact that it only depends on the kinetic energy of the electrons and the potential energy arising from their interaction. So far, no exact expression has been found for *F[n]*. This is because the kinetic energy of a system of *interacting* electrons, in addition to the Laplacian term in eq. (2.3), has an exchange and correlation term E_{xc} that can not be derived analytically. The approximations employed to evaluate this term are presented in section 2.2.3.

Moreover, the second theorem, also known as the variational principle of DFT, allows us to formulate the question of solving for $n(\vec{r})$ in a variational language. To put this in other words, one has to solve the following variational problem

$$\frac{\delta}{\delta n(\vec{r})}\left\{E[n(\vec{r})] - \lambda\left(\int n(\vec{r})d\vec{r} - N\right)\right\} = 0 \tag{2.9}$$

where λ is a Lagrange multiplier.

In the next section, we shall use the variational principle of DFT, specified by eq. (2.9), to find a suitable procedure for computing the ground state energy functional *E[n]*.

2.2.2 Kohn-Sham equations

In their paper published in 1965 [Kohn and Sham], Kohn and Sham used the following separation in writing eq. (2.6)

$$E[n] = T_0[n] + \int d\vec{r} n(\vec{r})[V_{ex} + \tfrac{1}{2}V_{ee}] + E_{xc}[n] \tag{2.10}$$

where T_0 is the kinetic energy of a system of non interacting electrons given by the Laplacian term in eq. (2.3).

The substitution of eq. (2.10) in eq. (2.9) and the differentiation of the later with respect to the density $n(\vec{r})$ yield

$$\frac{\delta E[n]}{\delta n(\vec{r})} = \frac{\delta T_0}{\delta n(\vec{r})} + V_{ex}(\vec{r}) + V_{ee}(\vec{r}) + \frac{\delta E_{xc}[n]}{\delta n(\vec{r})} = \lambda \tag{2.11}$$

Comparing eq. (2.11) with the corresponding equation for a system of non-interacting particles satisfying the normalisation condition given by eq. (2.8) and with an effective potential $\Phi(\vec{r})$,

$$\frac{\delta E[n]}{\delta n(\vec{r})} = \frac{\delta T_0}{\delta n(\vec{r})} + \Phi(\vec{r}) = \lambda \tag{2.12}$$

one can see that eq. (2.11) and (2.12) describe the same mathematical problem, provided that

$$\Phi(\vec{r}) = V_{ex}(\vec{r}) + V_{ee}(\vec{r}) + V_{xc}(\vec{r}) \tag{2.13}$$

where the exchange and correlation potential V_{xc} is given by

$$V_{xc} = \delta E_{xc} / \delta n(\vec{r}) \tag{2.14}$$

Consequently, for a given $\Phi(\vec{r})$, the density $n(\vec{r})$, for which these equations hold, can be obtained by solving the following one-particle Schrödinger equations

$$\{-\tfrac{1}{2}\nabla^2 + \Phi(\vec{r})\}\psi_i(\vec{r}) = \varepsilon_i \psi_i(\vec{r}) \tag{2.15}$$

and setting

$$n(\vec{r}) = \sum_{i=1}^{N} \left|\psi_i(\vec{r})\right|^2 \tag{2.16}$$

Equations (2.13)-(2.16) must be solved in a self-consistent manner: an assumed density $n(\vec{r})$ is used to calculate $\Phi(\vec{r})$ from eq. (2.13) and then a new density is obtained from eq. (2.15) and (2.16). Notice that the solutions of eq. (2.15) describe one-electron orbitals and hence, in eq. (2.16), the summation is performed over all the N electrons or spin-orbitals. The total energy is then given by

$$E = \sum_{i=1}^{N} \varepsilon_i - \frac{1}{2}\iint \frac{n(\vec{r})n(\vec{r}')}{|\vec{r} - \vec{r}'|} d\vec{r} d\vec{r}' + E_{xc} - \int V_{xc} n(\vec{r}) d\vec{r} \tag{2.17}$$

Subsequently, the quantities derivable from the total energy can be calculated. Thus by reducing the problem of finding the ground state properties of an interacting system to the solution of a single-particle equation of Hartree form in an exact fashion,

the density functional method has relieved us from all the complications of solving for the wave function of a large interacting system. The advantage of this approach becomes even more obvious, when one notices that there exist efficient methods for solving the single-particle Schrödinger equation with an effective potential and that there is no restriction on the size of the system under study.

2.2.3 Exchange and correlation energy

The exchange-correlation energy E_{xc} is defined as the difference between the *exact* energy of the many-particle system and the sum of the contributions of terms that can be evaluated numerically exactly [Jones *et al.*] i.e. the total energy calculated using the Hartree-Fock approximation. Despite its clarity and simplicity, this definition is obviously of no help in estimating E_{xc} in the context of calculating the ground state energy. Consequently, one is constrained to make approximations for this term. The local density approximation (LDA) is one of the most significant approaches developed so far. As its name suggests, the LDA method consists of presuming that E_{xc} solely depends on the local density and hence it can be computed by integrating $\varepsilon_{xc}[n(\vec{r})]$, the exchange and correlation energy per particle of a uniform electron gas of density $n(\vec{r})$.

$$E_{xc}^{LDA}[n(\vec{r})] = \int d\vec{r} n(\vec{r}) \varepsilon_{xc}[n(\vec{r})] \tag{2.18}$$

Neglecting the contribution of correlation, Kohn and Sham [Kohn and Sham] analytically derived an expression for the exchange-correlation potential in the case of a slowly varying density

$$\frac{\delta E_{xc}[n(\vec{r})]}{\delta n(\vec{r})} = \frac{d(n\varepsilon_{xc})}{dn} = -\frac{1}{\pi}\left\{3\pi^2 n(\vec{r})\right\}^{1/3} \tag{2.19}$$

This result differs from Slater's estimation by a factor of $\frac{2}{3}$ and it diverges from the similar expressions obtained by Dirac and, Hartree and Fock by multiplicative factors of $\frac{3}{4}$ and $\frac{6}{4}$, respectively. In spite of the fact that the LDA was originally developed for

slowly varying densities, which exclude the electron density of solid matter, it surprisingly gives accurate results in the case of inhomogeneous charge density, although the value of the total energy is very often overestimated. As a result, several inhomogeneity corrections have been put forward.

In their original papers [[Hohenberg and Kohn] and [Kohn and Sham]], Hohenberg, Kohn and Sham suggested a gradient expansion of the exchange and correlation energy obtained from the gradient expansion of the energy as follows

$$E_{xc}^{GEA}[n(\vec{r})] = \int d\vec{r}\varepsilon[n]n(\vec{r}) + \int d\vec{r}\varepsilon_{xc}^{(2)}[n]|\nabla n|^2 + O(\nabla^3 n) \tag{2.20}$$

where $\varepsilon_{xc}^{(2)}$ is the exchange-correlation portion of the second term in the energy expansion in powers of the gradient of the density. The first term of this expansion is identical to what LDA gives for the exchange –correlation energy. With regard to the rest of the terms in the expansion, they yield results worse than the estimations made using LDA. As pointed out by Hohenberg and Kohn, there is no general proof that such an expansion *exists* for any given system and it can be verified only in few special cases [Hohenberg and Kohn]. Moreover, the gradient expansion approximation (GEA) violates some of the conditions the density of the exchange hole must satisfy [Perdew and Yue 1986]. Thus, the corrections made to the exchange-correlation energy through the gradient expansion of the energy are essentially unphysical; hence the aberrant results of this technique.

Perdew and co-workers [[Perdew and Yue 1986] and [Perdew *et al.* 1992]] solved this problem by introducing the general gradient approximation (GGA), which gives the following expression for the exchange-correlation energy

$$E_{xc}^{GGA}[n] = -\frac{3}{4}\left(\frac{3}{\pi}\right)^{1/3}\int d\vec{r}n^{4/3}F^{GGA}(s) \tag{2.21}$$

where

$$F^{GGA}(\bar{s}) = \frac{1}{9}\int_0^{z_c} z dz \frac{\int d\hat{\bar{R}}}{4\pi}\bar{y}\Theta(\bar{y}) \tag{2.22}$$

The quantity $\vec{s} = \nabla n(\vec{r})/\{2k_F n(\vec{r})\}$, $k_F = [3\pi^2 n(\vec{r})]^{1/3}$ is the Fermi wave vector and the parameter $z_c = 2k_F R_c$ is determined by the condition

$$\frac{-1}{12\pi}\int_0^{z_c} dz z^2 \int \frac{d\hat{\vec{R}}}{4\pi}\bar{y}\Theta(\bar{y}) = -1 \tag{2.23}$$

The angular integration in eq. (2.22) is performed analytically and then the integration over z is performed numerically. In eq. (2.22)-(2.23), Θ denotes the step function as usual and $\bar{y}$ is given by

$$\bar{y} = J + 4L\hat{\vec{R}}\cdot\vec{s}/3 - 16M(\hat{\vec{R}}\cdot\vec{s})^2/27 - 16Ns^2/3 \tag{2.24}$$

where

$$J = 72[4 + z^2 - (4 - z^2)\cos z - 4z\sin z]/z^6 \tag{2.25a}$$

$$L = 9(2 - 2\cos z - z\sin z)/z^3 \tag{2.25b}$$

$$M = 9(-z\cos z + \sin z)/(16z) \tag{2.25c}$$

$$N = 3[8 - (8 - 4z^2)\cos z - (8z - z^3)\sin z]/(16z^4) \tag{2.25d}$$

Compared to LDA, GGA yields better results as far as the binding energy is concerned. Even though, the commercially available simulation packages like VASP have both LDA and GGA options for computing the exchange-correlation term of the total energy, most researchers nowadays utilize the GGA method because of its higher accuracy. In the present work, all the calculations are performed using the GGA approach.

2.3 Review of VASP algorithm

2.3.1 Outline of the VASP algorithm

As shown in figure (1), the algorithm consists of two loops: an outer loop that assures the self-consistency of the charge density and an inner loop intended to improve the calculated wave functions. One begins with a set of trial functions $\{\psi_n, n=1, .., N_a\}$ and a reasonable input density n_{in}, which corresponds to the superposition of the atomic pseudo charge densities of the constituents. From the input charge density, the effective potential and the corresponding double counting corrections are evaluated. Subsequently, an iterative method, which forms the aforementioned inner loop, is utilized to improve the N_a trial wave functions. The new eigenenergies ε_n are then used to calculate new partial occupancies f_i and new Fermi energy. It is noteworthy that different orthogonalisation and diagonalisation techniques may be used before or after the iteration, if required. The total free energy A for the current iteration is evaluated as the sum of the band energies plus the contribution of the entropy and the double counting corrections. At this point, the input charge density is held fixed and the eigenvectors are iterated until they are converged.

In order to achieve the self-consistency necessitated by Kohn-Sham equations with regard to the initial charge density n_{in}, one imposes that the residual quantity R,

$$R = n_{out} - n_{in} \tag{2.26}$$

would be zero. The output charge density n_{out} is calculated using the newly obtained wave functions. At this point, a charge density mixing procedure is used and the new charge density serves as the input charge density for the next self-consistency or outer loop and similarly the final wave functions of the iteration are utilized as the new trial functions. This procedure is repeated until the self-consistency of the charge density is reached, i.e. until $n_{out} = n_{in}$. In the next subsections, we shall briefly discuss the different iterative techniques for the diagonalisation of the Kohn-Sham Hamiltonian and the various charge density mixing methods.

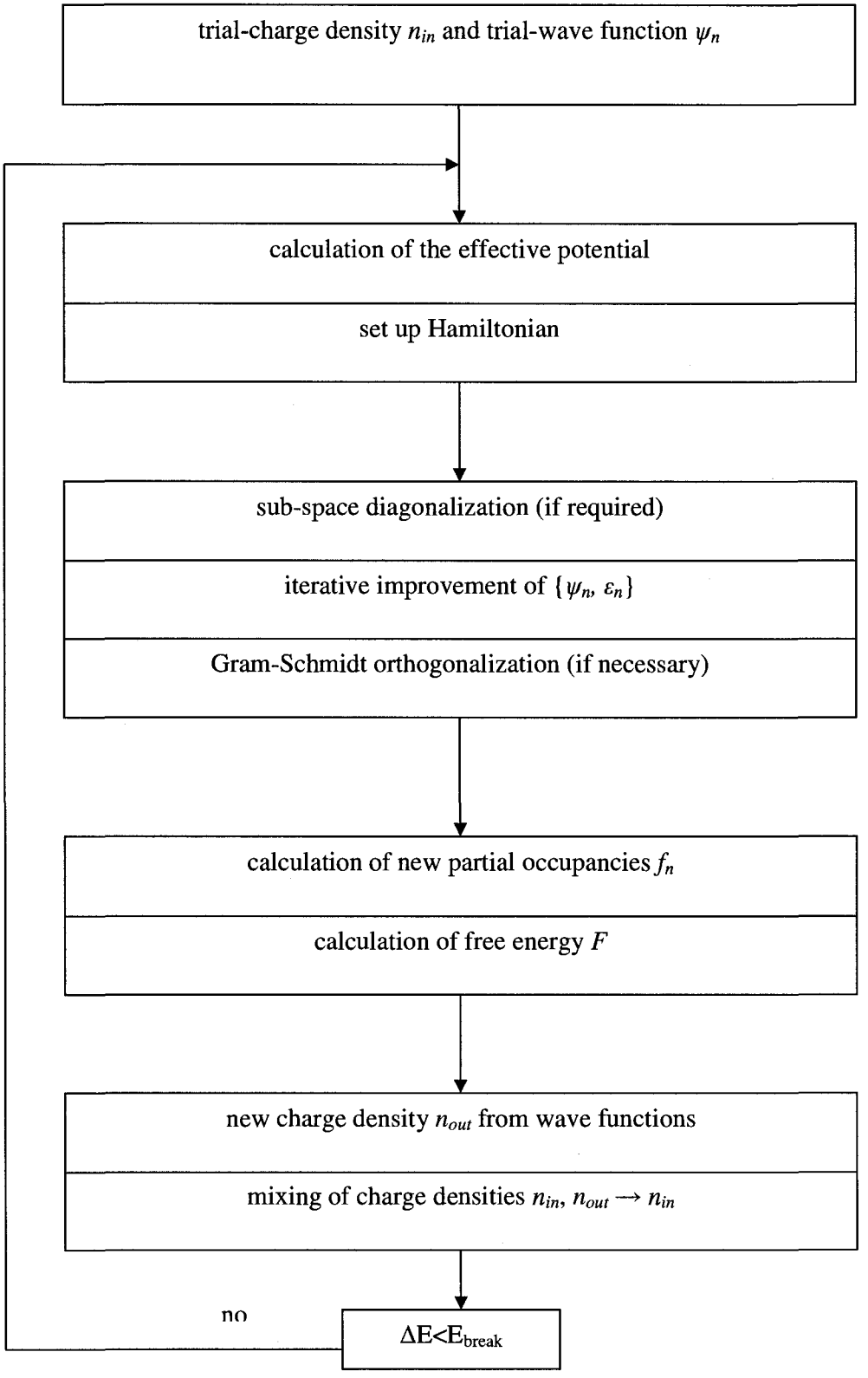

Figure 1: Outline of VASP algorithm taken from [Kresse *et al.* 1996a].

2.3.2 Iterative methods for the diagonalisation of the Kohn-Sham Hamiltonian

For the sake of clarity, it is convenient to state the mathematical problem at hand: we want to solve the generalized eigenvalue problem

$$H|\psi_n\rangle = \varepsilon_n S|\psi_n\rangle \tag{2.27}$$

where H is the Hamiltonian and, ε_n and $|\psi_n\rangle$ are the exact eigenvalues and eigenvectors for the n-th band, respectively. Notice that the only difference between eq. (2.27) and the usual formulation of the eigenvalue problems is the presence of the overlap operator or matrix S, which is also hermitian. The overlap matrix S accounts for the possible non-orthogonality of the basis vectors. In general, its elements can be evaluated as the scalar products of different basis vectors; however, if one uses pseudopotentials to set up the Hamiltonian, S will have a dependence on the projection states as well (see eq.2.51).

Mind that the solutions of eq. (2.27) have to meet the generalised orthonormality condition

$$\langle\psi_n|S|\psi_m\rangle = \delta_{nm} \tag{2.28}$$

All the iterative techniques discussed here start with an expansion set $\{|b_i\rangle, i = 1,..., N_a\}$to which one or several vectors are added at each iteration in order to obtain the best approximation to the exact eigenvalues and eigenvectors,

$$\varepsilon_n^{app}, |\varphi_n\rangle = \sum_m B_{mn}|b_m\rangle \tag{2.29}$$

As for the unblocked or sequential band by band methods, one starts with an expansion set containing only one vector, which should be a reasonable approximation to the exact eigenvector. In each iteration *i*, a single correction vector is added to the expansion set. In contrast, blocked methods optimize all bands or a set of them simultaneously. Thus, the size of the expansion set increases by N at each step.

In the case of both blocked and unblocked approaches, after the addition of the correction vector, the Rayleigh-Ritz (RR) technique is used to calculate a new best approximation of the eigenvalues and eigenvectors, which will serve as the initial expansion set for the next iteration. The RR scheme consists of solving the following eigenvalue problem

$$\sum_m \overline{H}_{lm} B_{mn} = \sum_m \varepsilon_n^{app} \overline{S}_{lm} B_{mn} \tag{2.30a}$$

where

$$\overline{H}_{lm} = \langle b_l | H | b_m \rangle \quad \text{and} \quad \overline{S}_{lm} = \langle b_l | S | b_m \rangle \tag{2.30b}$$

are the matrix elements of the Hamiltonian and the overlap matrix in the space spanned by the vectors of the expansion set. The transformations given in eq. (2.30b) are sometimes called subspace rotation. Mind that this space is actually a subspace of the Hilbert space over which $\boldsymbol{H}$ is defined; hence we are dealing with a diagonalisation problem that is simpler than one expressed in eq. (2.27)[2]. The m lowest eigenvalues and eigenvectors $\varepsilon_n^{app}, |\varphi_n\rangle$ constitute the approximation of the exact lowest m eigenvalues and eigenvectors within the subspace spanned by the extension set.

Before outlining specific methods, let's introduce the Rayleigh quotient, which is the expectation value

$$\varepsilon_n^{app} = \frac{\langle \varphi_n | H | \varphi_n \rangle}{\langle \varphi_n | S | \varphi_n \rangle} \tag{2.31}$$

If $\langle \varphi_n | S | \varphi_n \rangle = 1$, variation of this expectation value with respect to $\langle \varphi_n |$ gives the residual vector,

[2] In the case of small systems, the original eigenvalue problem given by eq. (2.27) can be solved using straightforward diagonalisation methods such as Choleski-Householder procedure. In the case of large systems, direct diagonalisation does not work; hence the necessity of transforming the problem to a simpler one.

$$|R(\varphi_n)\rangle = (H - \varepsilon_n^{app} S)|\varphi_n\rangle \tag{2.32}$$

whose product with the preconditioning matrix K estimates the error on the approximate eigenvector.

$$|\delta\varphi\rangle = K\,|R\rangle \tag{2.33}$$

and

$$|\psi_n\rangle = |\varphi_n\rangle + |\delta\varphi_n\rangle \tag{2.34}$$

The error calculation expressed in eq. (2.33) is called preconditioning. As for the preconditioning matrix K, it is normally constructed from the diagonal elements of the resolvent of the Hamiltonian. However, its explicit form slightly differs from one algorithm to another. For more details on the preconditioning process and the preconditioning matrix, the interested reader should consult reference [Kresse *et al.* 1996a] and the references therein.

The different iterative diagonalisation algorithms included in VASP are:

- *Blocked Davidson scheme (DAV2)*: In each step, the expansion set increases by N_b- where N_b is the number of bands included in the calculation. In each iteration i, the RR method is used to find lowest eigenvalue/eigenvector pairs from which the residual vectors are evaluated. These newly obtained residual vectors are then preconditioned as prescribed by eq. (2.33) and added to the expansion set. In the case of large systems, the storage of all the initial and residual vectors of different bands is memory consuming; as a result, the i should be restricted to small numbers.
- *Conjugate gradient minimisation (CG)*: In this sequential algorithm, the Rayleigh quotient (eq. 2.31) is optimised for each band by means of a conjugate gradient vector. At the outset, using Lagrange multipliers and the orthonormality condition $\langle\varphi_n|S|\varphi_n\rangle = 1$,one builds the following gradient vector for a specific band m and an initial expansion set

$$|g_m\rangle = \left(1 - \sum_n |\varphi_n\rangle\langle\varphi_n|S\right) H|\varphi_m\rangle \tag{2.35}$$

The conjugate gradient vector $|f_m^i\rangle$ of $|g_m\rangle$ for the *i*-th iteration is then given by

$$|f_m^i\rangle = |p_m^i\rangle + \frac{\langle p_m^i | g_m^i\rangle}{\langle p_m^{i-1} | g_m^{i-1}\rangle} |f_m^{i-1}\rangle \tag{2.36}$$

where $|p_m^i\rangle$ are the preconditioned gradients for the *i*-th step. In each step, the optimum new eigenvector $|\varphi_m^{i+1}\rangle$ is obtained by applying the RR scheme to the set $\{|\varphi_m^i\rangle, |f_m^i\rangle\}$. The new vector is added to the expansion set and the process is repeated until convergence is attained. The *CG* algorithm is quite stable and efficient, but it becomes memory and time consuming in the case of large-size systems. This is due to the fact that at each single band update, each vector must be orthonormalised to all the previous bands.

- *Residual minimisation method-direct inversion in the iterative subspace (RMM-DIIS)*: As discussed above, the main drawback of CG algorithm is the necessity of an explicit orthonormalisation of the preconditioned residual vector for each single band update. This problem has been solved in the RMM-DIIS approach by minimising the norm of the residual vector. At the end, the Gram-Schmidt technique[3] is used to guarantee the orthonormality of the new vectors.

These algorithms are included in the VASP code. Depending on the size of the system, one of them is selected for the diagonalisation of the Kohn-Sham Hamiltonian. A detailed treatment of these algorithms can be found in references [[Kresse *et al.* 1996a] and [Kresse *et al.* 1996b]].

[3] The Gram-Schmidt orthonormalisation procedure is explained in linear algebra textbooks, see for example reference [Nicholson].

2.3.3 Charge density mixing

The charge density mixing forms the outer loop in the main algorithm of VASP and constitutes its second key step. The goal is to attain self-consistency with respect to the input charge density. Mathematically, this means that the norm of the charge density residual R (see eq. 2.26)

$$\langle R[n_{in}] | R[n_{in}] \rangle \tag{2.37}$$

should be zero.

There exist several methods to achieve the aforementioned objective:

- *Simple mixing*: The new charge density is a linear function of R in this approach. At each step, the new charge density is calculated as the sum of the previous charge density and a certain amount of R. In this method, as in the iterative diagonalisation techniques, one can use a preconditioning matrix and add the preconditioned residual vector to the current charge density.
- *Pulay mixing*: In this approach the new optimal charge density is taken to be a linear combination of all previous charge densities. Assuming that the residual vector behaves linearly, that the new charge density must minimise the norm of R and that the sum of the coefficients used in the linear combination of the previous charge densities equals one, a series of equations for these coefficients can be found. These coefficients are then used to calculate the new charge density.
- *Broyden mixing*: In this approach, the inverse Jacobian of the residual vector is calculated and its product with R is added to the current charge density to obtain the new one. At each iteration, the inverse Jacobian is updated.

For more details on these techniques, consult reference [Kresse *et al.* 1996a] and the references therein.

2.3.4 Partial occupancies and Brillouin zone integration

The band occupancies are indicated by the partial occupancy f_i. For the i-th band f_i=1 if the band is occupied and f_i=0 if the band is empty. The partial occupancies are introduced to reduce the number of k-points, which are necessary in evaluating the band structure energy, in the first Brillouin zone (BZ), the Wigner-seitz unit cell in the reciprocal lattice.

At zero temperature, the band structure energy is given by

$$\sum_n \frac{1}{\Omega_{BZ}} \int_{\Omega_{BZ}} \varepsilon_{n,k} \Theta(\varepsilon_{n,k} - \mu) d^3k \tag{2.38}$$

where the summation is performed over all the bands and, Ω_{BZ} and μ denote the volume of the first Brillouin zone and the Fermi energy, respectively. For completely filled bands as in insulators and semiconductors, the integral in eq.(2.38) can be calculated accurately using a set of Monkhorst pack special k-points [MacDonald], which in the present work is always a set of Pack 8×8×8 k-points. Mind that in the aforementioned numerical technique the integral is replaced by a sum over the k-points. In the case of metallic systems, due to the discontinuous jumps from 0 to 1 at the Fermi level, the convergence of the sum is extremely slow. In order to enhance the speed of the calculation, the step function is replaced by a smoother function that allows f_i to vary continuously between 0 and 1. The Fermi-Dirac (eq. (2.39a)) distribution and the error function (eq.(2.39b)) are such functions.

$$f\left(\frac{\varepsilon-\mu}{\sigma}\right) = \frac{1}{\exp((\varepsilon-\mu)/\sigma)+1} \tag{2.39a}$$

$$f\left(\frac{\varepsilon-\mu}{\sigma}\right) = \frac{1}{2}\left(1-erf\left[\frac{\varepsilon-\mu}{\sigma}\right]\right) \tag{2.39b}$$

2.4 Pseudopotential approaches and the projector augmented waves (PAW) method

As the closed-shell core electrons of solids tend not to respond to low-energy perturbations, which are responsible for a large number of physical phenomena such as elastic and transport properties, it rapidly became evident that simplification of the electronic structure can safely be introduced. The underlying idea of this simplification is that one can separate the electron-ion potential in the solid in two distinct regions: (i) the *core region*, defined by the cut-off radius r_c, where the core states electrons are tightly bound together, and (ii) the *interionic region* occupied by the valence electrons. Thus, instead of the all-electron effective potential Φ, one uses a pseudopotential V that eliminates the need to include the core states, nodal structure of valence electrons and the strong potentials responsible for binding them. Mind that the pseudo-wave functions χ_i obtained from Kohn-Sham Hamiltonians with pseudopotentials are linear combinations of the all-electron wave-functions ψ_i. This implies that one can easily recover the true wave-functions simply by orthogonalizing the solutions χ_i to the core states [Zunger and Cohen 1978].

In the specific case of *norm-conserving pseudopotentials*, one explicitly requires that V fulfils the following conditions [Hamann *et al.*]:

(i) The real and pseudo valence eigenvalues agree for a given atomic configuration (e.g. atomic ground state);

(ii) The real and pseudo wave functions agree beyond the cut-off radius r_c;

(iii) The integrals from 0 to r of the real and pseudo charge densities agree for $r > r_c$ for each valence state (the norm conservation criterion);

(iv) The logarithmic derivatives of the real and pseudo wave functions and their first energy derivatives agree for $r > r_c$, that is

$$\frac{d}{d\varepsilon_i}\frac{d}{dr}\ln \chi_i\Big|_{r>r_c} = \frac{d}{d\varepsilon}\frac{d}{dr}\ln \psi_i\Big|_{r>r_c} \tag{2.40}$$

The first two conditions are simply the mathematical formulation of the simplification that led to the development of the concept of pseudo potential as discussed at the beginning of this section. The norm conservation criterion assures that the electrostatic potential produced outside r_c is identical for the real and pseudo charge distributions, whilst the fourth property guarantees that the scattering properties of the real ion cores are reproduced with minimum error. Notice that the conditions (iii) and (iv) together guarantee that the pseudo-charge contained in the sphere of radius r_c is identical to the real charge in that sphere and they can be mathematically expressed in terms of the following relation

$$-\psi_i^2 \frac{d}{d\varepsilon_i} \frac{d}{dr} \ln \chi_i \Big|_{r=r_c} = \int_o^{r_c} |\psi_i|^2 \, dr \tag{2.41}$$

As a result, Kerker suggested a new *fourth* criterion to be met by the pseudo wave functions, which consists of matching the first and second derivatives of the real and pseudo wave functions at the cut-off radius [Kerker].

The norm conserving pseudo potentials are successful at resolving the major difficulties encountered by the early pseudopotentials estimated based only on the first two aforementioned conditions. These difficulties essentially include the hard-core or the strong repulsive character of the pseudo potential at origin and discrepancies between the normalization factors of the real and pseudo wave functions in the regions where they have to agree (i.e. outside the core region). Nevertheless, the norm conserving pseudo potentials suffer from other shortcomings. These potentials are of limited utility when one treats systems with highly localized valence orbitals (e.g. transition-metal atoms) because of the difficulty of expressing the pseudo wave functions in a plane wave basis set. Two approaches have been put forth to deal with this difficulty, namely the ultrasoft[4] (US) pseudopotential approach and the projector augmented-wave (PAW) method. It has been shown that these techniques are mathematically equivalent in the sense that the US pseudopotential Hamiltonian can be derived from the corresponding PAW total energy

[4] The ultrasoft pseudopotentials are called thus, because they attain much smoother ("softer") wave functions.

functional through the linearization of some terms in the PAW Hamiltonian. The equivalence of these two approaches is discussed in details in reference [Kresse et al. 1999]; here we shall briefly outline them.

The US pseudopotentials, originally developed by Vanderbilt [Vanderbilt], are constructed by relaxing the norm conservation constraint and distinguishing the local (loc) and non local (NL) contributions to the Hamiltonian

$$H = T_0 + V_{loc} + V_{NL} \tag{2.42}$$

In order to account for the charge deficit caused by the relaxation of norm conservation constraint, for a large enough diagnostic radius R at and beyond which all real and pseudo quantities should agree, the generalised norm conservation criterion

$$Q_{ij} = 0 \tag{2.43}$$

where

$$Q_{ij} = \langle \psi_i | \psi_j \rangle_R - \langle \chi_i | \chi_j \rangle_R \tag{2.44}$$

is introduced. Notice that US pseudopotentials also require the cut-off radii r_c and r_c^{loc}. To set up the non local part of the potential, one needs to construct a set of localized projection states $\{|\beta_i\rangle\}$ defined as

$$|\beta_i\rangle = \sum_j (B^{-1})_{ji} |\eta_j\rangle \tag{2.45}$$

where

$$|\eta_i\rangle = (\varepsilon_i - T_0 - V_{loc}) |\chi_i\rangle \tag{2.46}$$

and

$$B_{ij} = \langle \chi_i | \eta_j \rangle \tag{2.47}$$

If one works within the formalism of generalised eigenvalue problems discussed in section 2.3.2, the generalised norm conserving constraint (eq. (2.43)) becomes completely unnecessary [Vanderbilt]. The non local part of the potential simply becomes

$$V_{NL} = \sum_{i,j} D_{ij} |\beta_i\rangle\langle\beta_j| \tag{2.48}$$

where

$$D_{ij} = B_{ij} + \varepsilon_j Q_{ij} \tag{2.49}$$

are the strength of the non local potential. In this case, instead of the norm conservation constraint, the pseudo wave functions have to satisfy the weaker condition

$$\langle\chi_i|S|\chi_j\rangle_R = \langle\psi_i|\psi_j\rangle_R \tag{2.50}$$

where

$$S = 1 + \sum_{i,j} Q_{ij} |\beta_i\rangle\langle\beta_j| \tag{2.51}$$

With these definitions and weaker constraints, one can easily verify [Vanderbilt] that the pseudo wave functions are solutions to eq. (2.27) with the overlap matrix defined as in eq. (2.51), and that their radial parts satisfy equations similar to eq. (2.41).

In the PAW approach elaborated by Blöchl, instead of approximating the potentials as such, one estimates the wave functions by pseudowaves subjected to the condition that they should match the real wave functions beyond some cut-off radius [Blöchl]. Thus, one starts with finding all-electron partial waves ς_i for a reference atom. Subsequently, the pseudo partial waves $\tilde{\varsigma}_i$ are calculated such that they are equivalent to the real partial waves outside the cut-off radius. Then, the real and pseudo wave functions can be related to each other through a linear transformation involving the real and pseudo partial waves

$$|\psi_k\rangle = |\chi_k\rangle + \sum_m \left(|\varsigma_m\rangle - |\tilde{\varsigma}_m\rangle\right)\langle\tilde{p}_m|\chi_k\rangle \tag{2.52}$$

where $\tilde{p}_i$ are projector functions that are dual[5] to the partial waves

$$\left\langle \tilde{p}_i \middle| \tilde{\varsigma}_j \right\rangle = \delta_{ij} \tag{2.53}$$

This transformation is then applied to the Kohn-Sham energy functional in order to express the total energy in terms of the pseudo wave functions and the projectors, which are easier to treat. Thus the PAW method directly deals with the all-electron potentials and requires only one cut-off radius, whereas the ultrasoft pseudopotential approach calls for several cut-off radii and therefore a large number of tests have to be carried out in order to obtain accurate pseudopotentials with high transferability to the all-electron potentials. In general, the results estimated by means of the PAW method are as accurate as relaxed core all-electron calculations, implying that all the approximations of the PAW method are well under control [Kresse *et al.* 1999]. In the present work, all the calculations are performed using the PAW technique.

2.5 Forces

The forces acting on the ions are related to the spatial derivatives of the total energy functional. One can naively differentiate the energy expectation value to obtain an expression for the forces along the direction j in the state $|\psi_i\rangle$

$$F_j = -\frac{\partial E}{\partial r_j} = -\langle \psi_i | \frac{\partial H}{\partial r_j} | \psi_i \rangle - \left\langle \frac{\partial \psi_i}{\partial r_j} \middle| H | \psi_i \right\rangle - \left\langle \psi_i | H \middle| \frac{\partial \psi_i}{\partial r_j} \right\rangle \tag{2.54}$$

The first term in eq. (2.54) is the Feynman-Hellmann force and the last two terms correspond to Pulay contributions [Pulay]. In the VASP code, the forces are calculated by taking the spatial derivatives of the generalised free energy A of the system, which is the

[5] A brief discussion on dual or biorthonormal basis sets can be found in section 5.2.1.

Kohn-Sham total energy functional plus the entropy contributions $S(f_n)$ for each band and for a given temperature T

$$A = E - \sum_n k_B TS\ (f_n) \tag{2.55}$$

where k_B is the Boltzmann constant.

This approach takes into account the Pulay effects. Mind that in the case of US pseudopotentials, there are no Pulay effects [Kresse et al. 1996a]. A detailed treatment of the Feynman-Hellmann forces can be found in references [[Feynman] and [Marchildon]].

Chapter III
Elastic Properties
of Covalent Systems

[This chapter is adapted from the paper *b* accepted by *Physical Review B*, see appendix G]

As discussed in chapter I, the results of the *ab initio* calculations often need to be rationalised in terms of microscopic features of solids and the nature of their bonding. This situation has given rise to the necessity of elaborating analytical and semi-empirical approaches, no matter how simple they might be. In this chapter, one such method is proposed to shed light on the atomic-scale parameters governing the elastic moduli of covalently bonded crystals. More specifically, we shall outline Philips' description of covalent bond and shall exploit it in order to determine the predominant causes of the brittleness of covalent systems. In addition, a quick review of the previous works in this field will be presented, since some partial results from these early studies will be used in assessing the bulk and shear moduli of the materials examined in this part of the thesis.

3.1 Elastic moduli

The elastic moduli are indicative of the strength of materials under various sorts of deformation. They are formally defined as the derivative of stress with respect to the appropriate strain and hence they are all related to the second derivatives of energy with

respect to different deformation parameters. In the present work, we shall focus on isothermal bulk modulus, which describes the tendency of an object's volume (Ω) to deform under expansion or compression, and shear modulus, which portrays the ease with which an object suffers deformation according to a given slip system with constant volume. Bulk modulus B and shear modulus G are mathematically expressed as [[Kittle] and [Roundy *et al.* 1999]]

$$B = \Omega \frac{\partial^2 E}{\partial \Omega^2} \tag{3.1}$$

$$G = \frac{1}{\Omega} \frac{\partial^2 E}{\partial \gamma^2}\Big|_{\gamma=\gamma_0} \tag{3.2}$$

where γ is the dimensionless shear parameter and γ_0 refers to the spatial equilibrium state of the crystal.

The elastic moduli, that signify the average elastic properties of materials, are also related to the stiffness constants C_{ij} (see appendix D). In the specific case of the cubic structure, to which all the materials examined in the present work belong, these relationships are quite simple

$$B = \frac{C_{11} + 2C_{12}}{3} \tag{3.3}$$

$$G = \frac{C_{11} - C_{12} + 3C_{44}}{5} \tag{3.4}$$

Due to Pugh, the G/B ratio is used as an indicator of the ductility of materials. He suggested that the resistance to plastic deformation is related to the product $G\vec{b}$, where $\vec{b}$ is the Burgers vector (see section 4.1) and that the fracture strength is proportional to the product Ba, where a corresponds to the lattice parameter [Pugh]. If $G\vec{b}/Ba$ is high for a given material, it will behave in a brittle manner. Consequently, the $G\vec{b}/Ba$ reflects the competition between the shear and cohesive strengths at the crack tip of fracture. As $\vec{b}$

and a are constants for specific materials, the $G\vec{b}/B$a can be simplified into G/B. This formula was recently exploited in the study of brittle versus ductile transition in intermetallic compounds from first-principles calculations [[Chen *et al.* 2003] and [Chen *et al.* 2004]].

3.2 Covalent systems

The basic idea underlying the concept of covalent bonds, which is the sharing of pairs of electrons between the atoms involved in the bonding, was first formulated in G. N. Lewis' theory of the cubical atom using the now well known (Lewis') dot notation [Lewis]. Three years later, in 1919, I. Langmuir published his octet theory, an extension of Lewis' approach, and coined the word covalence, which he defined as the number of electron pairs shared between two neighbouring atoms [Langmuir]. This is the description of covalent systems nowadays taught in all high schools, which we shall investigate in the next chapter in more depth and particularly in relationship with metallic bonds. However, in this section, the covalent bond in crystals will be portrayed according to the line of thought favoured by Phillips, in which the energy band gap is regarded as the characteristic feature of this kind of bonding.

3.2.1 Structure of diamond-like and sphalerite crystals

Phillips' method deals with tetrahedrally bounded crystals, which include the diamond-like, zincblende, wurtzite and rocksalt structures. In the present work, only diamond-like and sphalerite crystals are dealt with. There are two atoms in the primitive unit cells of either of these two structures and their conventional unit cells, as shown in figures 2-3, is an FCC based structure augmented with four atoms along the body diagonals.

In these structures, each atom has four first nearest neighbours (FNN). In other words, the crystals are of the form A_4B or AB_4, and therefore, effects occurring beyond the FNN range are negligible.

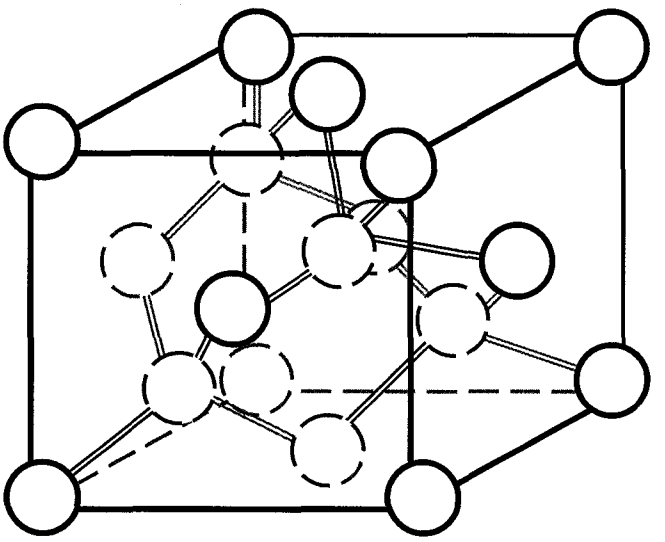

Fig. 2: the structure of monatomic diamond-like crystals.

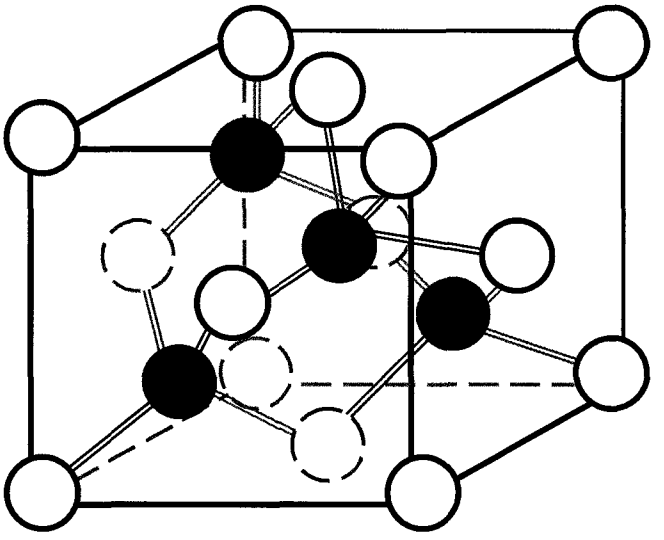

Fig. 3: The structure of sphalerite or zinc-blende crystals. In the particular case of ZnS, the Zn atoms (coloured white) are placed on the faces of the lattice; while, the S atoms (coloured blue and blue gray) are situated along the body diagonals.

3.2.2 Overview of band structure

The electron wave functions ψ_n in a crystal can be approximated by the single-particle Schrödinger equation (see eq. (2.15)) with a potential V that is periodic under symmetry transformations induced by the lattice translation vector $\vec{T}$.

$$V(\vec{r}) = V(\vec{r} + \vec{T}) \tag{3.5}$$

In one dimension, the Schrödinger equation in question reads

$$-\frac{1}{2}\frac{d^2\psi_n}{dx^2} + (V - E_n)\psi_n = 0 \tag{3.6}$$

where the eigenfunctions ψ_n have to satisfy periodic boundary conditions. The solutions to eq. (3.6) are the well known Bloch functions [[Bloch] and [Kramers]],

$$\psi_n(\vec{r}) = u_k(\vec{r})e^{i\vec{k}\cdot\vec{r}} \tag{3.7}$$

where $\vec{k}$ refers to the wave vector and the functions $u_k(\vec{r})$ are periodic,

$$u_k(\vec{r}) = u_k(\vec{r} + \vec{T}) \tag{3.8}$$

The eigenvalues of eq. (3.6) are the so-called energy bands

$$E = E_{n,k}, n = 0,1,2,.. \tag{3.9}$$

The allowed ranges of E are separated by forbidden energy zones, in which the solutions of eq. (3.6) are of the form (3.7) but with purely imaginary wave vectors [Kohn 1959]. In the case of metallic systems, the valence band, which is the last occupied band, is only partially filled and hence their transport properties are not affected by the energy

gap disconnecting the valence band from the conduction band or the first empty band. To the contrary, in semiconductors and insulators, which form the covalent systems, the valence band is completely occupied; as a result, the band gap energy E_g becomes an important parameter in these systems.

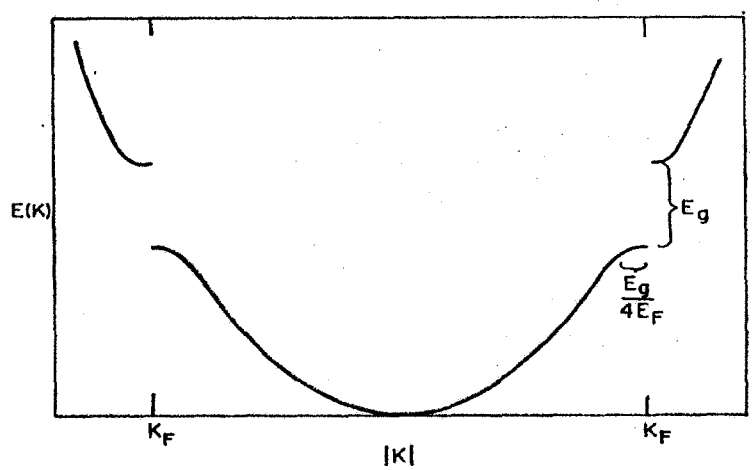

Fig. 4: energy as a function of wave number for semiconductors. From reference [Penn].

In figure 4, the behaviour of the energy of the valence and conduction bands as a function of wave number $|k|$ for semiconductors is displayed. Notice that k_F and E_F refer to Fermi wave number and Fermi energy, respectively. As can be seen, the energy exhibits a discontinuity between the valence band, also called the bonding region, and the higher empty bands which are usually referred to as antibonding region.

As shown by Penn, the band gap energy intervenes in the calculation of the dielectric function $\varepsilon_s(\vec{q})$ in the covalently bonded materials [Penn]. Later, Philips used Penn's dielectric function to set up a pseudopotential form factor $v_s(\vec{q})$ for isotropic covalent atoms

$$v_s(\vec{q}) = \frac{v_i(\vec{q})}{\varepsilon(\vec{q})} \tag{3.10}$$

where $v_i(\vec{q})$ is the free ion pseudopotential and the dielectric function $\varepsilon_s(\vec{q})$ accounts for the screening effects produced by the electrons. Using eq. (3.10) as the characteristic form factor for covalent systems, be they semiconductors or insulators, Philips showed that the energy of the valence electrons in the region corresponding to the overlap of the basis functions of the respective ions involved in the bond is of the form

$$E_h + C \tag{3.11}$$

where E_h corresponds to the purely covalent or homopolar energy contributions and C reflects a charge transfer from the atom to the bonds [Philips 1968b]. To this term other correction terms are added to obtain the total valence energy, for more details see references [[Philips 1968a]-[Philips 1968d]]. In the next subsection, the relation between the homopolar and heteropolar energies and the band gap energy will be examined.

3.2.3 The band gap energy Eg

Recall that the crystal structures studied here all have two atoms per unit cell; hence, it is convenient to chose the origin of the coordinate system half way between the atoms A and B bounded together in the primitive cell. The atomic orbitals associated with these atoms are labelled φ_A and φ_B. Moreover, as mentioned previously, the crystal potential is periodic. This implies that it can be written as a Fourier series

$$V(\vec{r}) = \sum_g V_g e^{i\vec{g}\cdot\vec{r}} \tag{3.12}$$

where $\vec{g}$ is a vector of the reciprocal lattice. In order to avoid the difficulties arising from the possible isoelectric nature of the electronic cores of atoms A and B, it is assumed that the coefficients V_g are estimated by the pseudopotentials $V_A(\vec{r})$ and $V_B(\vec{r})$ associated with atoms A and B, respectively.

$$V_g = V_A(\vec{g})e^{i\vec{g}\cdot\vec{r}_A} + V_B(\vec{g})e^{-i\vec{g}\cdot\vec{r}_B} \tag{3.13}$$

where $\vec{r}_A$ corresponds to the radius of atom A along the bond direction. After some algebra, eq. (3.13) can be expressed as follows [Philips 1970]

$$V_g = \{[V_A(\vec{g}) + V_B(\vec{g})]\cos\vec{g}\cdot\vec{\tau} + i[V_A(\vec{g}) - V_B(\vec{g})]\sin\vec{g}\cdot\vec{\tau}\}e^{i\vec{g}\frac{\vec{r}_A+\vec{r}_B}{2}} \tag{3.14}$$

where

$$2\vec{\tau} = \vec{r}_A - \vec{r}_B \tag{3.15}$$

In the limiting case where $V_A = 0 = V_B$, the bonding state, corresponding to a symmetric linear combination of φ_A and φ_B and the antibonding state, resulting from an antisymmetric linear combination of φ_A and φ_B, will have the same energies, which are set at zero for convenience. As discussed in the preceding subsection, in the Hamiltonian describing the valence bond, the matrix elements related to the overlap energies gained as a result of the formation of the crystal can be written as

$$\frac{1}{2}(E_h + iC) \tag{3.16}$$

Thus, the following Hamiltonian can be constructed for the valence band

$$\begin{pmatrix} 0 & \frac{1}{2}(E_h + iC) \\ \frac{1}{2}(E_h - iC) & 0 \end{pmatrix} \tag{3.17}$$

where the elements along the diagonal correspond to the pure bonding (*bon.*) and antibonding (*antb.*) states and the off diagonal terms describe the overlap effects. The eigenvalues of this Hamiltonian are the bonding and antibonding energies

$$E_{antb} = \frac{1}{2}\sqrt{\left(E_h^2 + C^2\right)} \tag{3.18a}$$

$$E_{bon} = -\frac{1}{2}\sqrt{\left(E_h^2 + C^2\right)} \tag{3.18b}$$

As the difference between these energies gives the band gap energy, from eq. (3.18a-b), it follows that

$$E_g^2 = E_h^2 + C^2 \tag{3.19}$$

Mind that the homopolar contribution E_h originates from the real part of V_g (see eq. (3.14)), while the ionic or heteropolar portion of the energy arises from the imaginary term in eq. (3.14) [Philips 1970]. Moreover, in the case of purely covalent materials like diamond and silicon (Si) whose bond formation process does not involve any charge transfer, the band gap energy is equal to the homopolar energy E_h. Assuming that E_h is an entire function of some power of the bond length d, which is simply the distance between the first nearest neighbours, Philips used the band gap energies of diamond and Si to scale E_h.

$$E_h = \frac{39.74}{d^{2.5}} \tag{3.20}$$

In eq. (3.20), the units of E_h are electron volts and d is in angstroms. Notice that the main motivation behind the assumption leading to eq. (3.20) is that the gap energy has to describe solely the strength of the valence band and hence, the peripheral effects created by the core electrons should be excluded from the band gap calculation. In this regard, the aforementioned postulation constitutes the easiest way of fulfilling this requirement.

As for C, based on the spectroscopic values available for this parameter, it can be expressed by the following formula

$$C = bq^2\left[\frac{Z_A}{r_A} - \frac{Z_B}{r_B}\right]e^{-k_s r_o} \tag{3.21}$$

where q is the elementary charge, b is a correction parameter,

$$k_s = \sqrt{\frac{4k_F}{\pi a_B}} \tag{3.22}$$

and

$$r_0 = \frac{1}{2}(r_A + r_B) = \frac{d}{2} \tag{3.23}$$

Mind that in eq. (3.22), a_B is the Bohr radius.

3.2.4 Ionicity fraction f_i

The ionicity fraction $f_i(A,B)$ is a measure of the ionic character of an AB bond. This notion was first introduce by Pauling in relationship with his concept of electronegativity. Since then, numerous definitions for ionicity have been proposed, including Pauling's. All these definitions meet the following intuitive conditions

$$f_i(A,B) = f_i(B,A) \tag{3.24}$$

and

$$0 \le f_i(AB) \le 1 \tag{3.25}$$

Notice that eq. (3.19) suggests that E_h and C can be regarded as Cartesian coordinates and hence, one can construct more symmetric polar coordinates whose radial part corresponds to the band gap energy E_g as displayed in figure 5.

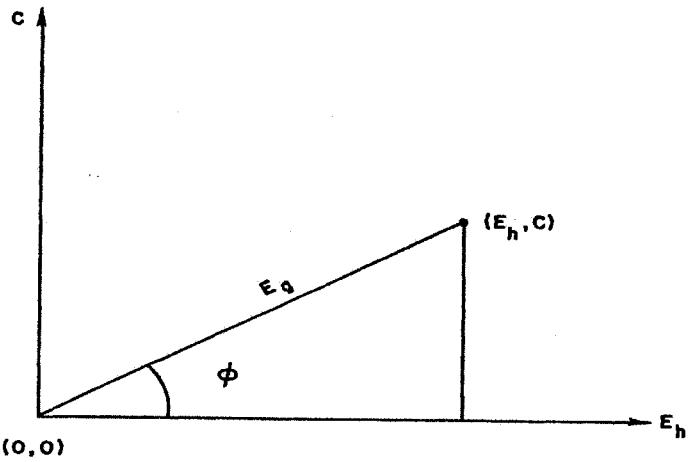

Fig. 5: a sketch showing the polar coordinates (E_g, ϕ) corresponding to the Cartesian coordinates (E_h, C).

The angle ϕ, which Philips calls the ionic phase angle, is given by

$$\tan \phi = C / E_h \tag{3.26}$$

These polar coordinates (E_g, ϕ) correspond to the Cartesian coordinates (E_h, C). This observation led Philips [Philips 1970] to suggest the following definition for the ionicity f_i

$$f_i = \sin^2 \phi = \frac{C^2}{E_g^2} \tag{3.27}$$

Using eq. (3.19) for a second time, eq. (3.27) can be rewritten as

$$f_i = 1 - \frac{E_h^2}{E_g^2} \tag{3.28}$$

This definition of ionicity clearly satisfies the conditions (3.24) and (3.25). Furthermore, as expected, it vanishes when there is no charge transfer, i.e. when $C = 0$. Expression (3.28) is more helpful for practical purposes, since it allows the estimation of the ionic character of the bond in terms of relatively easily measurable quantities, namely the bond length and the band gap energy. Additionally, as discussed in reference [Martin], the elastic moduli and constants have a rather linear dependence on Philips' ionicity

In a very similar fashion, one can also define the covalent fraction f_c

$$f_c = \cos^2 \phi = E_h^2 / E_g^2 \tag{3.29}$$

3.3 Overview of previous investigations

A survey of a number of covalent materials such as Ge, GaAs and ZnSe led M. L. Cohen to conclude that the homopolar energy E_h is the predominant energy parameter in covalent systems [Cohen 1985]. The aforementioned substances all have approximately the same lattice constant, and hence the same bond length. This entails that d is almost independent of C. The implication of this observation for bulk modulus and other elastic moduli like shear modulus is that they essentially depend on the purely covalent portion of band gap energy. This phenomenological conclusion can be rationalized by noticing that the core electrons are usually unaffected by small strains, which typify the elastic regime. As a result, one can only take into account the energy changes of the valence electrons, which are fully involved in the deformation process. Moreover, relationships connecting inherent traits of covalent crystals such as the thermal activation energies [Siethoff] and hardness [Gao *et al.*] to the homopolar band gap energy were recently elaborated. These works further confirm that the intrinsic properties of covalent materials are predominantly dictated by E_h.

Based on these considerations, eq. (3.20) allows us to estimate the second derivative of the energy as

$$\frac{\partial^2 E}{\partial \gamma^2} \propto \frac{1}{d^{4.5}} \tag{3.30}$$

where the deformation parameter γ is linearly related to the bond length d and its equilibrium value d_0 through the equation $d = d_0(1 \pm \gamma)$. The estimation given by eq. (3.30) was later justified by P. K. Lam and collaborators in more details [[Lam *et al.* 1984] and [Lam *et al.* 1987]].

The charge volume of covalent materials usually assumes a cylindrical shape along the bonding direction and hence linearly varies with the bond length d. M. L. Cohen has estimated this volume as [Cohen 1985]

$$\Omega \approx \pi (2a_B)^2 d \tag{3.31}$$

Combining eq. (3.1), (3.30) and (3.31), Cohen found the following explicit expression for bulk modulus [Cohen 1993]

$$B = \frac{N_c}{4} \frac{(1972 - 220\lambda)}{d^{3.5}} \tag{3.32}$$

where N_c is the bulk coordination number, B is in GPa and λ is an empirical ionicity parameter that takes the values 0, 1 and 2 for the IV, III-V and II-VI group semiconductors, respectively. Mind that N_c =4 in the case of crystals studied in the present work and that Cohen's ionicity parameter is an *ad hoc* adjustable empirical factor that does not satisfies eq. (3.25). In the next section, we shall set formulae for both bulk modulus and shear modulus using the results discussed in this section and the previous parts of this chapter.

3.4 Elastic moduli of covalent crystals

At this point, we are prepared to estimate both bulk modulus and shear modulus in atomistic terms. Based on eq. (3.1), (3.2), (3.30) and (3.31) and the fact that B and G are linear functions of ionicity, these elastic moduli are expected to exhibit the following explicit dependences on d and f_i:

$$G_j = \frac{\alpha_j - \beta_j f_i}{d^{5.5}} \tag{3.33}$$

$$B = \frac{\delta - \eta f_i}{d^{3.5}} \tag{3.34}$$

where α_j, β_j, δ and η are constants, and the subscript j refers to the two covalent crystal groups discussed below. These constants can be extrapolated from a selection of experimental data of covalent materials. The resulting expressions are:

$$G_a = \frac{5954.02 - 4538.404 f_i}{d^{5.5}} \tag{3.35a}$$

$$G_b = \frac{9058.22 - 6905.865 f_i}{d^{5.5}} \tag{3.35b}$$

$$B = \frac{1938.72 - 506.702 f_i}{d^{3.5}} \tag{3.36}$$

In eq. (3.35)-(3.36), all the elastic constants are in GPa and d is in angstroms as usual. Sixteen data selected from the twenty three experimental measurements in table 1 were used to interpolate coefficients α_j and β_j in eqs. (3.35a-b), and the linear fitting curves together with selected data are shown in fig.6. In the case of bulk modulus B, nine experimental data plotted in fig.7 were employed to determine constants δ and η in eq. (3.36).

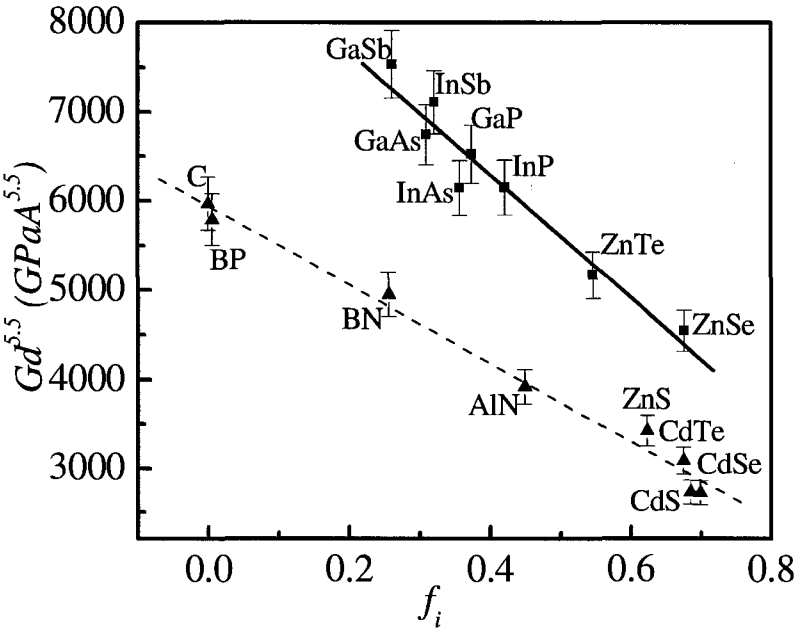

Figure 6: $Gd^{5.5}$ as a function of ionicity fraction f_i; the dash and solid lines are from eq. (3.35a) and (3.35b), respectively.

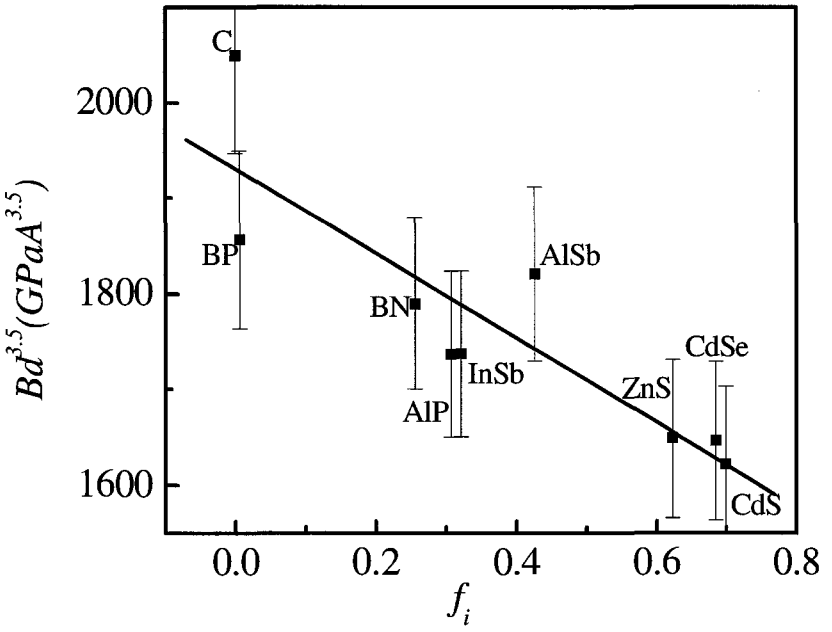

Figure 7: $Bd^{3.5}$ as a function of ionicity fraction f_i.

The calculated results presented in table 1 are in a good agreement with the experimental observations. In the case of shear modulus G, our predictions for Si, Ge, Pb, SiC, HgSe and HgTe, which were not included in fitting eq. (3.35a-b), are within 16% of the experimental values. As for B, our calculations for the crystals unexploited in the extrapolation process generally fall within 19% of the experimental values. As regards the compounds BeS, BeSe, BeTe, MgS, BAs and BSb, for which there exist no measurements known to the author, the predictions are very close to the results of *ab initio* calculations, which give B =111GPa and G = 81.2 GPa for BeS [Gonzalez-Diaz *et al.*], B = 98 GPa and G = 66.6 GPa for BeSe [Gonzalez-Diaz *et al.*], B = 70 GPa and G = 49.6 GPa for BeTe [Gonzalez-Diaz *et al.*], B = 61.3 GPa and G = 34.8 GPa for MgS [Drief *et al.*], B =152 GPa and G =149.6 GPa for BAs [Meradji *et al.*] and, B =116 GPa and G =116.2 GPa for BSb [Meradji *et al.*]. In the case of β-HgS, our estimations are comparable to the results obtained from valence-force-field approach, which yields B = 68.5 GPa and G = 19.6 GPa [Kumazaki]. As for shear moduli of compounds AlP, AlAs, GaN and InN whose experimental values are also unknown to the writer, the results assessed using eq. (3.35b) agree with the outcomes of first-principle calculations testified in reference [Rodriguez-Hernandez *et al.* 1992], which gives G = 55.2 GPa for AlP, reference [Chetty *et al.*], which gives G = 46.4 GPa for AlAs, and reference [Bouarissa *et al.*], which reports G = 122.7 GPa for GaN and G = 83.3 GPa for InN. Consequently, the reliability and accuracy of formulae 35-36 are well verified. It is noteworthy that in most cases, the reported *ab initio* values of bulk and shear moduli were extrapolated from the elastic constants through equations (3.3)-(3.4).

Because of different bond-bending and bond-stretching features, the materials under study are split into two groups as far as their shear moduli are concerned (see fig.6). This is due to the fact that the compounds of the first-row elements are not always directly comparable to those with heavier elements. This behaviour stems from the differences in the bonding that are related to the *s-p* hybridisation [Martin]. Thus, C, α-Sn and Pb together with compounds formed of first-row elements (e.g. BP and BN) or elements of first and second rows such as SiC and AlN belong to group a; whereas, Si, Ge and compounds consisting of first-row elements and heavier ones like BAs, BSb, GaN and InN fit in group b. Furthermore, group a contains compounds of II-VI family

Crystal	*d(Å)*	f_i	B_{exp}	B_{cal}	%	G_{exp}	G_{cal}	%	*Group*
C	1.55 [a]	0 [f]	442 [j]	418.2	5.4	535.7 [j]	534.5	0.2	a
α-Sn	2.81 [a]	0 [f]	53 [a]	52.1	1.7	...	20.3	...	a
Pb	3.17 [b]	0 [b]	41.7 [j]	34.2	17.9	10.1 [j]	10.4	2.9	a
BP	1.97 [a]	0.006 [f]	173 [k]	180.4	4.3	139 [k]	142.3	2.4	a
BN	1.57 [a]	0.256 [f]	369 [l]	373	1.1	414 [q]	400.9	3.2	a
AlN	1.90 [c]	0.449 [f]	201 [m]	180.9	10	114.8 [m]	114.7	0.1	a
SiC	1.88 [b]	0.177 [f]	211 [a]	202.9	3.8	175.8 [r]	160	8.9	a
BeS	2.10 [b]	0.312 [f]	...	132.7	...	...	76.7	...	a
BeSe	2.20 [b]	0.299 [f]	...	113.2	...	...	60.1	...	a
BeTe	2.40 [b]	0.169 [f]	...	86.5	...	...	42	...	a
MgS	2.43 [b]	0.639 [t]	...	72.2	...	...	23.1	...	a
ZnS	2.34 [a]	0.623 [f]	84.1 [j]	82.8	1.5	31.9 [j]	29.1	8.7	a
CdS	2.52 [a]	0.685 [f]	64.8 [n]	62.6	3.4	16.9 [n]	17.6	4.1	a
CdSe	2.62 [a]	0.699 [f]	55.7 [o]	54.4	2.3	13.6 [o]	13.9	2.2	a
CdTe	2.81 [a]	0.675 [f]	42.4 [a]	42.9	1.2	10.5 [s]	9.8	6.6	a
β-HgS	2.53 [d]	0.77 [g]	...	60.1	...	...	15	...	a
HgSe	2.63 [d]	0.62 [h]	48.5 [h]	55.1	13.6	16.5 [h]	15.4	6.6	a
HgTe	2.78 [d]	0.565 [h]	43.7 [j]	46.1	5.5	12.9 [j]	12.2	5.4	a
Si	2.35 [a]	0 [f]	100 [j]	97.4	2.8	70.8 [j]	82.4	16.4	b
Ge	2.45 [a]	0 [f]	77.8 [j]	84.2	8.2	56.6 [j]	65.5	15.7	b
BAs	2.07 [b]	0.002 [f]	...	151.8	...	...	165.4	...	b
BSb	2.24 [e]	0.03 [i]	...	114.3	...	...	104.8	...	b
AlP	2.36 [a]	0.307 [f]	86 [a]	88.3	2.7	...	61.7	...	b
AlAs	2.43 [a]	0.274 [f]	77 [a]	80.5	4.5	...	54.2	...	b
AlSb	2.66 [a]	0.426 [f]	59.3 [j]	56.1	5.4	31.1 [j]	28.2	9.32	b
ZnSe	2.45 [a]	0.676 [f]	62.4 [a]	69.3	11	32.9 [j]	31.7	3.6	b
ZnTe	2.64 [a]	0.546 [f]	51 [j]	55.6	9	24.8 [j]	25.4	2.4	b
GaP	2.36 [a]	0.374 [f]	88.8 [j]	86.6	2.5	58 [j]	57.6	0.7	b
GaAs	2.45 [a]	0.310 [f]	75.6 [j]	77.4	2.4	48.8 [j]	50.1	2.6	b
GaSb	2.65 [a]	0.261 [f]	57.4 [j]	59.6	3.8	35.4 [j]	34.1	3.7	b
GaN	1.94 [d]	0.5 [f]	190 [p]	164	13.7	...	144	...	b
InP	2.54 [a]	0.421 [f]	72.5 [j]	66.1	8.8	36.5 [j]	36.5	0	b
InAs	2.61 [a]	0.357 [f]	60 [a]	61.2	2	31.4 [j]	33.7	7.3	b
InSb	2.81 [a]	0.321 [f]	46.7 [j]	47.7	2.1	24.2 [j]	23.3	3.7	b
InN	2.16 [d]	0.578 [f]	137 [p]	111.1	18.9	...	73.3	...	b

[a] Reference [Lam *et al.* 1987]. [b] Reference [Christensen *et al.*]. [c] Reference [Gao *et al.*]. [d] Reference [Kumar *et al.*]. [e] Reference [Bouhafs *et al.*]. [f] Reference [Philips 1970]. [g] Reference [Kumazaki]. [h] Reference [Lehoczky *et al.*]. [i] Reference [Ferhat *et al.*]. [j] Reference [Simmons and Wang]. [k] Reference [Rodriguez-Hernandez *et al.* 1995]. [l] Reference [Knittle *et al.*]. [m] Reference [Wright]. [n] Reference [Bass]. [o] Reference [Cline *et al.*]. [p] Reference [Berrah *et al.*]. [q] Reference [Shimada *et al.*]. [r] Reference [Kamitani *et al.*]. [s] Reference [Dunstan *et al.*]. [t] Reference [Drief *et al.*].

Some of the data are calculated from the experimental values of the elastic constants using eq. (3.3)-(3.4). All the elastic constants are in GPa and "%" stands for the discrepancy between our predictions and the empirical data.

Table 1: Calculated and experimental values for bulk and shear moduli of covalent crystals.

(BeS, CdS, ZnS, HgTe etc.), while all the III-V semiconductors without any first-row elements (e.g. GaP, AlSb, InAs etc.) constitute the rest of group b. The only exceptions to these general criteria of classification are ZnSe and ZnTe, which fall in group b as shown in fig. 6. This reflects the existing difference between the band gaps of these crystals and that of ZnS [Khenata *et al.*]. In contrast to shear modulus, bulk modulus is not affected by the abovementioned angular properties of the chemical bond, and hence a universal linear relation between B and f_i can be obtained as displayed in fig.7. This results from the fact that bulk modulus quantifies the response of a crystal to a uniform volumetric tension. In this case, the solid suffers a symmetric deformation along the three main axes, and as a result no angular effects are created.

Using equations (3.35-36), we obtain the following expression for the ratio of shear modulus to bulk modulus

$$\frac{G_j}{B} = \frac{R_j(f_i)}{d^2} \tag{3.37}$$

with

$$R_j(f_i) = \frac{A_j - B_j f_i}{1938.72 - 506.702 f_i} \tag{3.38}$$

where j= a, and b and, A_j and B_j refer to the corresponding constants in equations (3.35a-b).

From fig. 8, it can be observed that as expected all the three R_j decrease with increasing ionicity and that they exhibit the same trend evinced by the corresponding curves in fig. 6. Notice that both curves display a nearly linear behaviour, which suggests that the effects of ionicity are less significant than those induced by the bond lengths. From expression (3.37), it is also evident that the ratio *G/B* assumes small values for large bond lengths. The three-dimensional surface plots displayed in fig.9 clearly demonstrate that the bond length plays a predominant role in the brittle behaviour of covalent materials, since even for relatively high ionicities, small values of d still yield *G/B* ratios larger or equal to 0.5, which is typical of brittle materials.

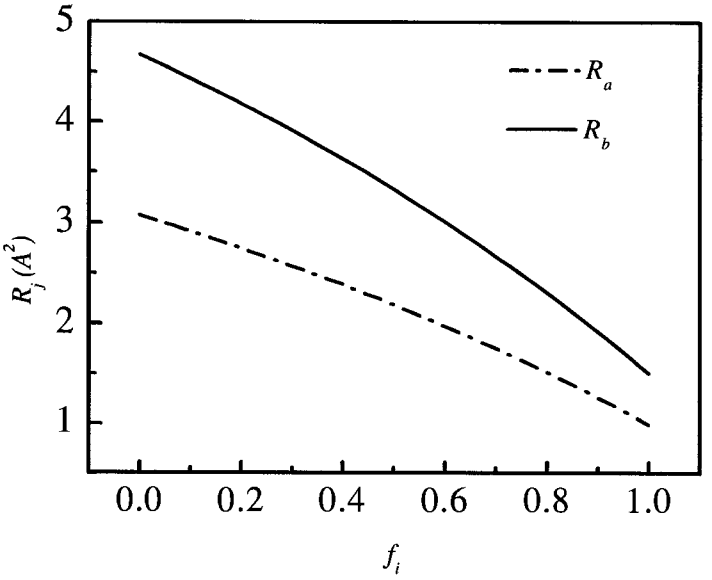

Figure 8: R_j as a function of ionicity fraction f_i.

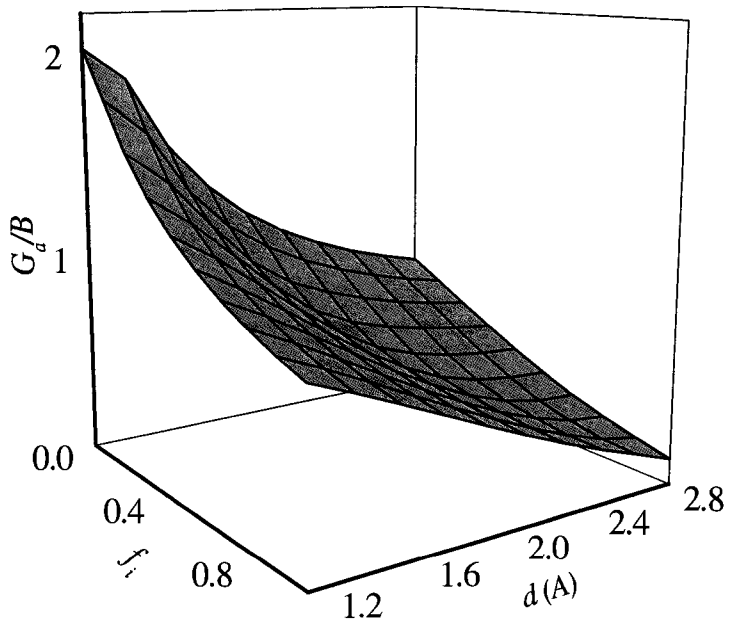

Figure (9a): The ratio G_a/B as a function of ionicity and bond length.

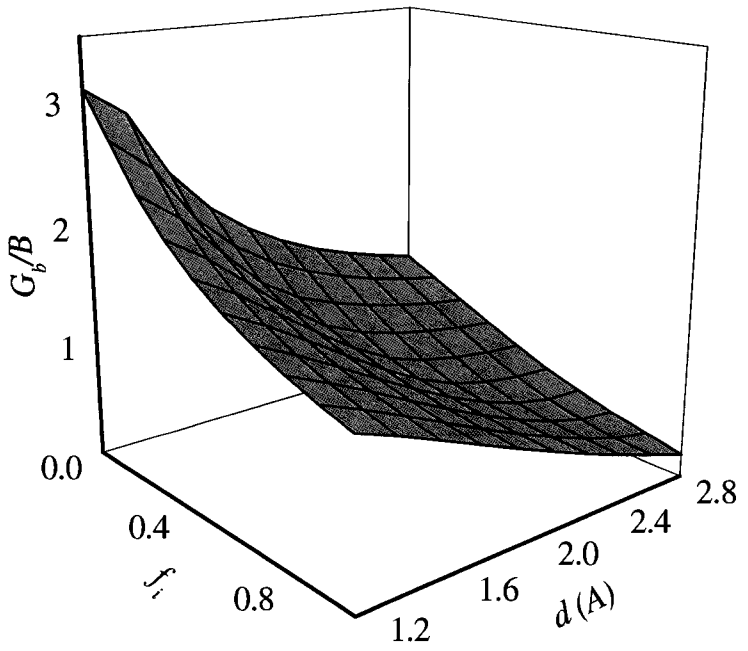

Figure (9b): The ratio G_b/B as a function of ionicity and bond length.

Chapter IV
Ideal Strengths of
FCC Metals

The investigation of the strength of materials under different types of deformation has always been of interest because of its practical importance and due to the fact that it is one of the few problems in mechanical behaviour of materials that can be solved using *ab initio* calculations. As the study of the strength of real crystals involves a deep understanding of a large number of mechanical phenomena like defects (e.g. voids, dislocations etc.) or the impurity effects, only perfect (i.e. defectless) pure monocrystals will be examined. Furthermore, our study will be focused on the FCC metals that are usually thought to be more ductile than their BCC counterparts. In this chapter, the structure of the FCC metals, their ideal strength under shear and tension will be investigated in relation to the geometrical features of their bonds and a new performance indictor will be proposed.

4.1 FCC Structure

The primitive unit cell of face-centred cubic (FCC) crystals is a rhombohedra and their conventional unit cell, which is the one used throughout the present work and in most cited researches, is a cubic structure enclosing four atoms distributed in its corners and on its faces as shown in figure 10.

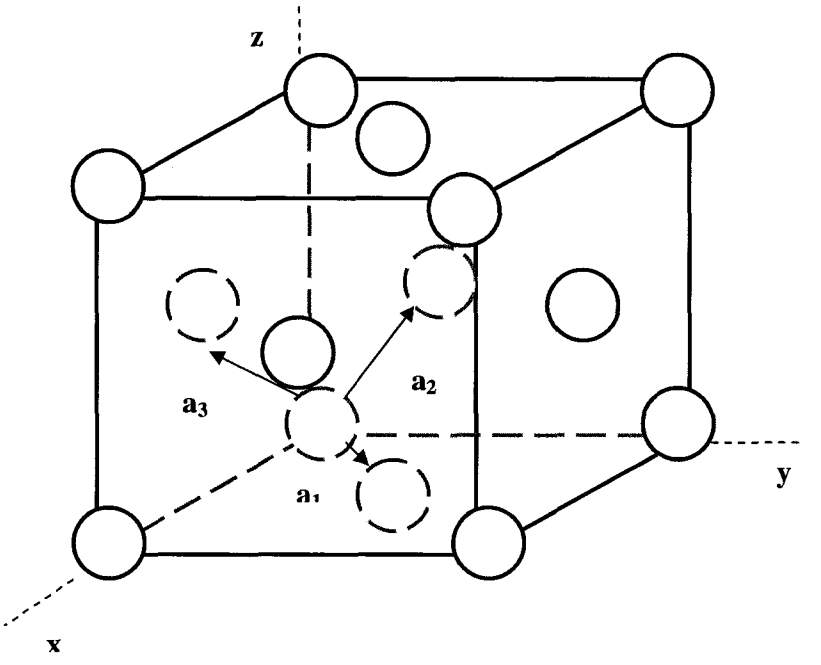

Figure 10: conventional FCC unit cell.

The primitive vectors of the FCC structure are displayed in figure 10. Their mathematical expression for a given lattice constant a is as follows

$$\mathbf{a}_1 = \tfrac{1}{2} a(\mathbf{e}_x+\mathbf{e}_y) \quad (4.1a)$$

$$\mathbf{a}_2 = \tfrac{1}{2} a(\mathbf{e}_y+\mathbf{e}_z) \quad (4.1b)$$

$$\mathbf{a}_3 = \tfrac{1}{2} a(\mathbf{e}_z+\mathbf{e}_x) \quad (4.1c)$$

All the directions <abc> and planes {hkl} are not equivalent in a crystal, since solid structures usually favour a small number of orientations when undergoing symmetry operations and they normally fail along a specific direction or plane when deforming. In the case of shear deformation, one needs to specify the composition plane, along which the shear processing occurs, and the direction of the shear, which is parallel to a vector lying in the composition plane. The vector indicating the shear direction is referred to as Burgers vector $\vec{b}$; for more information on Burgers vector, which is evoked in the description of lattice dislocations, see ref. [Kittel] p. 604. The combination of the

composition plane and the burgers vector is labelled the slip system, which is $\{111\}<11\bar{2}>$ in FCC metals.

As for tension, the weak direction of the FCC metals is reportedly <110> [Morris *et al.*]. Through tensile straining, one can transform an FCC crystal to a BCC structure and vice versa. This straining process is known as Bain path or Bain strain and it takes place, when the crystal is pulled along its weak direction in tension. Even though, in theory, defect-free FCC metals could withstand a Bain strain, no such transformation has been experimentally observed in the case of these crystals. Lastly, it should be noted that the inherent failure mechanism in FCC metals is in shear. Even when sustaining a tensile deformation along <110>, the FCC metals end up failing in shear in the well-known $\{111\}<11\bar{2}>$ system. This feature of FCC metals is related to the relaxations occurring parallel and perpendicular to the direction of tension; for more details, see reference [Morris *et al.*] and the references therein.

4.2 Calculation of Ideal Strength

The ideal strength of a material is defined as the maximal stress σ_m the crystal can undergo before its failure, i.e. before the crystal becomes structurally unstable and spontaneously deforms or breaks. Conversely, one can introduce an ideal deformability parameter identified with the strain corresponding to the ideal strength. In the case of tension, the maximal stress suffered by the crystal is labelled ideal tensile strength σ_m and the deformability parameter is called tensibility t_m. In a similar fashion, one can depict the behaviour of a crystal under shear processing in terms of its ideal shear strength τ_m and shearability s_m. It is worth mentioning that the notions of tensibility and shearability were first introduced by Ogata and collaborators [Ogata *et al.* 2004]. The practical significance of the concepts of ideal strength, shearability and tensibility, which serves as the foremost motivation for this kind of research, lies on the observation that ideal strength is an inherent material property and that it can be approached in real situations of scientific and engineering importance.

In simulating tension normal to the (hkl) plane, one proceeds by setting the vector <hkl> normal to the plane in question as the z axis, then the crystal lattice is recreated through the superimposition of different closed packed layers of the FCC lattice along the <hkl> direction and their repetition along the z axis with periodic boundary conditions. The layers necessary to reproduce the conventional FCC unit cell for planes {110} and {111} are evinced in figures 11a-b.

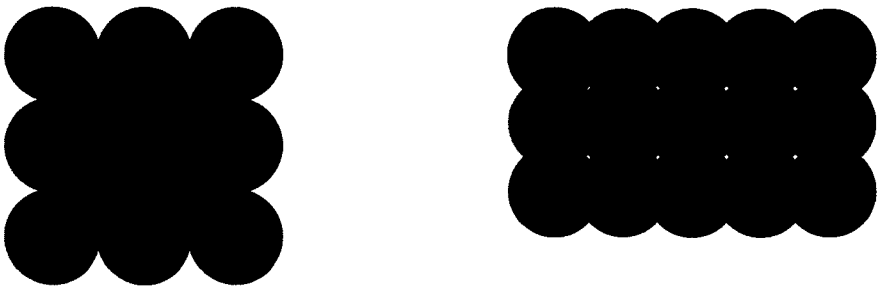

(a) (b)

Figure 11: (a) (110) face of FCC crystals (b) (111) face of FCC crystals. Upper layers are in dark blue while lower layers appear in light blue.

The next step consists of distorting the lattice through small amounts of deformation γ along the z axis and computing the total energy for each increment. As for shear processing, one has to transform the Cartesian coordinate system in accordance with eq. (4.2) so that the direction of shear becomes the new z axis. This transformation resembles a rotation [Paxton *et al.*]

$$\vec{a}_i' = S_i^j \vec{a}_j \tag{4.2a}$$

where

$$S^{i}_{j} = \delta^{i}_{j} + \gamma b^{i} n_{j} \qquad (4.2b)$$

In equations (4.2), $\vec{a}_i'$ correspond to the vectors of the coordinate system resulting from the rotation of the Cartesian reference frame described by $\vec{a}_j$, while b^i and n_j are the contravariant components of a unit vector parallel to the Burgers vector (or the shear direction) and the covariant components of a unit vector normal to the composition plane of the slip system, respectively. As mentioned in section 4.1, the Burgers vector is parallel to the <11 $\bar{2}$> direction and $\vec{n}$ should be along the <111> direction.

Once the transformation given by eq. (4.2) is performed, small amounts of deformation are introduced along the new z axis and the total energy is calculated for each increment of γ. As expected, the energy curves obtained for shear processing are identical in shape to those resulting from tensile distortion. As an example, the energy curve for Ni is given below (see figure 12).

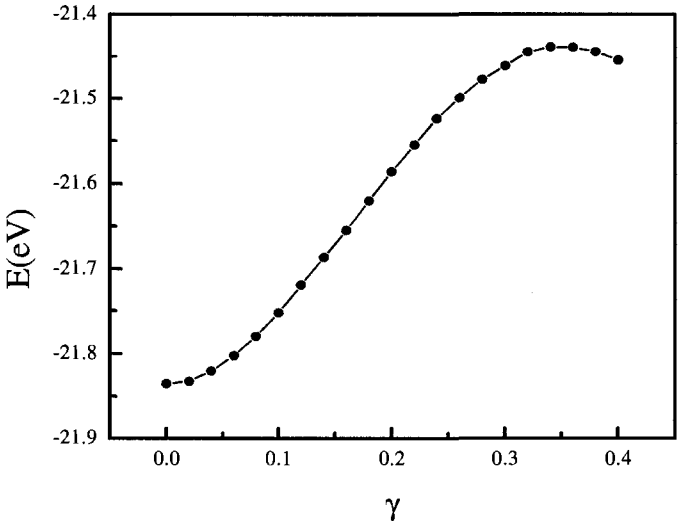

Figure 12: Total electronic energy of Ni as a function of the shear deformation parameter γ.

For the calculation of the total energy, the VASP package (see 2.3) was utilised with a cutoff energy equal to 375 eV and high precision for all the metals. In the case of Ni, which is a magnetic substance, the spin polarised option was chosen, whilst the computation of the total energy of the rest of the metals was performed with spins

unpolarised. The resulting energy curves are then approximated by a fourth order polynomial in order to extract their slope, which is related to the ideal strength through the following equation involving the volume Ω of the unit cell

$$\sigma = \frac{1}{\Omega}\frac{\partial E}{\partial \gamma} \tag{4.3}$$

The ideal strength is then given by the maximum value of the curve described by eq. (4.3). As an example, the shear stress curve of Ni is displayed in figure 13.

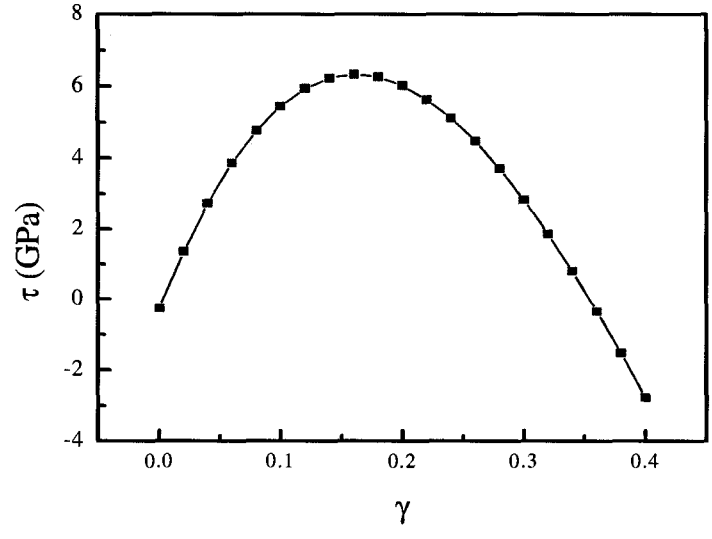

Figure 13: The shear stress curve of Ni as a function of the shear deformation parameter γ.

Crystals	*a*	τ_m	s_m	*G*	$\sigma_{m<110>}$	$t_{m<110>}$	$\sigma_{m<111>}$	$t_{m<111>}$
Al	4.05048	3.93	0.14	33.8	10.01	0.407	9.59	0.37
Ag	4.14003	2.31	0.122	27.64	10.77	0.34	8.99	0.237
Au	4.15639	0.953	0.13	10.37	13.91	0.393	7.26	0.232
Ni	3.51422	6.312	0.159	73.55	28.72	0.356	29.12	0.284
Cu	3.61945	3.84	0.125	49.20	19.60	0.396	18.34	0.244
Ir	3.8816	19.424	0.16	182.09	39.9	0.239	33.8	0.25
Pt	3.96920	2.57	0.126	33.91	28.86	0.474	21.73	0.275
Pd	3.9333	2.736	0.174	26.85	20.59	0.357	19.41	0.280

Table 2: values of shearability, tensibility, shear modulus and ideal shear and tensile strengths of FCC metals and their lattice constants from first-principle calculations. The stresses and the shear modulus are in GPa and the lattice parameter is in angstroms.

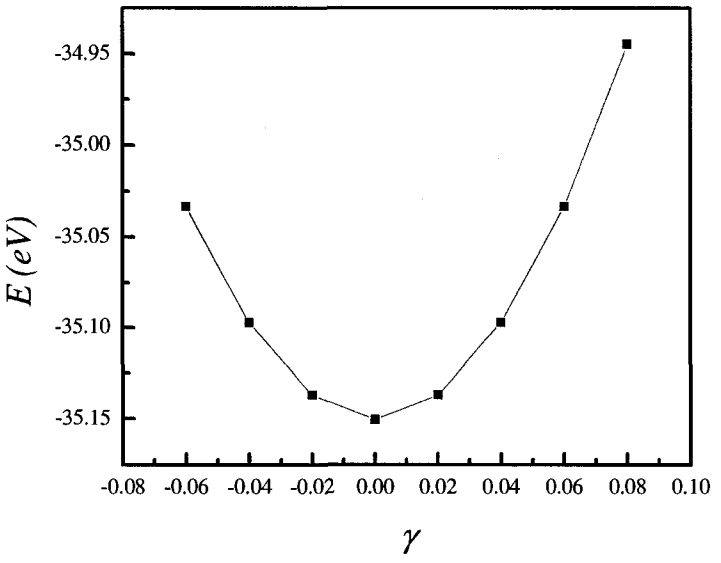

(a)

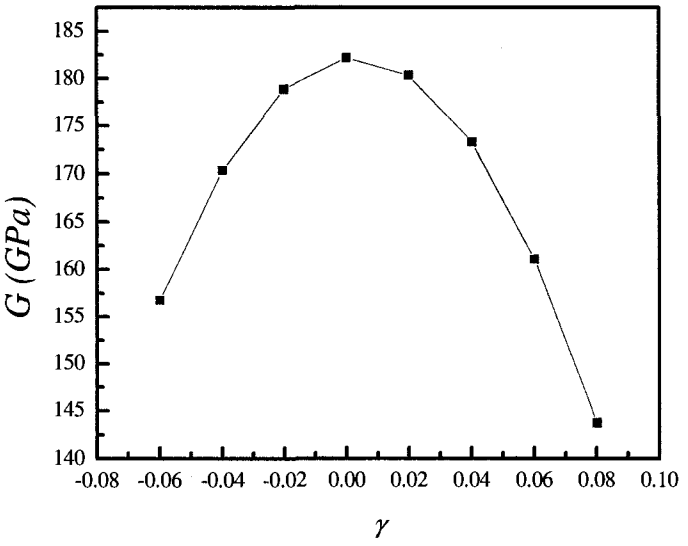

(b)

Figure 14: (a) energy curve around $\gamma = 0$ for Ir. (b) second derivative of the total energy of Ir.

In addition to shearability, tensibility and ideal shear and tensile strengths, the shear modulus of the FCC metals for the slip system$\{111\}\langle 11\bar{2}\rangle$ has been calculated according to eq. (3.2) by extracting the value of the second derivative of the energy curve around zero (see figures 14a-b) at $\gamma = 0$. The results of our calculations are shown in table 2. Mind that all the ideal strengths calculated in the present work are unrelaxed in the sense that all the strains have been zeroed with exception of the one corresponding to the direction of distortion.

Due to dislocations and defects, all crystals fail before reaching their ideal strength; consequently, it is impossible to measure the theoretical maximal stress they can withstand under shear or tension. To the knowledge of the author, only the ideal shear strengths of Al, Cu, Au Ag and Ni, and their volumetric tensile strengths have been computed and published in references [[Morris *et al.*], [Ogata *et al.* 2002] and [Ogata *et al.* 2004]]. As regards the calculations of the ideal shear strengths and shear moduli listed in table 2, they usually tend to be larger than the results reported in the references cited above. Only in the case of gold, the calculated ideal shear strength and shear modulus seem to be lower than similar computations. The discrepancies between our predictions and the results of the works cited above result from the type of unit cell used in the calculations, the range of thr cutoff energies and the choice of pseudopotentials or the alternative methods. In the present work, all the computations were performed using PAW approach with a conventional FCC unit cell and cutoff energies of the order of 375 eV. However, previous works suggest that in the case of some materials like Au and Cu, primitive unit cells or non conventional six-atom cells with US pseudopotentials are more effective.

As can be seen from table 2, Ir is stronger than the rest of the FCC metals both in shear and tension. Its high ideal strengths are a consequence of its abnormally large elastic moduli [Morris *et al.*], which will be investigated in the next chapter. Lastly, all the examined FCC metals appear to be weaker along the <111> direction in tension (see also appendix E).

4.3 Shearability and bond directionality

Recently, it has been suggested that the range of distortion suffered by a material is dictated by the angular features of its bonds [Ogata *et al.* 2004]. Crystals with spherically symmetric valence electron distributions can easily reform the broken bonds, once the shearing process stops; while, in the case of solids whose valence charge distributions exhibit directional features, the bond reformation process can difficultly occur due to the geometrical constraints imposed on the electrons by the angular character of the bonds. Thus, directionally bonded solid structures sustain a comparatively long range of deformation before they fail.

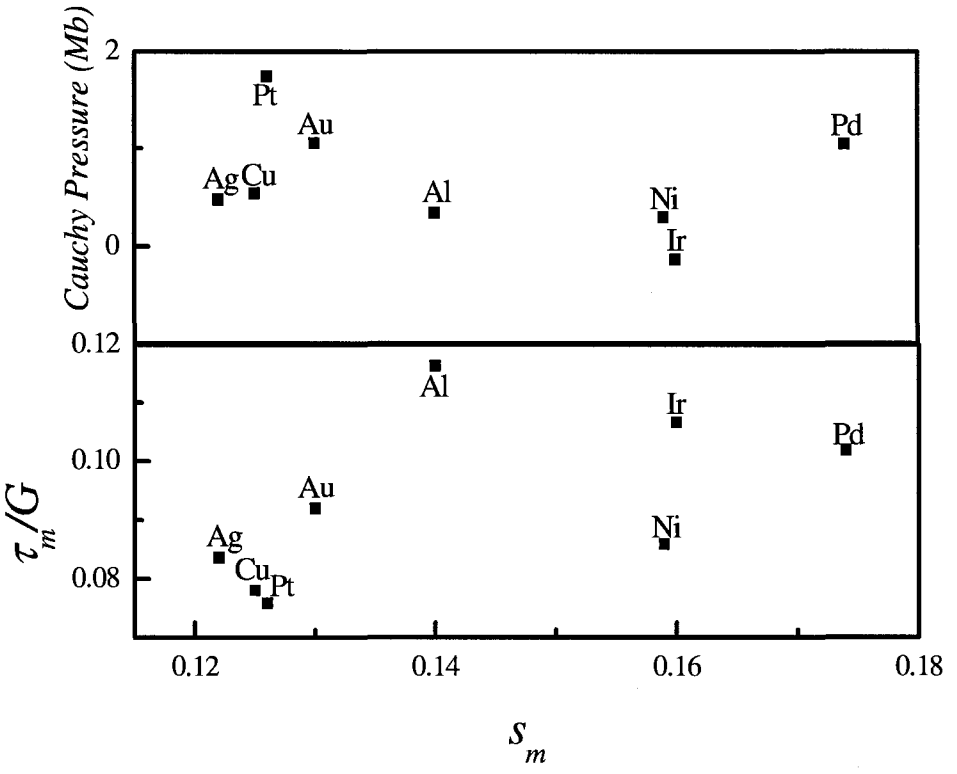

Figure 15: Cauchy pressure (mb) and the ratio of the ideal shear strength to the shear modulus are plotted as functions of shearability.

In figure 15, Cauchy pressure given by $C_{12} - C_{44}$ and the ratio τ_m / G are plotted as functions of shearability. The Cauchy pressure is often evoked as a macroscopic measure of bond directionality [Chen *et al.* 2003] and it exhibits an almost linear correlation with the maximal strain. Thus metals with symmetric charge distributions like Au, Pt (see fig. 21a-b) and Cu tend to have high Cauchy pressures and low shearabilities, whereas metallic FCC crystals with angular bonding such as Ni, Ir and Al assume small Cauchy pressures and display large shearabilities. As mentioned previously, the only exception to this observation is Pd, a very ductile metal with low ideal strength both in shear and tension. In addition, as discussed in section 4.2, in the absence of any published results for Pd, one can only have a very crude idea of the scale of the ideal strengths and strains of this metal. As can be observed from table 2, the maximal shear and tensile stresses sustained by Pd are very low, which is in concord with the high ductility of this metal; however, its shearability seems abnormally large and might be indicative of other electronic factors susceptible of influencing the range of deformation withstood by crystals.

4.4 Ideal strength and ductility

The competition between ductile and brittle failures can be depicted as the competition between the shear and tensile destabilisations. As a result, the ratio of the ideal shear strength to the theoretical tensile strength along the composition plane of the slip system, i.e. $\tau_m / \sigma_{<111>}$ for FCC metals, can be utilised as a performance indicator. The ratio G/B (see 3.1) is widely used to assess the ductility of crystals in a rather rough fashion mainly because of the experimental difficulties involved in measuring parameters directly related to plastic deformation. In the specific case of FCC metals, as shown in figure 16, the ratio of shear and tensile strengths is equivalent to the ratio of the elastic moduli in many regards; nonetheless, it allows segregating the directionally bonded metals from solids with spherical electron distributions.

As can be seen from figure 16, there is a linear correlation between the ratios of the elastic moduli and ideal strengths. The ratio $\tau_m / \sigma_{<111>}$ usually assigns larger values to metals with directional bonds like Al and Ir, and hence it portrays the ductility of metals with more nuances.

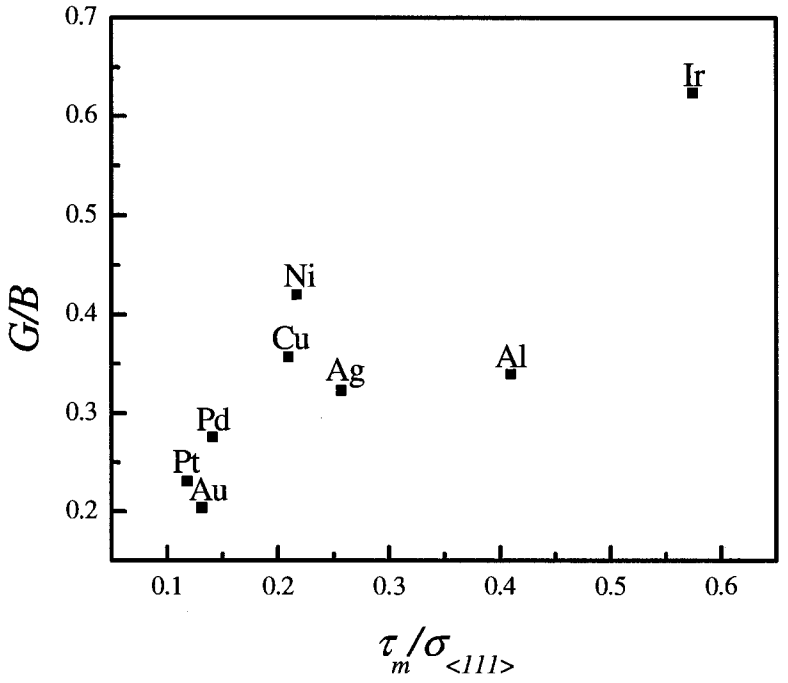

Figure 16: the ratio of elastic moduli plotted as a function of the ratio of the ideal strengths.

4.5 Analysis of the DOS of Al, Cu, Ir and Pd

In order to substantiate the observations made in the previous sections, the density of states[6] (DOS) of the valence electrons of Al, Cu, Ir and Pd have been calculated for $\gamma = 0$, which corresponds to the equilibrium state of the crystal, $\gamma = s_m / 2$ and

[6] For an elementary introduction to DOS see reference [Kittel] p.108-112

$\gamma = s_m$ (see figures 17a-d). The VASP code estimates the DOS $\bar{n}$ as the difference of the integrated DOS $N(\varepsilon_i)$ between two grid points as shown by eq. (4.4) [Kresse et al. 2005].

$$\bar{n}(\varepsilon_i) = (N(\varepsilon_i) - N(\varepsilon_{i-1}))\Delta\varepsilon \tag{4.4a}$$

where $\Delta\varepsilon$ is the energy difference and the integrated DOS is given by

$$N(\varepsilon_i) = \int_{-\infty}^{\varepsilon_i} \bar{n}(\varepsilon) d\varepsilon \tag{4.4b}$$

This method conserves the total number of electrons exactly. The resulting DOS curves display a large number of peaks of various sizes that are partly artefacts created by the software. In what follows only the large peaks near the Fermi level and the spacing between them, which have physical significance, will be analysed.

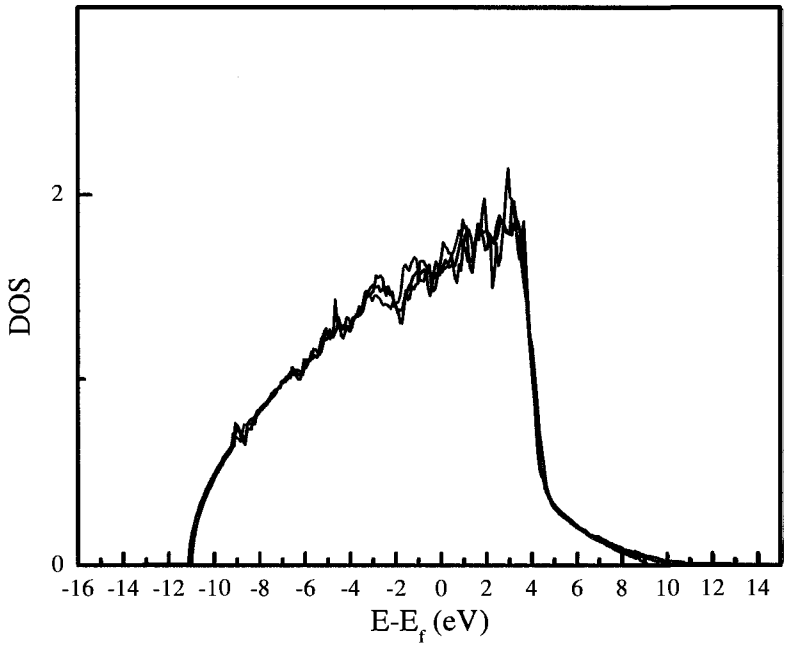

(a)

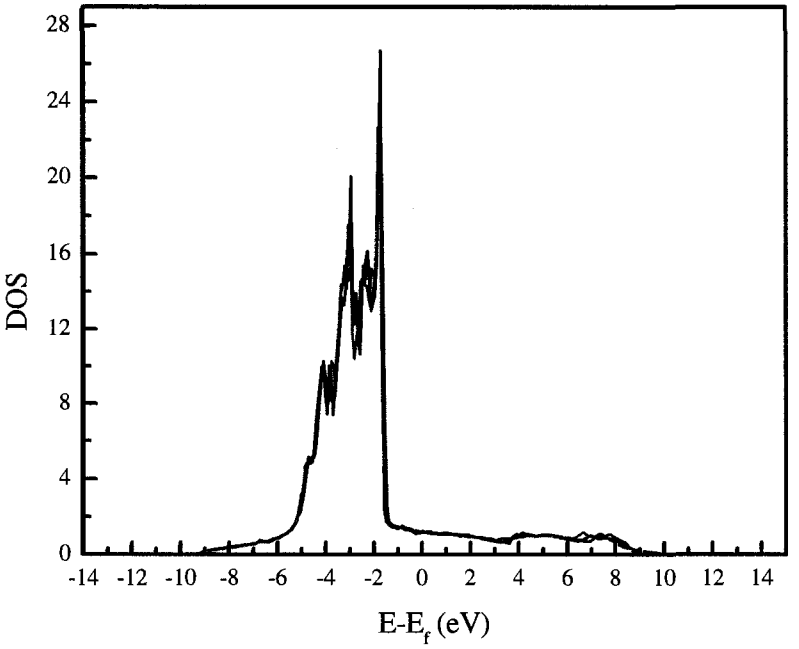
28
24
20
16
12
8
4
0
DOS
-14 -12 -10 -8 -6 -4 -2 0 2 4 6 8 10 12 14
E-E$_f$ (eV)

(b)

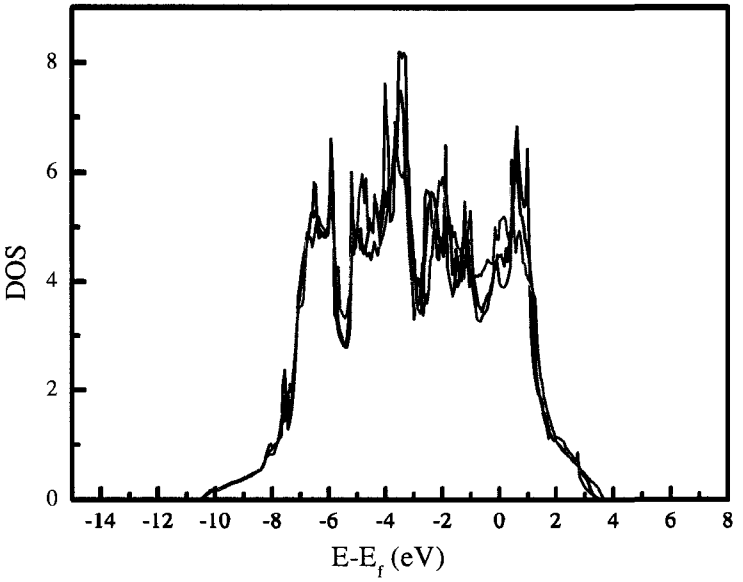
8
6
4
2
0
DOS
-14 -12 -10 -8 -6 -4 -2 0 2 4 6 8
E-E$_f$ (eV)

(c)

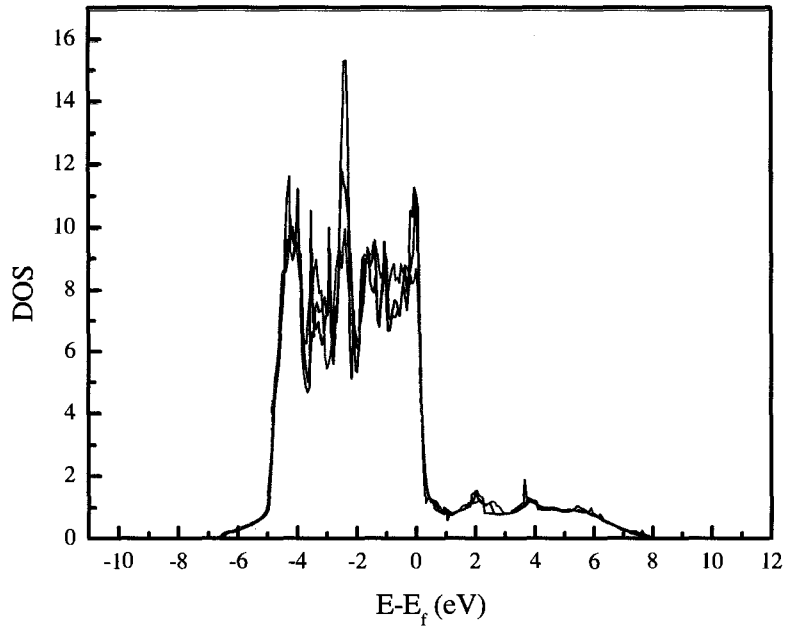

(d)

Figure 17: DOS curves of (a) Al, (b) Cu, (c) Ir and (d) Pd at $\gamma = 0$ (in black), $\gamma = s_m / 2$ (in blue) and $\gamma = s_m$ (in red).

With the exception of Al, all the metals exhibit a sharp peak near the Fermi energy, which is typical of FCC transition metals [Friedel]. In the particular case of Al, the *s-p* orbitals hybridisation is responsible for the relatively circular shape of the DOS curve. As can be seen from figures 17a-d, under shear processing, the spacing between the peaks near the Fermi energy is filled, which is indicative of an augmentation in the density of electrons around the Fermi level. This phenomenon is well noticeable in the case of Ir, which is well known for having directional bonds, and Pd that seems to undergo a surprisingly high range of shear deformation. Such increases in the valence electron concentration near the Fermi energy can be interpreted as the amplification of the angular features of the bonds or the creation of some degree of directionality in the electron distribution. This observation in concert with the relationship between bond directionality and shearability discussed in section 4.3 permits us to speculate the formation of angular features in the bonding of sheared Pd as the cause of its long range of deformation. It is

also worth mentioning that the occupied states occurring after the Fermi level in the antibonding region are usually suggestive of instability. These states, which are manifest in the DOS plots of Ir and Al but are wanting in the case of Cu, can be regarded as an indicator of the inherent capability of the metal to withstand a successful bond reformation. In the case of solids, such as Ir and Al, where these states are noticeable, once the crystal is deformed, it is difficult for the bonds to recover, whereas metals like Cu, which lack such states, can effectively reform their bonds once the shearing process is over.

Fermi E	*Al*	*Cu*	*Ir*	*Pd*
at $\gamma = 0$	7.939	3.649	9.795	4.412
at $\gamma = s_m/2$	7.929	3.642	9.787	4.418
at $\gamma = s_m$	7.914	3.638	9.735	4.420

Table 3: Fermi energy for different values of the deformation parameter.

Lastly, it is noteworthy that in the case of Al, Cu and Ir, the Fermi energy slightly decreases. However, the Fermi energy of the electron distribution of Pd rises to some extend, which sets this metal apart and suggests a destabilisation of its structure that may be related to its long range of distortion.

Chapter V
Origin of the Anomalous Elastic Properties of Iridium

[This chapter is adapted from the paper *a* accepted by *Journal of Physics: Condensed Matter*, see appendix G]

As discussed in the previous chapter, iridium distinguishes itself from the rest of FCC metals by its atypical elastic peculiarities. For a long time, it was believed that these abnormal features are produced by the impurities present in Ir samples. However, in 70's, Hecker and co-workers evidenced that even Ir samples with low impurity percentages behave in a brittle fashion [Hecker *et al.*]. This observation, which was later substantiated by P. Panfilov and collaborators [Panfilov *et al.*], led Hecker *et al.* to conclude that the directional character of Ir's bonds are responsible for its large elastic moduli. Since then, numerous investigations have been conducted in order to deduce the atomic-scale causes of these abnormalities in Ir. In particular, works done by Eberhart [Eberhart 2001], Wills and collaborators [Wills *et al.*], and Gornostyrev *et al.* [Gornostyrev *et al.*] need to be mentioned (see chapter I). Despite all these studies, the origin of iridium's unusual elastic properties is still unknown. In this chapter, concepts such as electron localisation and bond order will be introduced and used to elucidate the cause of the aforesaid singularities in regard to the very nature of metallic bonding.

5.1 Metallic bond

According to the generally accepted description of the chemical bonding, the metallic bond is characterised by the partial occupancy of the conduction band and hence, it stands in firm contrast to covalently bonded systems examined in chapter II. This theory of metallic systems, which is basically devised to explain the electric transport properties of metals and which is still widely taught, suffered its breakdown in 1937 with the experimental data on the electrical conductivity of various transition metal oxides measured by de Boer and Verwey [Edwards *et al.*]. Binary compounds such as NiO, CoO, MnO and iron oxides all have partially filled *d*-bands in the solid state, but as evinced by de Boer and Verwey's experiment, they are all insulators! The failure of the band theory, which is based on the reciprocal space representation of the crystal, has remained marginalised in the physics community but has attracted chemists, who have always hesitated to regard the metallic bond as a distinct type of bonding. In the new description of the metallic systems substantiated by B. Silvi and C. Gatti, the metallic bond is depicted as a partial covalent bond that distinguishes itself from purely covalent crystals by its delocalised electron distribution in the interionic regions [Silvi and Gatti]. This delocalisation generates a network of itinerant electrons around the ions, hence yielding the electrical conductivity of metals. It is worth mentioning that this portray of metallic systems resembles anisotropic conductors like gallium. In what follows, the electron localisation function (ELF) will be introduced and the bonding topology will be used to substantiate the novel depiction of the metallic bond.

5.1.1 Electron localisation

Despite the undeniable utility of the concept of localised/delocalised electrons both in solid state physics and chemistry, its mathematical formulation seems hard to pin down at first glance. In his pioneering paper published in 1964, Kohn used the concept of localised electrons within a mathematical formalism common to quantum mechanics and solid state physics to describe the insulating state without any need for an energetical band gap [Kohn 1964]. He suggested that Wannier functions should be used to describe

insulators, because they exhibit stationary properties that Bloch functions lack. Based on this line of thought, an electron localisation function is currently under development [Silvestrelli *et al.*] while others, inspired by Kohn's original idea, are attempting at elaborating another electron localisation function rooted in the electric polarisation of insulating materials [Resta *et al.*]. In 1990, A.D. Becke and K.E. Edgecombe derived an electron localisation function (ELF) that has been used extensively by chemists and physicists since then. The full derivation of this function is given in references [[Becke 1985]-[Becke *et al.*]]. Here we shall briefly outline its elaboration from the conditional pair probability and its applications.

The same-spin pair probability $P_2^{\sigma\sigma}(1,2)$, i.e. the probability of finding two particles of spin σ simultaneously at position 1 and 2 in a multielectron system, is given by

$$P_2^{\sigma\sigma}(1,2) = \rho_\sigma(1)\rho_\sigma(2) - \left|\rho_1^\sigma(1,2)\right|^2 \tag{5.1}$$

where

$$\rho_1^\sigma = \sum_i \psi_i^*(1)\psi_i(2) \tag{5.2}$$

is the σ-spin one-body Hartree-Fock density matrix (see section 5.2.1 for more details on density matrix). Mind that the summation is restricted to the orbitals of spin σ and that

$$\int\left|\rho_1^\sigma(1,2)\right|^2 d2 = \rho_1^\sigma(1,1) = \rho_\sigma(1) \tag{5.3}$$

If a particle is well localised at position 1, which will be called the reference hereafter for convenience, then the conditional probability $P_{cond}^{\sigma\sigma}(1,2)$ of finding another σ-spin electron at position 2 is calculated as

$$P_{cond}^{\sigma\sigma}(1,2) = P_2^{\sigma\sigma}(1,2)/\rho_\sigma(1) = \rho_\sigma(2) - \frac{\left|\rho_1^\sigma(1,2)\right|^2}{\rho_\sigma(1)} \tag{5.4}$$

As shown by Becke, the leading term of the Taylor expansion of the spherically averaged conditional pair probability (eq. 5.4) can be expressed as

$$P_{cond}^{\sigma\sigma}(\vec{r},s)=\frac{1}{3}\left[T_0^{\sigma}-\frac{1}{4}\frac{(\nabla\rho_\sigma)^2}{\rho_\sigma}\right]s^2+... \tag{5.5}$$

where the arguments $(\vec{r},s)$ denote the spherical average on a shell of radius s about the reference point $\vec{r}$ [[Becke 1985] and [Becke 1989]] and T_0^{σ} corresponds to the kinetic energy of a homogeneous system for spin σ. As expected, a small probability of finding a second same-spin electron near the reference (at position 2) implies that the reference electron is highly localised. Consequently, the localisation of the electron is dictated by the smallness of the expression

$$D_\sigma \equiv T_0^{\sigma}-\frac{1}{4}\frac{(\nabla\rho_\sigma)^2}{\rho_\sigma} \tag{5.6}$$

which is necessarily a positive quantity, since eq. (5.5) is a probability [Tal and Bader]. Notice that the relation between the electron localisation and eq. (5.6) is an inverse one; this means that high localisation implies small D_σ. Additionally, the quantity D_σ is not bounded from above. Thus, for convenience, it is suitable to introduce the following electron localisation function (*ELF*)

$$ELF=(1+\xi_\sigma^2)^{-1} \tag{5.7}$$

where $\xi_\sigma = D_\sigma / D_\sigma^0$ and

$$D_\sigma^0=\frac{3}{5}(6\pi^2)^{2/3}\rho_\sigma^{5/3} \tag{5.8}$$

corresponds to a uniform electron gas with spin density equal to the local value of $\rho_\sigma(\vec{r})$. Therefore, the ratio ξ_σ is a dimensionless localisation index which is calibrated with respect to homogeneous electron gas as reference. The transformation resulting in eq. (5.7) may well appear arbitrary, but it limits the range of ELF in a desirable fashion

$$0 \leq ELF \leq 1 \tag{5.9}$$

Thus, in the case of extreme delocalisation, ELF assumes values close to zero, while in the case of perfect localisation, it is equal to 1, and the ELF comes to 0.5 for an electron gas-like probability.

The ELF was first applied to analyse the shell structure of heavy atoms, as the typical approaches based on the features of the charge density are only reliable in the case of light atoms. Later, other chemists [[Silvi and Gatti] and [Silvi and Savin]] exploited ELF to study the nature of chemical bonding. Recently, De Santis and Resta utilised the ELF contour plots to investigate the aluminium surfaces and pointed out the advantages they have over the broadly used charge density plots [De Santis *et al.*]. Like the charge density, the ELF is a ground-state property, but it magnifies the bonding features and because of its dimensionless and bounded (see eq. (5.9)) character, it permits us to compare the bonding nature of different electron distributions on an absolute scale.

The ELF is implemented in the VASP code (see 2.3). As an example, the ELF contour plot of an isolated tungsten (W) atom is displayed in figure 18. It is worth mentioning that the ELF distribution is cut in the (001) x-y plane. For the sake of comparison, the ELF contour plots of Si, NaCl, Au, Pt and Al, which are displayed in the following sections, were calculated in addition to that of Ir. The computational model for FCC structure is illustrated in figure 10 and mind that VASP uses periodic boundary conditions.

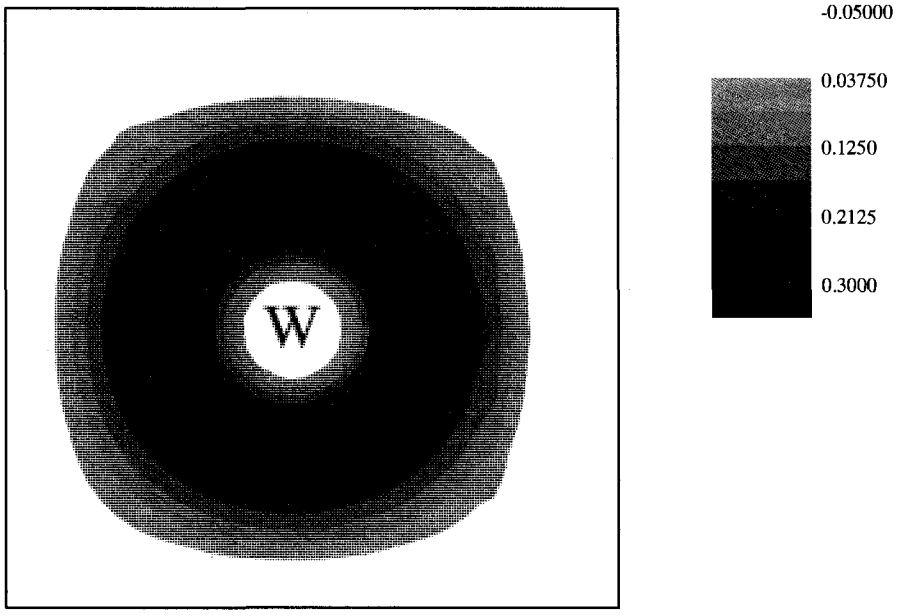

Figure 18: ELF contour plot cut in the (001) x-y plane for an isolated tungsten (W) atom.

5.1.2 Bonding topology and interactions

The gradient of the charge density is a dynamical system whose equilibrium points are the solutions of equation (5.10)

$$\vec{\nabla} \rho = 0 \qquad (5.10)$$

These critical points (CPs) are characterised by their *rank*, which is the number of nonzero eigenvalues of the Hessian matrix (the Jacobian of grad ρ) of the charge density scalar field and their *signature*, the algebraic sum of the signs of the eigenvalues. Thus, the critical points are noted (rank, signature). Equivalently, they can be typified by their index, which is the number of positive eigenvalues of the Hessian of the electron density. In the three-dimensional space, there are necessarily four types of critical points: local maxima of the potential or attractors of index 0 denoted as (3, -3) CPs, local minima or repellers of index 3 noted as (3, 3) CPs and two kinds of saddle points of index 2 labelled

(3, -1) CPs and (3, 1) CPs. Additionally, the number of critical points satisfies the Poincaré-Hopf formula

$$\sum_{CP}(-1)^{I(CP)} = \chi(M) \tag{5.11}$$

where the summation is performed over the CPs, I(CP) stands for the index of the critical point CP and $\chi(M)$ is the Euler characteristic of the manifold on which the gradient field is bounded, i.e. 1 for a molecule and 0 for a periodic system.

It has been observed that a bond connects two nuclei through a (3,-1) critical point, named a bond critical point, whose presence guarantees that the charge density along the bond path is always a maximum with respect to any neighbouring path. The local minima always appear in the middle of the cage structures and therefore, they are termed cage critical points. Similarly, the saddle points (3, 1) are called ring critical points, since they are always found in the middle of ring structures like that of the benzene molecule. The local maxima of the charge density correlate with the nuclei. Some local maxima, however, do not correspond to any atomic nucleus and they are consequently called pseudo-atoms. Pendas and co-workers have demonstrated that in materials with homonuclear bonds, the non-nuclear maxima (NNM) appear whenever there is an overlap between two regions in which the second radial derivative of the electron charge density is negative. Thus, NNM can be regarded as a normal step in the chemical bonding of homonuclear systems [[Pendás *et al.*] and [Luaña *et al.*]]

The basin of attraction of a dynamical system is defined as the set of points such that the initial conditions chosen in this set evolve to a particular ω-limit[7] point or attractor. Such sets are perceived only near the local maxima of the charge density. The union of a nuclear attractor or a local maximum and its basin of attraction are identified with the notion of chemical atom i.e. an open region containing a nuclear attractor with

[7] The ω-limit set is the set of all points to which a dynamical system approaches as $t\rightarrow\infty$. Similarly, the origin or the α-limit set is the set of all points to which the dynamical system converges as $t\rightarrow-\infty$. The points belonging to these sets are called ω-limit/ α-limit points (or the end and the origin of the trajectories of the dynamical system) for more details see reference [Hirsch *et al.*].

its basin of attraction and delimited by surfaces through which the flux of grad $\rho(\mathbf{r})$ is zero.

The laplacian of the charge density is related to the sum of the potential and kinetic energies through the virial theorem [Bader 1991]

$$\left(\hbar^2/4m_e\right)\nabla^2\rho = 2T + V \tag{5.12}$$

This implies that in the regions where $\nabla^2\rho < 0$, the potential energy has the dominant contribution to lowering the energy of the system, while for regions where the laplacian of the charge density assumes positive values, i.e. for $\nabla^2\rho > 0$, the main contribution to the total energy comes from the kinetic energy. These two regimes defined by the predominance of either potential or kinetic energy are actually associated with the competition between charge concentration in the interatomic surface defined by the directions corresponding to the negative eigenvalues of the Hessian of the charge density at bond CP and the charge depletion of the bonding path at this CP due to electron transfer from one ion to another. Consequently, only two types of bonding interactions can be distinguished. Following Bader's terminology, we shall refer to these interactions as shared-electron and closed-shell interactions.

In a shared-electron interaction, which gives rise to covalent, dative and metallic bonds and for which $\nabla^2\rho < 0$, the nuclei are bound together as a consequence of the diminution of the potential energy associated with charge shared between the nuclei. As for closed-shell interactions which generate ionic, hydrogen, electrostatic and van der Waals bonds and for which $\nabla^2\rho > 0$, the contribution of the kinetic energy to the local expression of the virial is larger than the contribution of the potential energy. This situation leads to a relative charge depletion of the interatomic surface [[Bader 1990] and [Bader 1991]].

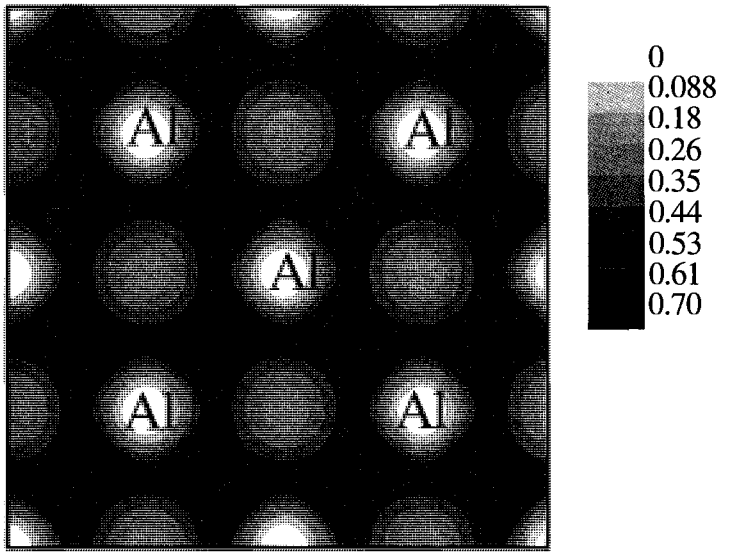

Figure 19a: ELF contour plot of Al on (001) x-y plane.

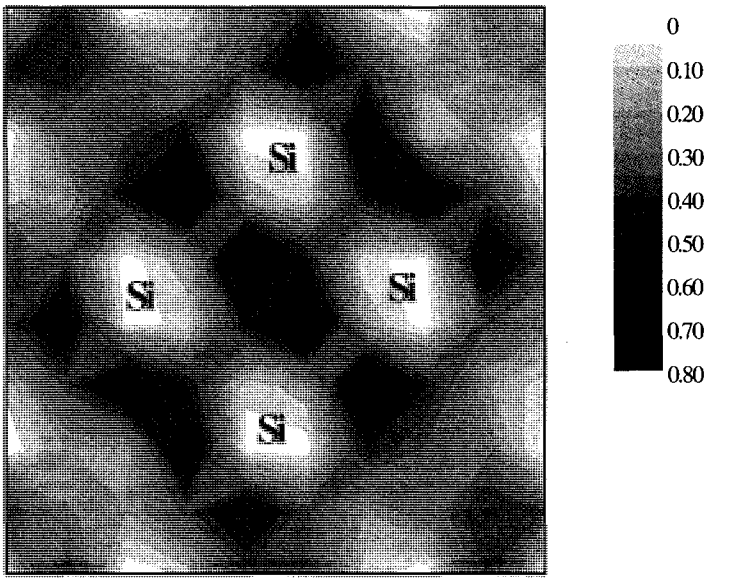

Figure 19b: ELF contour plot of Si on (001) x-y plane.

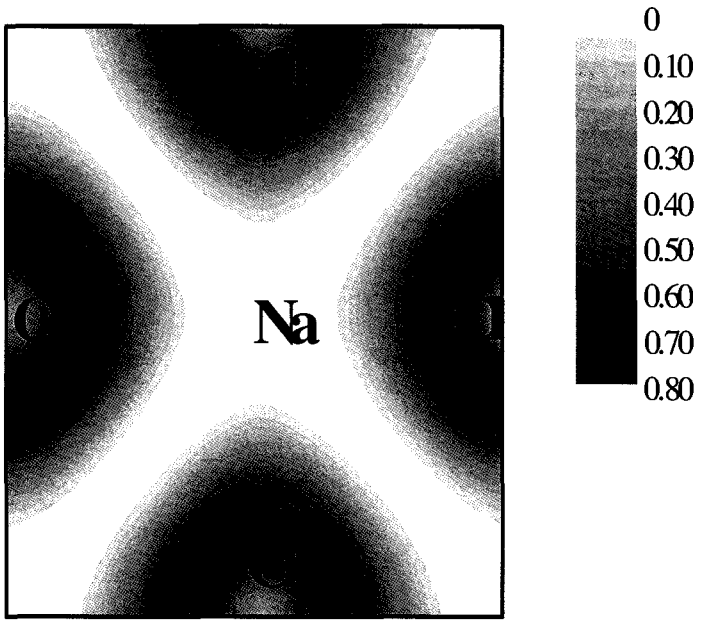

Figure 19c: ELF contour plot of NaCl on (001) x-y plane.

These descriptions of electron-shared and closed-shell interactions are illustrated in the ELF contour plots of typical metallic, highly localised covalent and ionic systems displayed in figures 19a-c. In the case of NaCl, the interionic region appears empty of any charge due to electron transfer which concentrates the valence shell charges around the acceptor atoms (i.e. Cl in the case of NaCl), whilst in the covalent systems, the valence shell charges are shared through spin-orbital overlaps in the internuclear region. Moreover, the main difference between the metallic systems and well-known covalent crystals such as silicon is the delocalisation of the electron distribution through out the interatomic space, which creates a charge network around the ions [Silvi and Gatti]. In the next section, we shall turn our attention to the quantitative treatment of the spin-orbital overlaps or bond order indices, which quantify the strength of the covalent bond.

5.2 Bond strength

The strength of the covalent bond is often quantified by means of bond order index, which measures the multiplicity of the chemical bond In Lewis' classical picture of covalent bond, bond order simply corresponds to the number of the shared electron pairs between the bonded atoms. In the quantum mechanical description of covalent bonding, where the covalence results from spin interactions between the ions, one can set up a mathematical definition in terms of the overlap of spin-orbital wave functions and the electronic density matrix. Before stating this definition and examining its consequences, it is of importance to recall the concept of biorthogonality, however.

5.2.1 Biorthonormal functions and density matrix

Let $\{\phi_i\}$ be a set of linearly independent functions. The vector space Ω spanned by this set contains all the linear combinations of these functions

$$\phi = C^i \phi_i \tag{5.13}$$

where the set $\{\phi_i\}$ constitutes a covariant basis set with respect to which the coefficients C^i form a contravariant vector. Mind that here the Einstein summation convention has been used. The overlap matrix between the basis functions is given by

$$S_{ij} = \langle \phi_i | \phi_j \rangle = \int \phi_i^* \phi_j d\tau \tag{5.14}$$

where $d\tau$ refers to all the variables on which the basis functions depend. The hermitian matrix $[S_{ij}]$ is also called the covariant metric and its inverse, the contravariant hermetian metric $[S^{ij}]$, allows us to construct the contravariant basis set $\{\phi^i\}$.

$$\phi^i = \phi_j S^{ji} \tag{5.15}$$

Similar to eq. (5.13), one can write a contravariant expansion whose coefficients form a covariant vector related to the corresponding contravariant vector through the metric

$$\phi = C_i \phi^i \tag{5.16}$$

$$C^i = S^{ij} C_j \tag{5.17}$$

Mind that by definition, the components of the covariant and contravariant metrics satisfy the following relationship

$$S_{ij} S^{jk} = S^{kj} S_{ji} = \delta_i^k \tag{5.18}$$

where δ_i^k is the Kronecker delta. From this relation, it follows that the dual basis sets meet the biorthonormality property expressed by equation (5.19)

$$\left\langle \phi^i \middle| \phi_j \right\rangle = \delta^i_j \tag{5.19}$$

For more details on biorthonormal functions, the reader can consult references [[Dahl] and [De Giambigi *et al.*]]

As for the density matrix, here we shall briefly outline some of its aspects; nonetheless, an extended discussion on this subject can be found in reference [McWeeny]. The density operator P for a system described by state vector $|\psi\rangle$ is defined as

$$P = |\psi\rangle\langle\psi| \tag{5.20}$$

In terms of wave functions, the density operator is identified with an integral whose kernel is constructed from any two functions $\psi_k(q)$ and $\psi_\lambda(q')$. The action of P on φ is then given by

$$P\varphi = \psi_\kappa(q)\int\psi_\lambda^*(q')\varphi(q')dq' = \psi_\kappa(q)\langle\psi_\lambda|\varphi\rangle \tag{5.21}$$

For a pure state, the density matrix meets the following properties

$$P^2 = P \tag{5.22}$$

$$trP = 1 \tag{5.23}$$

For an N-particle system, which is of interest to us, these conditions are slightly modified

$$P^2 = P \tag{5.24}$$

$$trP = N \tag{5.25}$$

Notice that for strongly interacting particles, it is not legitimate to apply the aforementioned procedure to obtain P from the wave functions, since one has to deal with the system as a whole. In order to extract information on the particles forming such systems, one resorts to the reduced density matrix, whose diagonal element determines the probability of finding any n of the N particles, in any order, at n selected points 1,2,…,n of the configuration space, and which is given by

$$P_n(1,2,..n;1',2',...n') = N(N-1)...(N-n+1)\int\psi(1,..N)\psi^*(1',...n',n+1,...N)d\tau_{n+1}...d\tau_N \tag{5.26}$$

where $d\tau$, as before, refers to all the variables on which the wave functions depend. The reduced density matrix is used in the calculation of ELF to estimate the von Weizsäcker kinetic energy functional D_σ.

5.2.2 Bond order (BO) index

The bond order (BO) index B_{AB} between atoms A and B is defined as [Mayer 1986]

$$B_{AB} = 2\sum_{\mu\in A}\sum_{\nu\in B}\left[(P^{\alpha}S)_{\mu\nu}(P^{\alpha}S)_{\nu\mu} + (P^{\beta}S)_{\mu\nu}(P^{\beta}S)_{\nu\mu}\right] \qquad (5.27)$$

where, as before, P is the first order density matrix for spins α and β, and S is the matrix of the overlap of the bases or their metric. The bond order index accounts for the non-classical exchange effects in the bonding as it is related to the electrostatic exchange energy components. The full derivation of these proportionalities between BO and different components of the exchange energy, which are summarily listed in appendix F, is given in reference [Mayer 1983b]. As pointed out at the beginning of this section, BO measures the degree at which the electrons are shared in the bond and hence it gives an estimation of the strength of bonds created through electron-shared interactions. Moreover, it is the theoretical equivalent of the classical concept of bond order or bond multiplicity.

In contrast to its classical counterpart, BO often assumes non integer values. The deviation from integer values can be interpreted as the effects of polarity differences between the ions or the electronic delocalisation [1Mayer 1986]. As we are studying transition metals, the discrepancy between the calculated values of BO and the expected value (i.e.1 pair of electrons per bond) can only reflect the lack of localisation along the bond path as discussed in section 5.1.2.

5.2.3 LCAO approach

In order to calculate the BO indices, an FCC-based cluster of 63 atoms, which is portrayed in figure 20, was constructed. To minimize the surface effects, which result from the lack periodicity of the crystals occupying the faces of the cluster, only the bond orders between the central atom, which is coloured gray in figure 20, and its first nearest neighbours (FNN) are computed. Notice that the values of BO for atoms separated by distances beyond the FNN range are negligible.

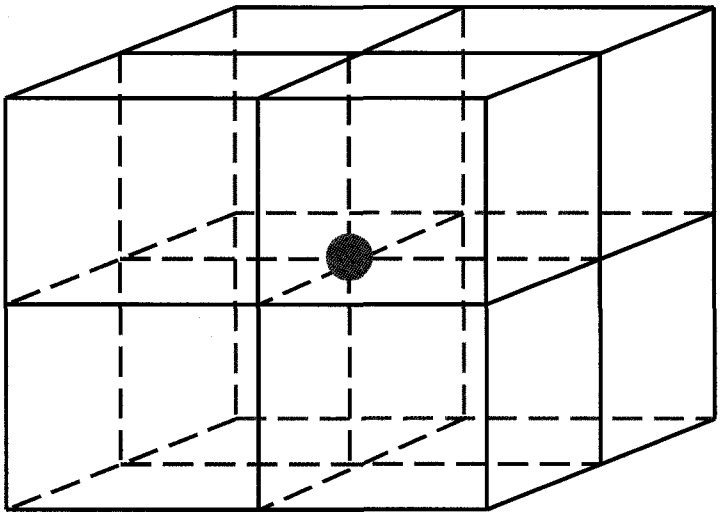

Figure 20: The 63-atom cluster model used in the calculation of bond order (BO). The model consists of eight identical FCC based unit cells as shown in figure 10.

The calculation of BO was performed using the DFT based DMol3 package (see chapter II for an outline of DFT) with a cutoff energy of 442 eV. This package differs from VASP in that it employs the linear combination of atomic orbitals (LCAO) technique to solve the Kohn-Sham equations. In this approach as in all self-consistent computational schemes, one starts with test functions $\phi_{k,\sigma}$ expressed as an expansion of a basis set $\{\varphi_j\}$, which allows transforming the Kohn-Sham equations to a generalised eigenvalue problem discussed in section 2.3.2. In contrast to VASP, which uses plane waves as its basis set, DMol3 extends the test functions in terms of a series of numerically tabulated spherical-atom orbitals. The numerical integrations are also performed using a different technique which is explained in reference [Delly]. Notice that this package like VASP has both GGA and LDA options for computing the exchange-correlation energy and as before, the GGA approach was used in all the calculations. The calculated values of BO for a selection of FCC metals are plotted in figure 22.

5.3 Rationalisation of the abnormal elastic properties of Ir

As shown in figure 21a, the ELF contour plot of Au displays a spherical distribution, whereas the valence electrons of Pt (fig. 21b) exhibit minor directional features, although they are relatively widely spread in the interatomic regions. As to Ir (fig.21c), its electrons tend to be localised between the ions, thus forming thick rod-like bonds somewhat similar to the cylindrical-shaped bonds of Si. However, in any of these cases, no strong covalent bonding can be detected, since the maximal value of ELF never exceeds 0.5 even for Ir. The observed directional features are simply related to the *d*-band filling, as all transition metals with partially occupied *d*-bands show such topological characteristics.

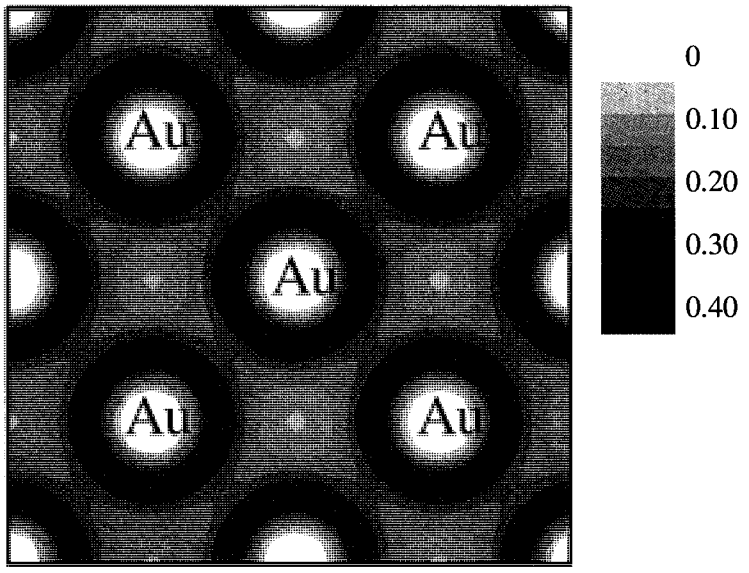

Figure 21a: ELF contour plot of Au on (001) x-y plane.

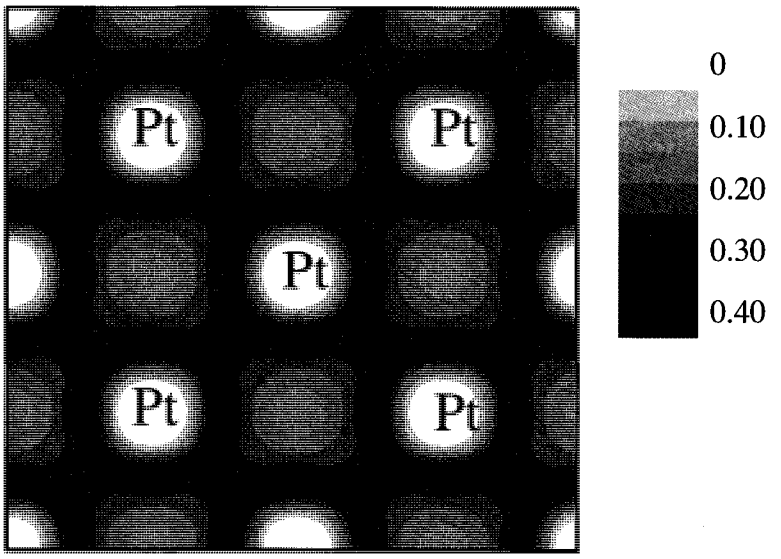

Figure 21b: ELF contour plot of Pt on (001) x-y plane.

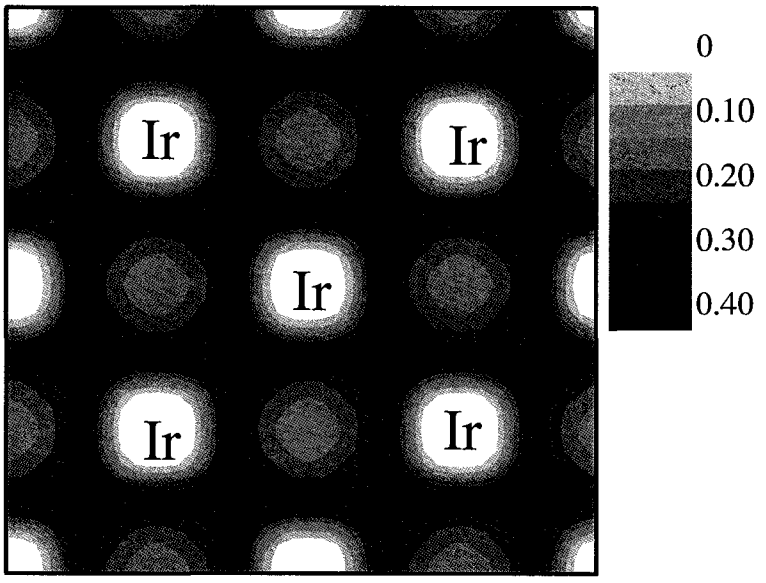

Figure 21c: ELF contour plot of Ir on (001) x-y plane

In the case of Al (see fig. 19a), the bulk of the electrons assume a jellium-like character, whilst sporadic high covalency (the dark spots in fig. 18a, for which ELF takes values close to 0.7) appears near the ions. Furthermore, the ELF plot of Al visibly shows rectangular directional bonds somewhat analogous to the valence electron distribution of Ir in the interionic regions. These angular features of the Al bonds, which originate from the *s-p* orbitals hybridisation, are responsible for the long range of deformation it sustains (see section 4.3) and their resemblance to the bond directionality of Ir electron distribution accounts for the observed similarity between its fatigue fracture and failure of Ir crystals [Panfilov *et al.*].

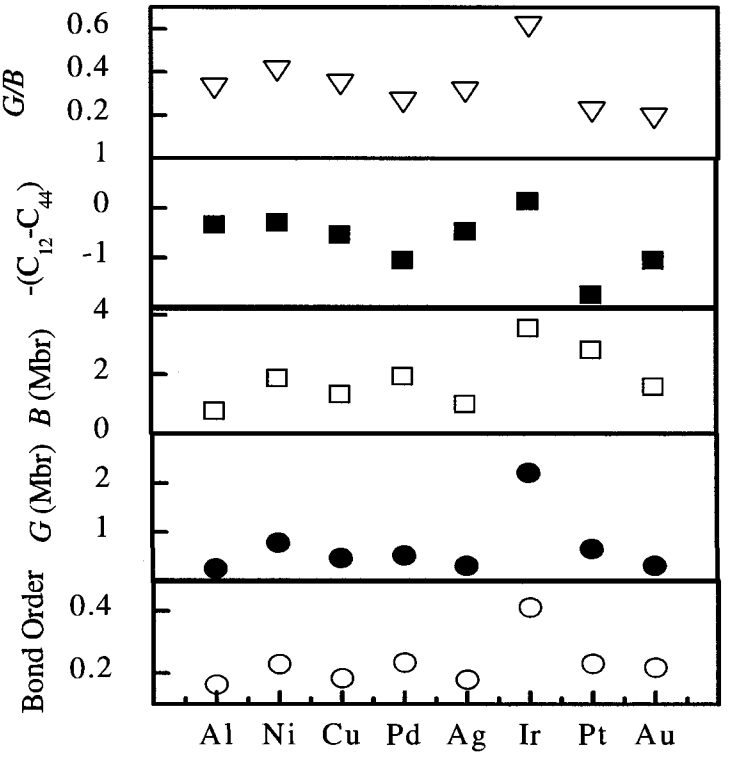

Fig. 22: The calculated bond orders of selected fcc elements versus experimentally measured [Simmons and Wong] shear (G), bulk (B) moduli, negative Cauchy pressure $-(C_{12}-C_{44})$ and G/B.

In figure 22 the BO values of a selection of FCC metals together with the experimental values of their shear modulus G and bulk modulus B [Simmons and Wang] are displayed. For convenience, the order of the elements along the x-axis in figure 22 is sorted according to their atomic numbers in the periodical table. With the purpose of investigating the correlation between BO, bond directionality and ductility of metals, the Cauchy pressure (– (C_{12}-C_{44})) and G/B ratio are also plotted. The Cauchy pressure provides a reliable macroscopic measure of bond directionality [Chen *et al.* 2003] and for a short discussion on G/B ratio, the reader is referred to section 3.1. It is evident from the plots that the BO, G and B curves present similar trends. All these three curves reach their peak values at Ir and have their minimum at Al. Nonetheless, the G curve is better correlated with BO, as is testified by the fact that the curve G as a function of BO has the largest linear correlation coefficient R_L (see table 4). Since the bond order index is proportional to the exchange component of the leading interatomic electrostatic term in the Hamiltonian of the system, it becomes clear that G is essentially related to the spin-orbital coupling which dictates the strength of the bonds.

BO *vs*	*G*	*B*	*G/B*	*Cauchy Pressure*
R_L	0.96957	0.89317	0.73139	0.34238

Table 4: The linear correlation coefficient R_L for different elastic constants plotted against BO.

Furthermore, The Cauchy pressure and G/B curves almost follow the same trend; however, they are only partly correlated to BO. The Cauchy pressure curve agrees with our ELF contour plots as it associates high values to metals with intense directional features (like Ir, Al and Ni) and low values to those with roughly symmetric electronic distributions (like Au and Pt). The partial correlation of G/B with BO and Cauchy pressure indicates that the brittleness is partly governed by the strength and directionality of the bonds. Thus the intrinsic brittleness of Ir can be explained as follows: the relatively high spin coupling of Ir atoms results in strong bonds that formidably resist deformation. In addition, once the bond is broken, its angular character renders the bond reformation hardly realisable (see also section 4.3), since the electrons have to be reorganized

according to specific angles [Ogata *et al.* 2002]. In other words, the directional character of Ir bonds reduces their mobility [Haydock], hence the brittle failure of the material.

Chapter VI
Conclusion

6.1 Thesis Achievements

Within the frame of the present work, different computational tools, namely DFT based VASP package, which allows calculating the total electronic energy, DOS and ELF, and DMol3 package, which has been exploited in computing the BO values of a selection of FCC metals, were used to investigate the ideal strengths of FCC metals and in particular the abnormal shear modulus of Ir. Furthermore, through a semi-empirical approach, bulk and shear moduli of covalently bonded crystals were studied. The results of these researches can be summarised as follows:

1- I have developed semi-empirical formulae for the shear modulus of covalently bonded solids for the first time and I have improved Cohen's bulk modulus for covalent crystals by using Philip's ionicity parameter. These formulae were then employed in analysing the effects of atomic-scale parameters on the ratio *G/B* and it was found that the bond length is the predominant cause of brittleness in covalent crystals, despite the fact that ionicity enhances ductility;

2- Using VASP, the ideal strengths of eight FCC metals, specifically Ag, Al, Au, Cu, Ir, Ni, Pd and Pt, were calculated both for shear along {111}<112> slip system and for tension along {110} and {111} planes. My results show that directionally bonded metals usually withstand longer ranges of deformation as expected and that FCC metals attain smaller ideal tensile strengths when pulled

along {111} direction. Moreover, the ratio of ideal shear and tensile strengths, $\tau_m / \sigma_{<111>}$, was proposed as a new indicator of ductility that assigns values larger than 0.5 to brittle crystals but contrary to the ratio *G/B*, it distinguishes metals with angular bonding like Al from those with symmetric electron distributions;

3- In the study of the peculiarly high shear modulus of Ir, I found that the intrinsic properties of Ir bonds are involved different fashions. Amongst the FCC metals examined in the present thesis, Ir bonds exhibit the highest BO value, which is an indicator of spin coupling and hence bond strength. Moreover, the ELF contour plot of Ir demonstrates the intensely directional features of its bonds, while indicating that Ir bonds have larger covalence only compared to other FCC metals. Thus, I concluded that the anomalously high shear modulus of Ir results from the fact that the strong bonds of Ir formidably resist distortion and once they are broken, the extremely angular features of its bond do not allow the bond reformation process to occur successfully. This observation is also indicative of the limited bond mobility of Ir;

4- The comparative study of the EFL contour plots of Al and Ir permitted to elucidate the similarities observed between iridium's brittle failure and the fatigue fracture in Al, as both metals possess rectangular valence electron distributions. These directional features also account for the long ranges of deformation suffered by these two FCC crystals. It is noteworthy to mention that in the case of Ir, the electrons tend to be concentrated in the bonding region between the ions, whilst Al electrons are rather widely spread in that region. This observation, together with BO calculations, rationalises the notable differences between their elastic moduli;

Based on these results, two articles have been written, which were accepted for publication in scientific journals (see appendix G), and a third paper is in preparation.

6.2 Suggested future Work

As for the future work, more research needs to be carried out in the following areas:

1- The formulae for shear modulus of covalent crystals can be improved by introducing parameters describing bond bending and bond stretching features and the investigation of the effects of these geometric factors on brittleness of covalent materials is wanted;

2- The semi-empirical formulae found for covalent materials can be generalised to include simple and transition metals, ionic crystals and alloys;

3- The abnormally large shearability of Pd, a very ductile metal, needs more investigation;

4- A criterion similar to the ratio, $\tau_m / \sigma_{<111>}$, can be elaborated for BCC metals, which would allow for broader comparison between different metals;

5- Some alloys of Ir have been scrutinised by K. Chen and collaborators recently; however, more investigation is required to determine the effects of the low bond mobility of Ir on its alloying capabilities;

6- Appropriate mathematical techniques can be used to reduce the information provided by ELF to a number of scalar parameters of manageable size, so that the localised character of the electron distribution would be linked to the mechanical properties of materials in a quantitative fashion;

References

[Ángyán *et al.*] J. G. Ángyán, M. Loos and I. Mayer, *Journal of Physical Chemistry*, "Covalent bond orders and atomic valence indices in the topological theory of atoms in molecules", 98, 5244-5248 (1994).

[Bader 1990] R. F. W. Bader, *Atoms in Molecules-A Quantum Theory*, University of Oxford Press (1990).

[Bader 1991] R. F. W. Bader, *Chemical Reviews*, "A quantum theory of molecular structure and its Applications", 91, 893-928 (1991).

[Bass] J. D. Bass, *Mineral Physics and Crystallography, A Handbook of Physical Constants* (1995), available at http://www.agu.org/reference/minphys/7_bass.pdf.

[Becke 1985] A. D. Becke, *International Journal of Quantum Chemistry*, "Local exchange-correlation approximations and first-row molecular dissociation energies", 27, 585-594 (1985).

[Becke 1989] A. D. Becke, *International Journal of Quantum Chemistry: Quantum Chemistry Symposium*, "Basis-set-free density-functional quantum chemistry", 23, 599-609 (1989).

[Becke *et al.*] A. D. Becke and K. E. Edgecombe, *Journal of Chemical Physics*, "A simple measure of electron localization in atomic and molecular systems", 92, 5397-5403 (1990).

[Berrah *et al.*] S. Berrah, H. Abid, A. Boukortt and M. Sehli, *Turkish Journal of Physics*, "Band Gap of Cubic AlN, GaN and InN Compounds Under Pressure", 30, 513-518 (2006).

[Bloch] F. Bloch, *Zeitschrift für Physik A*, "Über die Quantenmechanik der Electronen in Kristallgittern", 52, 555-600 (1929).

[Blöchl] P. E. Blöchl, *Physical Review B*, "Projector augmented-wave method", 50, 17953-17979 (1994).

[Bouarissa *et al.*] N. Bouarissa and K. Kassali, *Superlattices and Microstructures*, "elastic constants of lattice matched and mismatched $Ga_{1-x}InN_yAs_{1-y}$ alloys", 35, 115-124 (2004).

[Bouhafs *et al.*] B. Bouhafs, H. Aourag and M. Certier, *Journal of Physics: Condensed Matter*, "Trends in band-gap pressure coefficients in boron compounds BP, BAs and BSb", 12, 5655-5668 (2000).

[Chen *et al.* 2003] K. Chen, L. Zhao and J. S. Tse, *Journal of Applied Physics*, "*Ab initio* study of elastic properties of Ir and Ir_3X compounds", 93, 2414-2417 (2003).

[Chen *et al.* 2004] K. Chen, L. Zhao and J. S. Tse, *Physics Letters A*, "Elastic properties of platinum Rh and Rh_3X compounds", 331, 400-403 (2004).

[Chetty *et al.*] N. Chetty, A. Munoz and R. M. Martin, *Physical Review B*, "First-principles calculation of the elastic constants of AlAs", 40, 11934-11936 (1989).

[Christensen *et al.*] N. E. Christensen, S. Satpathy and Z. Pawlowska, *Physical Review B*, "Bonding and ionicity in semiconductors", 36, 1032-1050 (1987).

[Clerc 1998] D. G. Clerc, *Journal of Materials Science Letters*, "Mechanical hardness: atomic-level calculations for diamond-like materials", 17, 1461-1462 (1998).

[Clerc 1999] D. G. Clerc, *Journal of Physics and Chemistry of Solids*, "Mechanical hardness and elastic stiffness of alloys: semiempirical models", 60, 83-102 (1999).

[Clerc *et al.*] D. G. Clerc and H. M. Ledbetter, *Journal of Physics and Chemistry of Solids*, "Mechanical hardness: a semiepirical theory based on screened electrostatics and elastic shear", 59, 1071-1095 (1998).

[Cline *et al.*] C. F. Cline, H. L. Dunegan and G. W. Henderson, *Journal of Applied Physics*, "Elastic Constants of Hexagonal BeO, ZnS, and CdSe", 38, 1944-1948 (1967).

[Cohen 1985] M. L. Cohen, *Physical Review B*, "Calculation of bulk moduli of diamond and zinc-blende solids", 32, 7988-7991 (1985).

[Cohen 1993] M. L. Cohen, *Science*, "Predicting Useful Materials", 261, 307-308 (1993).

[Cohen 2000] M. L. Cohen, *Annual Review of Materials Science*, "The theory of real materials", 30, 1-26 (2000).

[Dahl] J. P. Dahl, *International Journal of Quantum Chemistry*, "Biorthonormal basis sets and the interaction between one-electron atoms", 14, 191-207 (1978).

[De Giambigi *et al.*] M. S. De Giambiagi, M. Giambiagi and F. E. Jorge, *Theoretica Chimica Acta*, "Bond index: relation to second-order density matrix and charge fluctuations", 68, 337-341 (1985).

[Delley] B. Delley, *Journal of Chemical Physics*, "An all-electron numerical method for solving the local density functional for polyatomic molecules", 92, 508-517 (1990).

[De Santis *et al.*] L. De Santis and R. Resta, *Surface Science*, "Electron localization at metal surfaces", 450, 126-132 (2000).

[Drief *et al.*] F. Drief, A. Tadjer, D. Mesri and H. Aourag, *Catalysis Today*, "First principles study of structural, electronic, elastic and optical properties of MgS, MgSe and MgTe", 89, 343-355 (2004).

[Dunstan *et al.*] D. J. Dunstan, A.D. Prins, B. Gil and J.P. Faurie, *Physical Review B*, "Phase transitions in CdTe/ZnTe strained-layer superlattices", 44, 4017-4020 (1991).

[Eberhart 1996] M. E. Eberhart, *Acta Materialia*, "The metallic bond: elastic properties", 44, 2495-2504 (1996).

[Eberhart 2001] M. E. Eberhart, *Physical Review Letters*, "Charge-density-shear-moduli relationships in aluminium-lithium alloys", 87, 205503 (2001).

[Eberhart 2002] M. E. Eberhart, *Foundations of Chemistry*, "Quantum mechanics and molecular design in the twenty first century", 4, 201-211 (2002).

[Edwards *et al.*] P. Edwards and M. J. Sienko, *International Reviews in Physical Chemistry*, "What is a metal?", 3, 83-137 (1983).

[Ferhat *et al.*] M. Ferhat, B. Bouhafs, A. Zaoui and H. Aourag, *Journal of Physics: Condensed Matter*, "First-principles study of structural and electronic properties of BSb", 10, 7995-8006 (1998).

[Feynman] R. P. Feynman, *Physical Review*, "Forces in molecules", 56, 340-343 (1939).

[Friedel] J. Friedel, *Physics of Metals*, Cambridge University Press, 340-408 (1969).

[Fu] C. L. Fu, *Journal of Materials Research*, "Electronic, elastic and fracture properties of trialuminide alloys: Al_3Sc and Al_3Ti", 5, 971-979 (1990).

[Gao *et al.*] F. Gao, J. He, E. Wu, S. Liu, D. Yu, D. Li, S. Zhang and Y. Tian, *Physical Review Letters*, "Hardness of covalent crystals", 91, 015502 (2003).

[Giambiagi et al.] M. Giambiagi, M. S. De Giambiagi, D. R. Grempel and C. D. Heynmann, *Journal de Chimie Physique*, "Sur la définition d'un indice de liaison (TEV) pour des bases non orthogonales. Propriétés et applications", 72, 15-22 (1975).

[Gilman] J. Gilman, *Electronic Basis of the Strength of Materials*, Cambridge University Press (2003).

[Gonzalez-Diaz *et al.*] M. Gonzalez-Diaz, P. Rodriguez-Hernandez and A. Munoz, *Physical Review B*, "Elastic constants and electronic structure of beryllium chalcogenides BeS, BeSe and BeTe from first-principles calculations", 55, 14043-14046 (1997).

[Gornostyrev *et al.*] Yu. N. Gornostyrev, M. I. Katsnelson, N. I. Medvedeva, O. N. Mryasov, A. J. Freeman and A. V. Trefilov, *Physical Review B*, "Pecularities of defect structure and mechanical properties of iridium: Results of *ab initio* electronic structure calculations", 62, 7802-7808 (2000).

[Hafner] J. Hafner, *Acta Materialia*, "Atomic-scale computational materials science", 48, 71-92 (2000).

[Hamann *et al.*] D. R. Hamann, M. Schlüter and C. Chiang, *Physical Review Letters*, "Norm-conserving pseudopotentials", 12, 1494-1497 (1979).

[Haydock] R. Haydock, *Journal of Physics C: Solid State Physics*, "The mobility of bonds at metal surfaces", 14, 3807-3816 (1981).

[Hecker *et al.*] S.S. Hecker, D.L. Rohr and F. Stein, *Metallurgical Transcriptions A*, "Brittle fracture in iridium", 9A, 481-488 (1978).

[Hirsch *et al.*] M. W. Hirsch, S. Smale and R. Devaney, *Differential equations, dynamical systems and an introduction to chaos*, 2nd edition, Elsevier Academic Press (2003).

[Hohenberg and Kohn] P. Hohenberg and W. Kohn, *Physical Review*, "Inhomogeneous electron gas", 136, B864-871 (1964).

[Ihm *et al.*] J. Ihm, A. Zunger and M. L. Cohen, *Journal of Physics C: Solid State Physics*, "Momentum-space formalism for the total energy of solids", 12, 4409-4422 (1979).

[Jones *et al.*] R. O. Jones and O. Gunnarsson, *Reviews of Modern Physics*, "The density functional formalism, its applications and prospects", 61, 689-746 (1989).

[Kamitani *et al.*] K. Kamitani, M. Grinsditch, J.C. Nipko, C. K. Loong, M. Okada and I. Kimura, *Journal of Applied Physics*, "The elastic constants of silicon carbide: A Brillouin-scattering study of 4H and 6H SiC single crystals", 82, 3152-3154 (1997).

[Kamran *et al.*] S. Kamran, K. Chen, L. Chen and L. Zhao, "A literature review on the quantum origins of elastic properties and mechanical hardness", report published by National Research Council Canada (NRC), Institute for Aerospace Research, Structure and Materials Performance Laboratory, LTR-SMPL-2006-0091, Ottawa (2006).

[Kerker] G. P. Kerker, *Journal of Physics C: Solid State Physics*, "Non-singular atomic pseudopotentials for solid state applications", 13, L1 89-94 (1980).

[Khenata *et al.*] R. Khenata, A. Bouhemadou, M. Shanoun, Ali, H. Reshak, H. Baltache and M. Rabah, *Computational Materials Science*, "Elastic, electronic and optical properties of ZnS, ZnSe and ZnTe under pressure", 38, 29-38 (2006).

[Kittel] C. Kittel, *Introduction to Solid State Physics*, 8th edition, John Wiley & Sons (2004).

[Knittle *et al.*] E. Knittle, R. M. Wentzcovitch, R. Jeanloz and M. L. Cohen, *Nature*, "Experimental and theoretical equation of state of cubic boron nitride", 337, 349-352 (1989).

[Kohn 1959] W. Kohn, *Physical Review*, "Analytic Properties of Bloch waves and Wannier Functions", 115, 809-821 (1959).

[Kohn 1964] W. Kohn, *Physical Review*, "Theory of the insulating state", 133, A171-181 (1964).

[Kohn and Sham] W. Kohn and L. J. Sham, *Physical Review*, "Self-consistent equations including exchange and correlation effects", 140, A1133-1138 (1965).

[Kontsevoi et al.] O. Y. Kontsevoi, Y. N. Gornostyrev and A. J. Freeman, *Journal of Minerals, Metals and Materials* (*JOM*), "Modeling the dislocation properties and mechanical behavior of Ir, Rh and their refractory alloys", 43-47 (March 2005).

[Kramers] H. A. Kramers, *Physica*, "Das Eigenwertproblem im eindimensionalen periodischen Kraftfelde", 2, 483-490 (1935).

[Kresse *et al.* 1996a] G. Kresse and J. Furthmüller, *Computational Materials Science*, "Efficiency of *ab-initio* total energy calculations for metals and semiconductors using a plane-wave basis set", 6, 15-50 (1996).

[Kresse *et al.* 1996b] G. Kresse and J. Furthmüller, *Physical Review B*, "Efficient iterative schemes for *ab initio* total-energy calculations using a plane-wave basis set", 54, 11169-11185 (1996).

[Kresse *et al.* 1999] G. Kresse and D. Joubert, *Physical Review B*, "From ultrasoft pseudopotentials to the projector augmented-wave method", 59, 1758-1775 (1999).

[Kresse *et al.* 2005] G. Kresse and J. Furthmüller, *VASP the GUIDE*, Institut für Materialphysik, Universität Wien, available at http://cms.mpi.univie.ac.at/VASP/ (2005).

[Kumar *et al.*] V. Kumar and B. S. R. Sastry, *Crystal Research and Technology*, "Thermal Expansion Coefficient of Binary Semiconductors", 36, 565-569 (2001).

[Kumazaki] K. Kumazaki, *Physica Status Solidi (a)*, "Elastic properties and ionicity of zero-gap semiconductors", 33, 615-623 (1976).

[Lam *et al.* 1984] P. K. Lam and M. L. Cohen, *Physics Letters*, "Dependence of lattice constants and bulk moduli on pseudopotential properties", 100A, 293-296 (1984).

[Lam *et al.* 1987] P. K. Lam, M. L. Cohen and G. Martinez, *Physical Review B*, "Analytic relation between bulk moduli and lattice constants", 35, 9190-9194 (1987).

[Langmuir] I. Langmuir, *Journal of the American Chemical Society*, "Isomorphism, isosterism and covalence", 41, 1543-1559 (1919).

[Lehoczky et al.] A. Lehoczky, D. A. Nelson and C. R. Whitsett, *Physical Review*, "Elastic Constants of Mercury Selenide", 188, 1069-1073 (1969).

[Levine] B. F. Levine, *Journal of Chemical Physics*, "Bond susceptibilities and ionicities in complex crystal structures", 59, 1463-1486 (1973).

[Levy] Mel Levy, *Proceedings of the National Academy of Sciences of the United States of America*, "Universal variational functions of electron densities, first-order density matrices, and natural spin-orbitals and solution of the v-representability problem", 76, 6062-6065 (1979).

[Lewis] G. N. Lewis, *Journal of the American Chemical Society*, "The atom and the molecule", 38, 762-785 (1916).

[Li et al.] T. Li, J. W. Morris and D. C. Chrzan, *Physical Review B*, "Ideal tensile strength of *B2* transition-metal aluminides", 70, 054107 (2004).

[Luaña *et al.*] V. Luaña, P. Mori-Sánchez, A. Costales, M. A. Blanco and A. Martin Pendás, *Journal of Chemical Physics*, "Non-nuclear maxima of the electron density on alkaline metals" 119, 6341 (2003).

[MacDonald] A. H. MacDonald, *Physical Review B*, "Comments on special points for Brillouin-zone integrations", 18, 5897-5899 (1978).

[Marchildon] Louis Marchildon, *Mécanique Quantique*, De Boeck, Belgium (2001).

[Martin] R. M. Martin, *Physical Review B*, "Elastic properties of ZnS structure semiconductors", 1, 4005-4011 (1970).

[Mayer 1983a] I. Mayer, *Chemical Physics Letters*, "Charge, bond order and valence in the *ab initio* SCF theory", 97, 270-274 (1983).

[Mayer 1983b] I. Mayer, *International Journal of Quantum Chemistry*, "Towards a chemical Hamiltonian", 23, 341-363 (1983).

[Mayer 1984] I. Mayer, *Chemical Physics Letters*, "Comments on the quantum theory of valence and bonding: choosing between alternative definitions", 110, 440-444 (1984).

[Mayer 1986] I. Mayer, *International Journal of Quantum Chemistry*, "Bond orders and valences from *ab initio* wave functions", 29, 477-483 (1986).

[McWeeny] R. McWeeny, *Reviews of Modern Physics*, "Some recent advances in density matrix theory", 32, 335-369 (1960).

[Meradji *et al.*] H. Meradji, S. Drablia, S. Ghermid, H. Belkhir, B. Bouhafs and A. Tadjer, *Physica Status Solidi* (*b*), "First-principles elastic constants and electronic structure of BP, BAs, and BSb", 1-5 (2004).

[Morris *et al.*] J. W. Morris, D. M. Clatterbuck, D.C. Chrzan, C. R. Krenn, W. Luo and M. L. Cohen, *Materials Science Forum*, "Elastic stability and the limits of strength", 426-432, 4429-4434 (2003).

[Nicholson] W. K. Nicholson, *Elementary Linear Algebra*, McGraw-Hill Ryerson, Toronto (2001).

[Norbeck et al.] J. M. Norbeck and R. McWeeny, *Chemical Physics Letters*, "The use of biorthonormal sets in valence bond calculations", 34, 206-210 (1975)

[Ogata *et al.* 2002] S. Ogata, Ju Li and S. Yip, *Science*, "Ideal pure shear strength of aluminium and copper", 298, 807-811 (2002).

[Ogata *et al.* 2004] S. Ogata, J. Li, N. Hirosaki, Y. Shibutani and S. Yip. *Physical Review B*, "Ideal shear strain of metals and ceramics", 70, 104104 (2004).

[Panfilov *et al.*] P. Panfilov, A. Yermakov, V. Dmitriev and N. Timofeev, *Platinum Metals Reiew*, " The plastic flow of iridium", 35, 196-200 (1991).

[Paxton *et al.*] A. T. Paxton, P. Gumbsch and M. Methfessel, *Philosophical Magazine Letters*, "A quantum mechanical calculation of the theoretical strength of metals", 63, 267-274 (1991).

[Pendas *et al.*] A. Pendás, M.A. Blanco, A. Costales, P. Mori-Sánchez and V. Luaña, *Physical Review Letters*, "Non-nuclear Maxima of the Electron Density", 83, 1930-1933 (1999).

[Penn] D. R. Penn, *Physical Review*, "Wave-number-dependent dielectric function of semiconductors", 128, 2093-2097 (1962).

[Perdew and Yue 1986] J. P. Perdew and W. Yue, *Physical Review B*, "Accurate and simple density functional for the electronic exchange energy: Generalized gradient approximation", 33, 8800-8802 (1986).

[Perdew *et al.* 1992] J. P. Perdew, J. A. Chevary, S. H. Vosko, K. A. Jackson, M. R. Pederson, D. J. Singh, and C. Fiolhais, *Physical Review B*, "Atoms, molecules, solids and surfaces: Applications of the generalized gradient approximation for exchange and correlation", 46, 6671- 6687 (1992).

[Philips 1968a] J. C. Philips, *Journal of Chemical Physics*, "Energy bands in cubic boron nitride", 48, 5740-5741 (1968).

[Philips 1968b] J. C. Philips, *Physical Review*, "Covalent bond in crystals I: elements of a structural theory", 166, 832-838 (1968).

[Philips 1968c] J. C. Philips, *Physical Review*, "Covalent bond in crystals II: Partially ionic binding", 168, 905-911 (1968).

[Philips 1968d] J. C. Philips, *Physical Review Letters*, "Dielectric definition of electronegativity", 20, 550-553 (1968).

[Philips 1970] J. C. Philips, *Reviews of Modern Physics*, "Ionicity of the chemical bond in crystals", 42, 317-356 (1970).

[Pugh] S. F. Pugh, *Philosophical Magazine*, "Relations between the elastic moduli and the plastic properties of polycrystalline pure metals", 45, 823-843 (1954).

[Pulay] P. Pulay, *Molecular Physics*, "*Ab initio* calculation of force constants and equilibrium geometries in polyatomic molecules I: Theory", 17, 197-204 (1969).

[Resta *et al.*] R. Resta and S. Sorella, *Physical Review Letters*, "Electron localization in the insulating state", 82, 370 (1999).

[Rice] J. P. Rice, *Journal of the Mechanics and Physics of Solids*, "Dislocation nucleation from a crack tip: An analysis based on the Peierls concept", 40, 239-271 (1992).

[Rodriguez-Hernandez *et al.* 1992] P. Rodriguez-Hernandez and A. Munoz, *Semiconductor Science and Technology*, "*Ab initio* calculations of electronic structure and elastic constants in AlP", 7, 1437-1440 (1992).

[Rodriguez-Hernandez *et al.* 1995] P. Rodriguez-Hernandez, M. Gonzalez-Diaz and A. Munoz, *Physical Review B*, "Electronic and structural properties of cubic BN and BP", 51, 14705-14708 (1995).

[Roundy *et al.* 1999] D. Roundy, C. R. Krenn, M. L. Cohen and J. W. Morris, *Physical Review Letters*, "Ideal shear strengths of fcc aluminum and copper", 82, 2713-272716 (1999).

[Roundy *et al.* 2001] D. Roundy, C. R. Krenn and M. L. Cohen, *Philosophical Magazine A*, "The ideal strength of tungsten", 81, 1725-1747 (2001).

[Shimada *et al.*] K. Shimada, T. Sota and K. Suzuki, *Journal of Applied Physics*, "First-principles study on electronic and elastic properties of BN, AlN, and GaN", 84, 4951-4958 (1998).

[Siethoff] H. Siethoff, *Journal of Applied Physics*, "Homopolar band gap and thermal activation parameters of plasticity of diamond and zinc-blende semiconductors", 87, 3301-3305 (2000).

[Silvestrelli *et al.*] P. L. Silvestrelli, N. Marzari, D. Vanderbilt and M. Parrinello, *Solid State Communications*, "Maximally-localized Wannier functions for disordered systems: Application to amorphous silicon", 107, 7-11 (1998).

[Silvi and Gatti] B. Silvi and C. Gatti, *Journal of Phyical Chemistry A*, "Direct space representation of the metallic bond", 104, 947-953 (2000).

[Silvi and Savin] B. Silvi and A. Savin, *Nature*, "Classification of chemical bonds based on topological analysis of electron localization functions", 371, 683-686 (1994).

[Simmons and Wang] G. Simmons and H. Wang, *Single Crystal Elastic Constants and Calculated Aggregate Properties: a Handbook*, 2nd edition, M.I.T. Press (1971).

[Srebrenik and Bader] S. Srebrenik and R. F. W. Bader, *Journal of Chemical Physics*, "Towards the development of the quantum mechanics of a subspace", 63, 3945-3961 (1975).

[Tal and Bader]Y. Tal and R. F. W. Bader, *International Journal of Quantum Chemistry Quantum Chemistry Symposium*, "Studies of the energy density functional approach I: kinetic energy", 12, 153-168 (1978).

[Teter *et al.*] M. P. Teter, M. C. Payne and D. C. Allan, *Physical Review B*, "Solutions of Schrödinger's equation for large systems", 40, 12255-12263 (1989).

[Vanderbilt] David Vanderbilt, *Physical Review B*, "Soft self-consistent pseudopotentials in a generalized eigenvalue formalism", 41, 7892-7895 (1990).

[Wills *et al.*] J. M. Wills, O. Eriksson, P. Söderlind and A. M. Boring, *Physical Review Letters*, "Trends of the elastic constants of cubic transition metals", 68, 2802-2805 (1992).

[Wood and Zunger] D. M. Wood and Alex Zunger, *Journal of Physics A: Mathematics and General*, "A new method for diagonalising large matrices", 18, 1343-1359 (1985).

[Wright] A. F. Wright, *Journal of Applied Physics*, "Elastic properties of zinc-blende and wurtzite AlN, GaN, and InN", 82, 2833-2839 (1997).

[Zunger and Cohen 1978] Alex Zunger and Marvin L. Cohen, *Physical Review B*, "first-principles nonlocal-pseudopotential approach in the density-functional formalism I: Development and application to atoms", 18, 5449-5472 (1978);

[Zunger and Cohen 1979] Alex Zunger and Marvin L. Cohen, *Physical Review B*, "first-principles nonlocal-pseudopotential approach in the density-functional formalism II: Application to electronic and structural properties of solids", 20, 4082-4108 (1979).

Appendix A: Atomic units

Atomic units (au) constitute a suitable unit system for atomic physics, electromagnetism, quantum electrodynamics and all the related fields such as DFT whose focus is the investigation of the properties of electrons. In the calculations performed in the aforementioned disciplines, one frequently encounters the following combinations $\hbar / m_e$ and $k_c q^2$, where $\hbar$ is the Planck's constant, m_e refers to the electron rest mass, k_c corresponds to the Coulomb electrostatic force constant and q is the elementary electron charge. For convenience, one wishes to set these expressions equal to unity, that is

$$\frac{\hbar}{m_e} = 1[E][L]^2 \tag{A1a}$$

$$k_c q^2 = 1[E][L] \tag{A1b}$$

where $[L]$ and $[E]$ refer to the new fundamental units of length and energy that fulfil eq. (A1). From these equations, it follows that

$$[L] = \frac{\hbar^2}{m_e k_c q^2} = 0.529177 \times 10^{-10}\, m = 1 bohr \tag{A2}$$

$$[E] = \frac{m_e \left(k_c q^2\right)^2}{\hbar^2} = 27.2113 eV = 1 hartree \tag{A3}$$

Thus the Bohr radius and the Hartree energy, which is the absolute value of the electric potential energy of a hydrogen atom, should be chosen as length and energy units. Furthermore, the basic properties of electron, i.e. its rest mass and elementary charge, will also serve as mass and charge units. This allows us to explicitly set $\hbar$ and k_c equal to unity. All the fundamental atomic units and their values in the SI system [Marchildon] are listed in table 5.

Quantity	*au Unit*	*Symbol*	*SI Value*
Length	Bohr radius	a_0	0.5291772×10^{-10} m
Mass	Electron rest mass	m_e	9.1093826×10^{-31} kg
Charge	Elementary charge	q	1.60217653×10^{-19} C
Angular momentum	Planck's constant	$\hbar$	1.05457168×10^{-34} Js
Energy	Hartree energy	E_h	4.35974417×10^{-18} J
Electrostatic force constant	Coulomb's constant	k_c	8.9875516×10^{9} Nm^2/C^2

Table 5: Fundamental atomic units (au) and their values in the SI system.

Appendix B: Adiabatic approximation

Assuming that the ions are held fixed at positions $\vec{r}_a$, the electronic wave function $\psi(\vec{r}_a,\vec{r}_i)$ satisfies equation 2.3. In order to show that the ionic wave function $v(\vec{r}_a)$ meet eq. (2.4), let's substitute eq. (2.2) in the Schrödinger equation corresponding to Hamiltonian 2.1

$$\left\{\sum_a \frac{1}{2M_a}\nabla^2 + \varepsilon(\vec{r}_a) - E(\vec{r}_a,\vec{r}_i)\right\} v(\vec{r}_a)\psi(\vec{r}_a,\vec{r}_i) = 0 \qquad \text{(B1)}$$

Here, as before, $\varepsilon(\vec{r}_a)$ is the electronic energy which satisfies eq. (2.3). The multiplication of eq. (B1) by $\psi^*(\vec{r}_a,\vec{r}_i)$ and its integration over $d\vec{r}_i$ yields eq. (2.4) provided that one neglects the terms involving the derivatives of $\psi(\vec{r}_a,\vec{r}_i)$ with respect to $\vec{r}_a$ and that the wave functions are normalised. For more details see reference [Marchildon] p. 439-441.

Appendix C: Proofs of the DFT theorems

Let's reformulate the two theorems in terms of the ground state (gs) properties E_{gs}, ψ_{gs} and n_{gs}

Theorem I

$$\int d\vec{r} v_{ex}(\vec{r}) n(\vec{r}) + Q[n] \geq E_{gs} \tag{C1}$$

Theorem II

$$\int d\vec{r} v_{ex}(\vec{r}) n_{gs}(\vec{r}) + Q[n_{gs}] = E_{gs} \tag{C2}$$

where $V_{ex} = \sum_{i=1}^{N} v_{ex}$ and

$$Q[n] = \min \langle \psi_n | T_0 + V_{ee} | \psi_n \rangle \tag{C3}$$

Here V_{ee} is the electron-electron interaction operator. It is also convenient to introduce the notation $|\psi_n^{\min}\rangle$ to denote a state that satisfies the right hand side of eq. (C3).

Proof of theorem I.

By the definition in eq. (C3), we can write

$$\begin{aligned} \int d\vec{r} v_{ex}(\vec{r}) n(\vec{r}) + Q[n] &= \int d\vec{r} v_{ex}(\vec{r}) n(\vec{r}) + \langle \psi_n^{\min} | T_0 + V_{ee} | \psi_n^{\min} \rangle \\ &= \langle \psi_n^{\min} | T_0 + V_{ee} + V_{ex} | \psi_n^{\min} \rangle \end{aligned} \tag{C4}$$

But by the minimal property of the ground state energy, we have

$$\left\langle \psi_n^{\min} \middle| T_0 + V_{ee} + V_{ex} \middle| \psi_n^{\min} \right\rangle \geq E_{gs} \tag{C5}$$

Addition of the eq. (C4) and (C5) completes the proof.

Proof of theorem II.

Again, using the minimal property of the ground state energy, we can write that

$$\left\langle \psi_{n_{gs}}^{\min} \middle| T_0 + V_{ee} + V_{ex} \middle| \psi_{n_{gs}}^{\min} \right\rangle \geq E_{gs} \tag{C6}$$

or

$$\left\langle \psi_{n_{gs}}^{\min} \middle| T_0 + V_{ee} + V_{ex} \middle| \psi_{n_{gs}}^{\min} \right\rangle \geq \left\langle \psi_{gs} \middle| T_0 + V_{ee} + V_{ex} \middle| \psi_{gs} \right\rangle \tag{C7a}$$

or

$$\int d\vec{r} v_{ex}(\vec{r}) n_{gs}(\vec{r}) + \left\langle \psi_{n_{gs}}^{\min} \middle| T_0 + V_{ee} \middle| \psi_{n_{gs}}^{\min} \right\rangle \geq \left\langle \psi_{gs} \middle| T_0 + V_{ee} + V_{ex} \middle| \psi_{gs} \right\rangle + \int d\vec{r} v_{ex}(\vec{r}) n_{gs}(\vec{r}) \tag{C7b}$$

which means that

$$\left\langle \psi_{n_{gs}}^{\min} \middle| T_0 + V_{ee} \middle| \psi_{n_{gs}}^{\min} \right\rangle \geq \left\langle \psi_{gs} \middle| T_0 + V_{ee} \middle| \psi_{gs} \right\rangle \tag{C8}$$

However, the definition of $\left| \psi_{n_{gs}}^{\min} \right\rangle$ implies that

$$\left\langle \psi_{n_{gs}}^{\min} \middle| T_0 + V_{ee} \middle| \psi_{n_{gs}}^{\min} \right\rangle \leq \left\langle \psi_{gs} \middle| T_0 + V_{ee} \middle| \psi_{gs} \right\rangle \tag{C9}$$

The last two equations hold simultaneously if and only if

$$\left\langle \psi_{n_{gs}}^{\min} \middle| T_0 + V_{ee} \middle| \psi_{n_{gs}}^{\min} \right\rangle = \left\langle \psi_{gs} \middle| T_0 + V_{ee} \middle| \psi_{gs} \right\rangle \tag{C10}$$

or

$$\left\langle \psi_{gs} \middle| T_0 + V_{ee} \middle| \psi_{gs} \right\rangle = Q[n_{gs}] \tag{C11}$$

Since,

$$\left\langle \psi_{gs} \middle| T_0 + V_{ee} + V_{ex} \middle| \psi_{gs} \right\rangle = E_{gs} \tag{C12}$$

substitution of eq. (C11) in eq. (C12) yields

$$\left\langle \psi_{gs} \middle| V_{ex} \middle| \psi_{ex} \right\rangle + Q[n_{gs}] = \int d\vec{r} v_{ex}(\vec{r}) n_{gs}(\vec{r}) + Q[n_{gs}] = E_{gs} \tag{C13}$$

In their original paper [Hohenberg and Kohn], Hohenberg and Kohn proved these theorems only for *v*-representable densities that is the densities obtained from antisymmetric wave functions associated with a Hamiltonian fixed by some external potential. The proofs presented here are due to Levy and cover a larger class of densities called the *N*-representable densities, which are simply defined for some antisymmetric wave functions [Levy]. Additionally, eq. (C11) implies that Levy's functional $Q[n]$ is identical to $F[n]$ defined by Hohenberg and Kohn (see eq. (2.7)) for *v*-representable densities.

Appendix D: The stiffness and compliance constants

The notion of stress is a generalisation of the concept of pressure, which refers to a force applied perpendicular to an area. In order to define a given stress σ, one needs to specify the direction normal to the plane subjected to the stress and the direction of the

stress itself. This is achieved through the use of subscripts, the first one of which refers to the direction of the stress, while the other one corresponds to the normal of the plane. Thus, we have the following second order stress tensor

$$[\sigma_{ij}]=\begin{pmatrix}\sigma_{11} & \sigma_{12} & \sigma_{13}\\ \sigma_{21} & \sigma_{22} & \sigma_{23}\\ \sigma_{31} & \sigma_{32} & \sigma_{33}\end{pmatrix} \tag{D1}$$

where 1, 2 and 3 refer to the main axes x, y and z, respectively.

In a similar fashion, one can write a 3×3 matrix representing the elements of the corresponding strain tensor $[\varepsilon_{ij}]$. Consequently, Hooke's law can be generalised as

$$\sigma_{ij} = \sum_{k,l} C_{ijkl}\,\varepsilon_{kl} \tag{D2}$$

or

$$\varepsilon_{ij} = \sum_{k,l} S_{ijkl}\,\sigma_{kl} \tag{D3}$$

where the C_{ijkl} are labelled elastic stiffness coefficients and the S_{ijkl} are referred to as the elastic compliance constants. The fourth order stiffness and compliance tensors are related to each other through the following equation

$$\sum_{i,j} C_{ijkl}\,S_{ijmn} = \delta_{kn}\delta_{lm} \tag{D4}$$

where δ_{ij} is Kronecker delta as usual.

In the case of a homogeneous cubic crystal, the nine elements of stress tensor and the corresponding strain tensor are reduced to six components due to symmetry.

Moreover, symmetry arguments allow us to reduce the number of independent stiffness constants as well

$$\begin{pmatrix}\sigma_{11}\\ \sigma_{22}\\ \sigma_{33}\\ \sigma_{23}\\ \sigma_{31}\\ \sigma_{12}\end{pmatrix} = \begin{pmatrix}C_{11} & C_{12} & C_{12} & 0 & 0 & 0\\ C_{12} & C_{11} & C_{12} & 0 & 0 & 0\\ C_{12} & C_{12} & C_{11} & 0 & 0 & 0\\ 0 & 0 & 0 & C_{44} & 0 & 0\\ 0 & 0 & 0 & 0 & C_{44} & 0\\ 0 & 0 & 0 & 0 & 0 & C_{44}\end{pmatrix}\begin{pmatrix}\varepsilon_{11}\\ \varepsilon_{22}\\ \varepsilon_{33}\\ \varepsilon_{23}\\ \varepsilon_{31}\\ \varepsilon_{12}\end{pmatrix} \quad \text{(D5)}$$

For more details, see reference [Kittel] p.73-80 and reference [Gilman] p. 9-23.

Appendix E: Supplement to Chapter IV

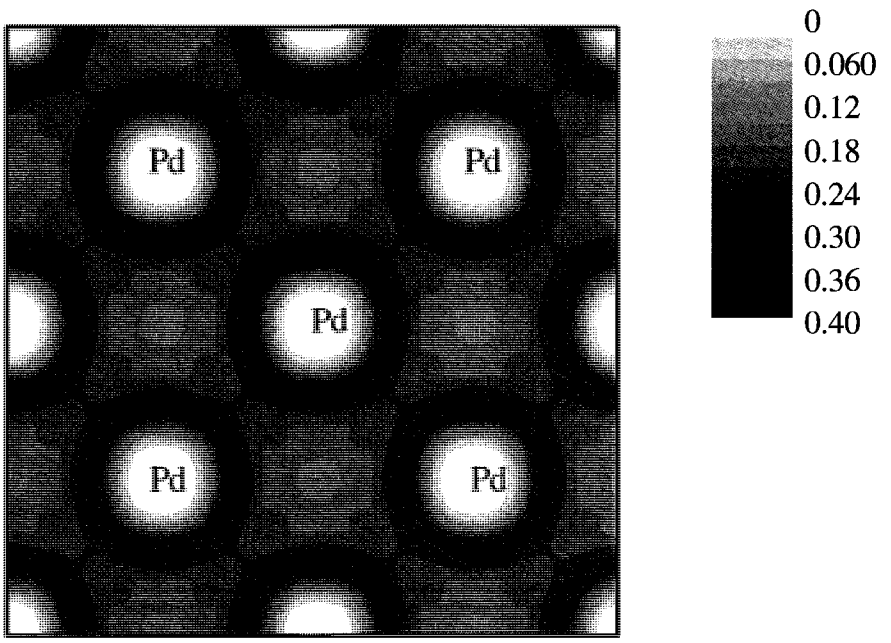

Figure 23: ELF contour plot of palladium.

Crystals	τ_{cle}	γ_{cle001}	σ_{100}	γ_{100}	σ_{vol}	γ_{vol}
Al	5.41	0.32	11.25	0.317	11.44	0.16
Ag	...	...	12.18	0.312	...	...
Au	...	...	14.39	0.279	...	...
Ni	...	...	34.52	0.324	...	...
Cu	...	...	23.07	0.345	...	...
Rh	15.18	0.34	...	...	34.91	0.15
Ir	22.5	0.28	51.014	0.262	48.96	0.14
Pt	12.19	0.35	30.09	0.286	31.67	0.15
Pd	9.37	0.36	22.757	0.322	21.43	0.15

Table 6: Cleavage tension τ_{cle} normal to (100) plane, tension normal to (100) plane σ_{100} and volumetric tension σ_{vol} with the corresponding strain values. Notice that all the stresses are in GPa and that the cleavage tension was calculated using the method explained in reference [Fu].

Appendix F: Proportionality of BO with the electrostatic terms in the Born-Oppenheimer Hamiltonian

In the case of a diatomic molecule with ionic constituents A and B, the electronic Born-Oppenheimer Hamiltonian in atomic units is given by

$$H = \sum_{A<B} \frac{Z_A Z_B}{R_{AB}} - \frac{1}{2}\sum_i \nabla_i^2 - \sum_{A,i} \frac{Z_A}{r_{Ai}} + \frac{1}{2}\sum_{\substack{i,j \\ (i\neq j)}} \frac{1}{r_{ij}} \qquad \text{(F1)}$$

Here, as in chapter II, the subscripts i and j refer to the electronic coordinates. Mayer uses the second quantization formalism for nonorthogonal orbitals in order to rewrite the physical Hamitonian expressed in eq. (F1) as a chemical Hamiltonian, which allows partitioning the energy into different terms that are chemically relevant. The chemical Hamiltonian he obtains is composed of six terms, amongst which three are proportional to BO. The details of the derivation can be found in reference [Mayer 1983b]. Here we shall simply state the aforementioned terms and their proportionality relation with BO:

a. H_2 describes the electrostatic interactions in the point-charge approximation; in other words, it corresponds to the largest Coulomb electrostatic interactions between the ions and electrons;

b. H_3 corresponds to the electrostatic effects arising from the deviation of the real charge distribution from the pointlike distribution treated by H_2;

c. H_4 accounts for the effects induced by the overlaps between the atomic orbitals;

These three terms are given by

$$\langle H_2 \rangle = \sum_{A<B} \left(\varepsilon_{AB}^{point} + \varepsilon_{BA}^{point} \right) \tag{F2}$$

$$\langle H_3 \rangle = \sum_{A<B} \left(\varepsilon_{AB}^{penetr} + \varepsilon_{BA}^{penetr} \right) \tag{F3}$$

$$\langle H_4 \rangle = \sum_{A<B} \left(\varepsilon_{AB}^{overl} + \varepsilon_{BA}^{overl} \right) \tag{F4}$$

where

$$\varepsilon_{AB}^{point} = \frac{1}{2} \cdot \frac{1}{R_{AB}} \left((Z_A - q_A)(Z_B - q_B) - \sum_{\lambda \in A} \sum_{\omega \in B} (PS)_{\omega\lambda} (PS)_{\lambda\omega} \right) \tag{F5}$$

$$\begin{aligned} \varepsilon_{AB}^{penetr} = & - \sum_{\eta,\mu,\nu \in A} S^{-1}_{(A)\nu\mu} \left(\left\langle \chi_\mu \left| \left(\frac{Z_B}{r_B} \right) \right| \chi_\eta \right\rangle - \frac{Z_B}{r_{AB}} S_{\mu\eta} \right) (PS)_{\eta\nu} \\ & + \frac{1}{2} \sum_{\kappa,\mu,\nu \in A} \sum_{\rho,\tau,\lambda \in B} S^{-1}_{(A)\nu\mu} S^{-1}_{(B)\lambda\tau} \left([\mu\tau \mid \kappa\rho] - \frac{S_{\mu\kappa} S_{\tau\rho}}{R_{AB}} \right) \times \left[(PS)_{\kappa\nu} (PS)_{\rho\lambda} - (PS)_{\kappa\lambda} (PS)_{\rho\nu} \right] \end{aligned} \tag{F6}$$

$$\varepsilon_{AB}^{overl} = -\sum_{\eta\in A}\sum_{\mu,\nu\in B} S^{-1}_{(AB)\mu\nu}\left\langle \chi_\nu \left| \left(\frac{Z_B}{r_B}\right) \right| \chi_\eta \right\rangle (PS)_{\eta\mu} + \sum_{\eta,\mu,\nu\in A} S^{-1}_{(A)\mu\nu}\left\langle \chi_\nu \left| \left(\frac{Z_B}{r_B}\right) \right| \chi_\eta \right\rangle (PS)_{\eta\mu}$$
$$+\frac{1}{2}\sum_{\kappa\in A}\sum_{\rho\in B}\sum_{\lambda,\mu,\nu,\tau\in AB} S^{-1}_{(AB)\mu\lambda} S^{-1}_{(AB)\nu\tau}[\lambda\tau \mid \kappa\rho]\left[(PS)_{\kappa\mu}(PS)_{\rho\nu} - (PS)_{\kappa\nu}(PS)_{\rho\mu}\right] \qquad \text{(F7)}$$
$$-\frac{1}{2}\sum_{\kappa,\mu,\lambda\in A}\sum_{\rho,\nu,\tau\in B} S^{-1}_{(A)\mu\lambda} S^{-1}_{(B)\nu\tau}[\lambda\tau \mid \kappa\rho]\left[(PS)_{\kappa\mu}(PS)_{\rho\nu} - (PS)_{\kappa\nu}(PS)_{\rho\mu}\right]$$

Here the symbol $\mu \in A$ is used to denote the assignment of spin-orbital χ_μ to atom A and the short notation $[\lambda\tau \mid \kappa\rho]$ stands for

$$[\lambda\eta \mid \kappa\rho] = \int\int \chi^*_\lambda(1)\chi^*_\eta(2)\frac{1}{r_{12}}\chi_\rho(1)\chi_\kappa(2)d\tau_1 d\tau_2 \qquad \text{(F8)}$$

where $d\tau_i$ refers to all the variables on which the spin-orbitals depend.

Appendix G: Curriculum Vitae

Full name Sami Kamran

Education

BSc. University of Ottawa, Ottawa, Canada (2002-2005)

MSc. University of Ottawa, Ottawa, Canada (2006-2007); Supervisors: Dr. Liang Chen and Dr. Kuiying Chen

Papers accepted for publication

a- S. Kamran, K. Chen, L. Chen and L. Zhao, "Electronic origin of anomalously high shear modulus and intrinsic brittleness of FCC Ir", accepted by *Journal of Physics: Condensed Matter.*

b- S. Kamran, K. Chen, L. Chen and L. Zhao, "Semi-empirical formulae for elastic moduli and brittleness of diamond-like and zinc-blende covalent crystals" accepted by *Physical Review B.*

A third paper on the ideal strengths of FCC metals is in preparation.

Publication

S. Kamran, K. Chen, L. Chen and L. Zhao, "A literature review on the quantum origins of elastic properties and mechanical hardness", report published by National Research Council Canada (NRC), Institute for Aerospace Research, Structure and Materials Performance Laboratory, Ottawa, LTR-SMPL-2006-0091 (2006).

Presentation

S. Kamran, "Electronic origins of elastic and mechanical properties of materials", *graduate symposium of Ottawa-Carlton Institute for Physics*, Ottawa, Canada, May 2007.